Rep. Prog. Phys. **61** (1998) 1575–1664. Printed in the UK PII: S0034-4885(98)07487-9

Atomic beam diffraction from solid surfaces

Daniel Farías and Karl-Heinz Rieder
Fachbereich Physik, Freie Universität Berlin, Arnimallee 14, 14195 Berlin, Germany

Received 29 June 1998

Abstract

Atomic beam techniques are presently being used in many branches of surface physics such as studies of the particle–surface physisorption potential, surface structure, surface phonons, nucleation and growth on metal and insulator surfaces, surface diffusion and accommodation and sticking of molecules. This review concentrates on diffractive phenomena from surfaces, which up to now were investigated mainly with helium. The theoretical background for diffraction calculations is outlined and representative examples of different applications are given. The main subjects covered are: structural determinations of chemisorbed and physisorbed systems, investigations of disordered surfaces, selective adsorption resonances, diffusion and nucleation studies and investigations of growth and phase transitions on surfaces. Diffraction results obtained with Ne, Ar, H_2 and D_2 are also summarized.

0034-4885/98/121575+90$59.50

Contents

1. Introduction

The rapid progress in combining ultra-high-vacuum techniques with high-pressure nozzle beam production systems (reviewed by Scoles 1988, 1992) has allowed the scattering of monoenergetic beams of neutral (mostly rare gas) particles from single crystalline solid surfaces to be intensively pursued under greatly improved scientific conditions since the end of the 1970s. Because of the low energies used (10–300 meV), the incident atoms (or nonreactive molecules) probe the topmost layer of the substrate surface in an absolutely nondestructive manner, and are equally applicable to insulators, semiconductors and metals. Using light particles (especially He) at low energies the scattering is predominantly elastic and, as the de Broglie wavelengths are of the order of several tenths to a few Ångströms, diffraction effects dominate. Measurements of diffraction spectra allow not only the determination of the size and orientation of the surface unit cells but also, by means of analysing diffraction intensities, yield the surface corrugations which very often provide direct pictures of the geometrical arrangement of the surface atoms (Engel and Rieder 1982, Rieder 1992, Manson 1992). In the diffraction regime, accurate determination of the particle–surface physisorption potential becomes possible via resonant scattering into bound-state channels (Hoinkes and Wilsch 1992). The extreme sensitivity of He beams to dilute adsorbates allows an accurate determination of minute amounts of surface impurities (down to $\sim$0.001 ML) with interesting consequences with respect to technologically important investigations of surface diffusion as well as two-dimensional condensation and growth phenomena (Poelsema and Comsa 1989).

Producing short He beam pulses and applying time-of-flight (TOF) techniques, the dispersion of surface phonons (especially the low-lying branches) can be determined with high resolution (0.5 meV) by analysing inelastic scattering events (Toennies 1982, 1984, 1991). Furthermore, detailed studies of the microscopic steps involved in surface adatom diffusion become possible through quasi-elastic helium atom scattering (Frenken and Hinch 1992). Upon scattering of heavier atoms multiphonon processes gain increasingly more importance and a distinction between direct (phononic) inelastic scattering and inelastic events resulting from trapping and subsequent desorption is necessary, which experimentally again requires use of TOF techniques (Barker and Auerbach 1985). Scattering of molecules is even more involved as the low-energy rotational and vibrational internal states can be influenced in the surface collision process, so that both TOF and state-specific detection must be applied. By combining beam techniques with optical methods for detecting the internal states of the scattered molecules, important insight into the dynamical phenomena involved in accommodation and sticking processes could be gained (Gerber 1987, Arumainayagam and Madix 1991). Finally, using relaxation and/or TOF techniques valuable information on surface chemical reactions can be obtained (D'Evelyn and Madix 1983).

Although the equipment required in the field of neutral particle/surface scattering is voluminous and expensive, and therefore not many groups are involved worldwide, it is a very active field of surface research. In this review we consequently restrict ourselves to investigations of solid surfaces by means of atomic beam diffraction. In order to make our presentation accesible to a broader readership, we introduce in section 2 some basic concepts relevant to the interpretation of the experimental results presented in the following three sections. We also adopted a pragmatic point of view in the sense that we write

down the relevant formulae, but refer for their derivation to the original literature. In view of helium scattering studies, notice that the two acronyms HAS (helium atom scattering) and TEAS (thermal energy atom scattering) have been coined by different groups. We maintain both abbreviations throughout this work, since they already hint at diffraction and structural studies (HAS) on the one hand and at investigations of disordered surfaces through measurements of the specular reflected beam (TEAS) on the other.

Helium diffraction results are summarized in section 3. Quantitative structural determinations on well-ordered clean and adsorbate-covered surfaces are illustrated by several examples. The emphasis was put on systems where HAS presents clear advantages in comparison with other techniques such as adsorption of hydrogen and weakly bonded adsorbates (water, polar molecules). A complete update of all adsorbate overlayers analysed with HAS is also given. Also summarized in this section are investigations of structural disorder on surfaces, an area in which enormous progress has recently been achieved. It includes characterization of step-edge defects and single adsorbates as well as substitutionally and structurally disordered adlayers by means of HAS. These fascinating results demonstrate that HAS is also capable of performing a crystallography of disordered surfaces. Studies of order–disorder and order–order phase transitions on surfaces as well as investigations of the Debye–Waller factor and selective adsorption resonances in atom–surface scattering are also covered in this section.

The main goal of section 4 is to provide a comprehensive description of some new applications of TEAS developed since the publication of the book by Poelsema and Comsa (1989) such as studies of adatom diffusion, nucleation and growth and thin film growth. These results clearly show that much insight into microscopic processes can be gained by modelling deposition curves, which can be easily measured for a variety of systems. With respect to growth studies, a major advantage of TEAS as compared with other techniques is its high sensitivity to step distributions in the topmost surface layer, which allows a quite simple interpretation of the data. In particular, the evolution of the defect density during growth can be monitored by in-phase measurements of the specular reflected beam. A list of all growth studies performed with TEAS is also given.

Finally, diffraction results obtained with Ne, Ar and H_2/D_2 molecular beams are presented in section 5. Ne-diffraction studies of hydrogen-covered systems are described in some detail, since, due to the absence of anticorrugating effects, they provide a more faithful picture of atom arrangements than He-diffraction data. The observation of sharp diffraction peaks in the scattering of Ar from 2H-W(100) demonstrates that quantum effects are important even for such large species and suggests that similar experiments may be extended to other systems. Diffraction studies with H_2/D_2 molecular beams have received renewed interest in recent years. This was certainly motivated by the possibility of (i) carrying out six-dimensional quantum mechanical calculations, which showed that precise information regarding the *reactive potential* within the unit cell can be obtained from diffraction experiments and (ii) performing experiments over a wide range of incident energies and with an angular resolution high enough to allow investigation of rotationally inelastic diffraction peaks. A summary of these very promising new results is given at the end of section 5.

We have performed an intensive literature search with modern computer resources including more than the last decade, up to December 1997. However, despite these efforts some of the relevant papers escaped our attention and were found just by chance, so that we cannot regard our list of articles as complete despite its length. Due to the existence of earlier reviews (Poelsema and Comsa 1989, Holpke 1992) we concentrate mainly on results obtained since 1990.

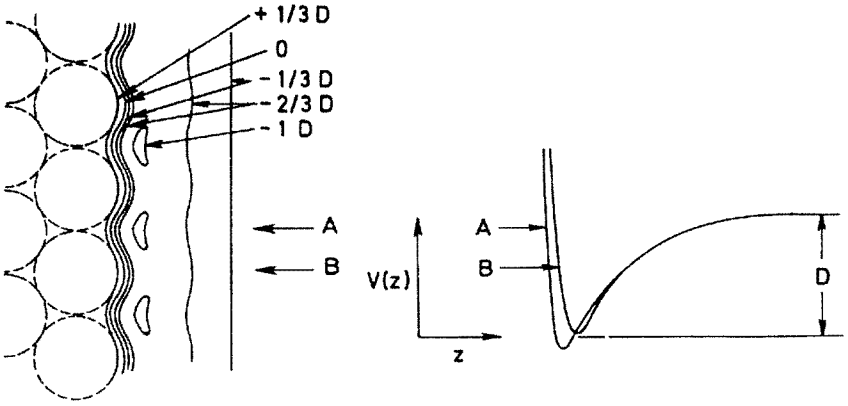

Figure 1. Schematic diagram showing equipotential lines for the interaction of an atom with an ordered surface. The (negative) potential energies are given in terms of the depth of the potential well D. On the right-hand side, the potential as a function of z (normal to the surface) for two different positions A and B is illustrated. After Stickney (1969).

2. Theoretical foundations

2.1. The particle–surface interaction potential

Diffraction experiments give information on both the dimensions of the unit cell via the angular location of the diffraction peaks and the distribution of the scattering centres within the unit cell via the intensity distributions in the spectra. Before discussing in more detail the way in which this information is recovered from experimental data, a brief description of the He–surface interaction potential will be presented. The discussion will be limited to the case of scattering with atoms of thermal energies, i.e. from 10 to 100 meV. At distances not too far away from the surface, the impinging atoms feel an attraction due to van der Waals forces. Closer to the surface, they will be repelled due to the overlap of their electronic wavefunctions with those of the atoms forming the solid surface (Pauli exclusion); this causes the repulsive part of the interaction potential to rise steeply. One way to obtain an at least qualitatively correct picture of the interaction potential is to start from individual particle–atom potentials (for example, of the Lennard-Jones type) and to perform a summation over all binary interactions between the particle and the atoms in the solid (for a more detailed description of this subject see Hoinkes 1980, Celli 1992). The result of such calculation for a monatomic solid is shown in figure 1 (Stickney 1969).

It illustrates schematically the most important features of a typical particle–surface potential. In general, the classical turning points are farther away for particles impinging on top of the surface atoms than for particles impinging between them; this gives rise to a periodic modulation of the repulsive part of the potential. The locus of the classical turning points follows a surface of constant total electron density (Esbjerg and Nørskov 1980), where every point constitutes a scattering centre; the resulting scattering surface is called the *corrugation function* $\zeta(\boldsymbol{R})$ ($\boldsymbol{R}$ denotes a two-dimensional vector in the surface plane). As shown by Esbjerg and Nørskov (1980), $\zeta(\boldsymbol{R})$ corresponds in first order to a contour of constant surface electronic charge density $\rho(\boldsymbol{r})$ related linearly to the particle energy $E(\boldsymbol{r})$,

$$E(\boldsymbol{r}) = \alpha\rho(\boldsymbol{r}). \tag{2.1}$$

It implies that the classical turning points are about 2–3 Å away from the surface atom cores, and that with thermal He atoms densities between 1×10^{-4} and 2×10^{-3} au

can be mapped. Therefore, the arrangement of the surface atoms can be obtained by relating the experimental corrugation $\zeta(\boldsymbol{R})$ to calculations of surface charge-density profiles. Note that according to this picture the corrugation is expected to increase with increasing kinetic energy, because high-energy atoms penetrate deeper into the electron-density profile. However, experimentally it was found that, in some cases, the corrugation remains constant (or even decreases) after increasing the incoming energy by a factor of 3 (as for Ni(110), Rieder (1982a)) indicating that the simple Esbjerg–Nørskov approach does not hold. Annett and Haydock (1984) were the first to theoretically discuss an extension of this simple picture leading to the possibility of anticorrugating effects, as discussed in more detail in section 5.1. Since anticorrugating effects concern changes in corrugation amplitudes of no more than a few hundredths of an Ångström, they are not expected to affect seriously the main conclusions obtained by applying the simple Esbjerg–Nørskov model to a clean metal surface.

The fundamental problem in relating models of surfaces to atom diffraction data is that of determining the surface charge density implied by a model in regions where the density is about 10^{-4} electrons per $(\text{au})^3$. This is a serious theoretical problem, because at these densities the effects of inhomogeneities in the electron gas become very important. Charge-density profiles are usually calculated by overlapping atomic charge densities using the approach introduced by Haneman and Haydock (1982), whereby the atomic wavefunctions are computed with a Herman–Skillman-like program (Herman and Skillman 1963). Superposition of atomic charge densities allows much simpler and faster calculations which enable us to compare different surface–structure models with the experimental data. This approach works well as long as bonding effects can be neglected, which is most likely for clean metals. For ordered hydrogen adlayers, good results have been obtained by adding a negative excess charge of $-0.4e$ to the H-atoms (Parschau *et al* 1990, 1991, Apel *et al* 1995b). For reconstructed semiconductor surfaces, an alternative procedure (the modified atomic charge superposition (MACS)) has been developed by Sakai *et al* (1986). The validity of the Esbjerg and Nørskov ansatz (2.1) for semiconductors has recently been demonstrated by Buongiorno Nardelli (1996) in a density functional study of the interaction of He with the InSb(110) surface.

2.2. Diffraction theory from two-dimensional structures

Before discussing the methods employed for calculating diffraction intensities, a brief description of diffraction kinematics for periodic two-dimensional systems is required. Consider a beam of particles of mass m and energy E_i impinging on a surface at an angle θ_i as measured from the surface normal. The particle wavelength λ is related to the beam energy according to the de Broglie relation

$$\lambda = \frac{h}{\sqrt{2mE_i}}. \tag{2.2}$$

The incoming wavevector $\boldsymbol{k}_i$ is related to the wavelength λ by $|\boldsymbol{k}_i| = 2\pi/\lambda$.

For mathematical simplicity, it is useful to separate the wavevector $\boldsymbol{k}$ into a component $\boldsymbol{K}$ parallel to the surface and a component $\boldsymbol{k}_z$ perpendicular to the surface. With this notation, the incoming and outgoing wavevectors read $\boldsymbol{k}_i = (\boldsymbol{K}, k_{iz})$ and $\boldsymbol{k}_G = (\boldsymbol{K}_G, k_{Gz})$, respectively. The well known Bragg condition for diffraction from a two-dimensional periodic array relates the wavevectors $\boldsymbol{k}_i$ and $\boldsymbol{k}_G$ by

$$\boldsymbol{K} + \boldsymbol{G} = \boldsymbol{K}_G \tag{2.3}$$

where $\boldsymbol{G} = j\boldsymbol{b}_1 + l\boldsymbol{b}_2,\ j, l \in N$ denotes a reciprocal lattice vector and $\boldsymbol{b}_1$, $\boldsymbol{b}_2$ are related to the unit cell vectors $\boldsymbol{a}_1$ and $\boldsymbol{a}_2$ through $\boldsymbol{a}_p \cdot \boldsymbol{b}_q = 2\pi\delta_{pq},\ p, q = 1, 2$. The particle

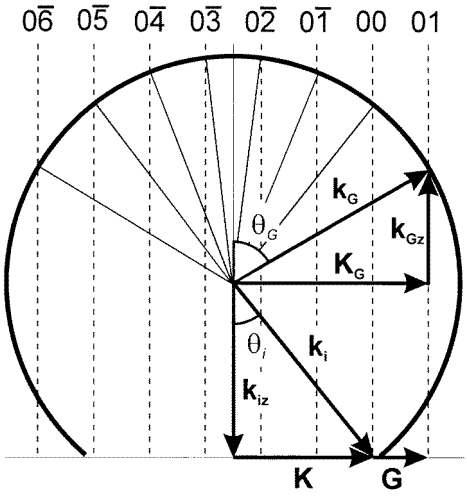

Figure 2. The Ewald construction for diffraction from surfaces. The notation used in this section is illustrated for the reciprocal vector $\boldsymbol{G} = (01)$.

energy remains unchanged during diffraction, so that $k_i = k_G$. This restricts the number of reciprocal lattice vectors for which diffraction can occur to the finite set $\boldsymbol{F}$ (the so-called propagating waves) that satisfy ${k_{Fz}}^2 = {k_i}^2 - |\boldsymbol{K} + \boldsymbol{F}|^2 > 0$.

The Bragg condition (2.3) can be represented graphically by the Ewald construction, as shown schematically in figure 2. Measurements of the angular locations of the diffraction peaks allow the determination of the dimensions of the surface unit cell as well as its orientation relative to the incoming beam. For a two-dimensional corrugation function $\zeta(x, y)$, two angles specifying the scattering direction have to be measured. Assuming that the incoming wavevector $\boldsymbol{k_i}$ is parallel to $\boldsymbol{a}_2$, the following formulae for the beam (jl), located at θ_{jl} and ϕ_{jl} can be derived:

$$\sin\phi_{jl} = -\lambda\frac{j}{a_1} \tag{2.4}$$

$$\sin\theta_{jl} = \frac{1}{\cos\phi_{jl}}\left[\sin\theta_i + \lambda\frac{l}{a_2}\right] \tag{2.5}$$

where θ_{jl} is measured in the scattering plane (which is spanned by the wavevector $\boldsymbol{k_i}$ and the surface normal) and ϕ_{jl} is measured away from this plane (the so-called 'out-of-plane' angle). The corresponding equations for arbitrary scattering conditions can be found in the book by Engel and Rieder (1982, p 74).

2.3. Calculation of diffraction intensities

2.3.1. Close-coupling calculations. The general problem of calculating diffraction intensities for a given scattering geometry and corrugation function consists of solving the time-independent Schrödinger equation

$$\frac{-\hbar^2}{2m}\nabla^2\Psi(\boldsymbol{r}) + V(\boldsymbol{r})\Psi(\boldsymbol{r}) = E\Psi(\boldsymbol{r}) \tag{2.6}$$

with a given model potential $V(\boldsymbol{r})$. This problem can be solved exactly in the most general case using the close-coupling method developed by Wolken (1973a, b). This method is very

time consuming and consequently not appropriate for determining the corrugation function $\zeta(\boldsymbol{R})$ from measured intensities, that must be made by means of trial and error procedures (see section 2.3.5). Manolopoulos *et al* (1990) have proposed a very promising procedure to overcome this problem. The method is based in the *log derivative Kohn approach*, and was applied to the diffractive scattering of He from LiF(100) (Manolopoulos and Wyatt 1988). The computer time required to achieve convergence was found to increase quite slowly with the number of channels N. This should be compared with the computer time required for a standard close-coupling calculation, which scales as N^3 (Blake 1984). These results are very encouraging and will certainly motivate new structural studies of highly corrugated surfaces. Also, a variety of approximate methods have been developed to calculate diffraction intensities, a detailed description of which is given by Manson (1992). In the following sections, we limit ourselves to briefly discussing the two most employed ones, namely the GR method and the eikonal approximation.

2.3.2. Approximate methods: the hard corrugated wall model. As mentioned above, close-coupling calculations are often very time consuming and consequently not appropriate for fitting experimental data. A very convenient approach for this purpose is the so-called 'hard-corrugated-wall model' (HCW), in which the particle–surface potential is represented by

$$V(\boldsymbol{R}, z) = \begin{cases} 0 & \text{for } z > \zeta(\boldsymbol{R}) \\ \infty & \text{for } z \leqslant \zeta(\boldsymbol{R}) \end{cases} \tag{2.7}$$

with z denoting the direction of the surface normal. Historically, this assumption was put forward by Lord Rayleigh (Strutt 1896) a century ago in his investigations related to the scattering of sound waves from corrugated surfaces. The analogous quantum theory for the scattering of atoms from surfaces was introduced by Garibaldi *et al* (1975). Neglect of the attractive part of the potential is a reasonable assumption as long as the particle energy E_i is much higher than the potential well D. For He, D values are usually between 5 and 10 meV, so that with a 63 meV room temperature He beam this condition is well fulfilled. For cases where E_i is comparable to D, however, the existence of the attractive well leads to another diffraction phenomenon called resonant scattering (or selective adsorption, see section 3.4), which can influence considerably the intensities of the diffraction peaks making calculations based on the HCW model doubtful. Nevertheless, in situations where the depth of the attractive well D cannot be neglected in comparison with the incoming energy E_i, but where selective adsorption still does not play an important role, calculations based on the HCW model can be performed by taking into account the depth D in a very simple form (Garibaldi *et al* 1975, García *et al* 1979). This modification where E_{iz} is replaced in the calculations by the 'effective' energy $E_{iz} + D$ with which the particle hits the surface, is known as Beeby's correction (Beeby 1971). Physically, it means that the particle beam is accelerated on its way to the surface and refracted towards the surface normal, so that the beam hits the repulsive wall under a smaller effective angle of incidence θ_i' given by

$$\sin\theta_i' = \frac{|\boldsymbol{k_i}|}{|\boldsymbol{k_i'}|}\sin\theta_i = \frac{\sin\theta_i}{\sqrt{1+\frac{D}{E_i}}}. \tag{2.8}$$

Therefore, to a first approximation the attractive well can be taken into account by replacing $|\boldsymbol{k_i}|$ and θ_i in the calculations by $|\boldsymbol{k_i'}|$ and θ_i'. This procedure gives reliable results for shallow corrugations and small angles of incidence.

A method to calculate diffraction intensities on a quantum mechanical basis for hard-corrugated surfaces and general scattering geometries has been developed as a result of

the effort of several groups (Cabrera *et al* 1970, Masel *et al* 1975, 1976, Goodman 1977, Toigo *et al* 1977, García and Cabrera 1978, Armand and Manson 1978). One of the most applied ones is the so-called RR′ method, a numerical algorithm developed by García and Cabrera (1978). It leads to the exact solution of the scattering of waves from a hard-corugated surface, providing in consequence a good frame of reference for testing the validity of approximated HCW calculations. Model calculations performed for one-dimensional corrugations of different shapes and amplitudes confirmed that the RR′ method always gives a convergent solution, irrespective of the scattering geometry. Calculations performed for the highly-corrugated Ge(111)–c(2 × 8) reconstruction suggest that also for two-dimensional problems the RR′ method yields convergent solutions for all cases of physical interest (Farías *et al* 1997c). Of course, the price to pay for this unlimited range of convergence consists of the mathematical complexity of this approach, which makes it very time consuming and consequently unappropriate for systematic fit procedures. Therefore, some simplifying physical assumptions must be introduced in order to obtain methods of calculation which converge faster than RR′, as discussed below. A mapping procedure to generate a set of starting parameters for close-coupling calculations from a HCW best-fit corrugation function has been developed by Aten and Engel (1985).

2.3.3. The GR method. A very simple and effective procedure to calculate diffraction intensities within the HCW approximation was developed by García (1976, 1977) and is usually referred to as the GR method. The starting point is the so-called Rayleigh assumption (Strutt 1896), which states that the incoming and outcoming beams can be considered as plane waves up to the surface, e.g. the total particle wavefunction reads

$$\Psi(\boldsymbol{R}, z) = \exp[\mathrm{i}(\boldsymbol{K}\cdot\boldsymbol{R} + k_{iz}z)] + \sum_{\boldsymbol{G}} A_{\boldsymbol{G}} \exp\{\mathrm{i}[(\boldsymbol{K}+\boldsymbol{G})\cdot\boldsymbol{R} + k_{Gz}z]\}. \tag{2.9}$$

The first term represents the incident beam of wavevector $\boldsymbol{k_i} = (\boldsymbol{K}, k_{iz})$ and the others the diffracted beams with wavevectors $\boldsymbol{k_G} = (\boldsymbol{K_G}, k_{Gz})$ and scattering amplitudes $A_{\boldsymbol{G}}$, corresponding to each two-dimensional reciprocal vector lattice $\boldsymbol{G}$. In principle, the sum extends over all $\boldsymbol{G}$'s, i.e. over the finite number of propagating waves (for which ${k_{Gz}}^2 > 0$) as well as over the remaining infinite set of evanescent waves (for which ${k_{Gz}}^2 \leqslant 0$ and $|\theta_f| > 90^\circ$)). To determine the amplitudes $A_{\boldsymbol{G}}$ we impose on (2.9) the boundary condition $\Psi[\boldsymbol{R}, z = \zeta(\boldsymbol{R})] = 0$ to obtain

$$\sum_{\boldsymbol{G}} A_{\boldsymbol{G}} \exp\{\mathrm{i}[\boldsymbol{G}\cdot\boldsymbol{R} + k_{Gz}\zeta(\boldsymbol{R})]\} = -\exp[\mathrm{i}k_{iz}\zeta(\boldsymbol{R})]. \tag{2.10}$$

Rearranging (2.10) by multiplying each side by $\exp[-\mathrm{i}k_{iz}\zeta(\boldsymbol{R})]$, we obtain the matrix equation

$$\sum_{\boldsymbol{G}} A_{\boldsymbol{G}} M_{\boldsymbol{GR}} = -1 \tag{2.11}$$

with

$$M_{\boldsymbol{GR}} = \exp\{\mathrm{i}[(k_{Gz} - k_{iz})\zeta(\boldsymbol{R}) + \boldsymbol{G}\cdot\boldsymbol{R}]\}. \tag{2.12}$$

Equation (2.12) must be satisfied for every point $\boldsymbol{R}$ in the unit cell. If one now chooses a finite set of n vectors $\boldsymbol{R}_n$ uniformly distributed over the surface unit cell and relates them to the same number of uniformly distributed reciprocal lattice vectors $\boldsymbol{G}$, one can regard (2.12) as a set of n linear equations which can be solved by matrix inversion for the $A_{\boldsymbol{G}}$'s. This is the basis of the GR method developed by García (1977, see also Stoll *et al* 1984). The scattered intensities $P_{\boldsymbol{G}}$ are finally obtained by using

$$P_{\boldsymbol{G}} = \frac{|k_{Gz}|}{|k_{iz}|} A_{\boldsymbol{G}} A^*_{\boldsymbol{G}} \tag{2.13}$$

where the kinematic factor is due to the cross section ratio of impinging and emerging beams. As all the scattering from the rigid hard wall is elastic, the diffracted intensities have to satisfy the unitarity condition

$$\sum_{\boldsymbol{G}} P_{\boldsymbol{G}} = 1. \tag{2.14}$$

As can be easily seen, the series (2.10) might be in general divergent because of the increasing exponential $\exp[\mathrm{i}k_{Gz}\zeta(\boldsymbol{R})]$. The limits of convergence of (2.10) (also known as the 'Rayleigh limit', because it is just a consequence of the Rayleigh assumption (2.9)) were investigated analytically by many authors (García 1977, García and Cabrera 1978, Hill and Celli 1978). It was found that, independent of the incident wavelength λ, convergence is guaranteed if $\zeta_m \leqslant 0.14a$ for a one-dimensional sinusoidal corrugation, and if $\zeta_m \leqslant 0.18a$ for a two-dimensional quadratic corrugation described by a sum of cosines in both x- and y-directions, where a denotes the lattice constant and ζ_m the maximum corrugation amplitude. In practice, however, it is found that the hard-wall boundary condition can be satisfied to a good approximation with a finite number of terms in the expansion (2.10), *even though the expansion eventually diverges*. In such cases, calculations can be performed beyond the Rayleigh limit but convergence is more difficult to achieve as λ increases (Stoll *et al* 1984). Comparison of solutions obtained with the GR and the RR′ methods have shown that, wherever unitarity is verified, the diffraction probabilities are the same independently of the formalism used (García and Cabrera 1978). That is, deviations from (2.14) should be used as an indicator for the adequacy of the Rayleigh ansatz and the minimum required number N of vectors to be included for a given accuracy. If the corrugation is not too large the result will appear to converge closer and closer to the exact solution as N is increased up to a certain value, after which the solution diverges with further increase of N. Depending on the form of the corrugation and the size of the unit cell, the dimension N of the matrix $M_{\boldsymbol{GR}}$ may be very large, making the calculations rather time consuming. Typical values of N lie between 400 and 600, although they can be reduced by a factor of 2 for every mirror symmetry present in the corrugation function. Further reduction of computing time can be achieved by taking into account additional symmetries in the experiment, as proposed by Varga and Füstöss (1991).

2.3.4. The eikonal approximation. Starting from (2.10), we multiply both of its sides by $\exp\{-\mathrm{i}[\boldsymbol{G}'\cdot\boldsymbol{R} + k_{G'z}\zeta(\boldsymbol{R})]\}$ and integrate over the unit cell to obtain the matrix equation

$$\sum_{\boldsymbol{G}} M_{\boldsymbol{GG}'} A_{\boldsymbol{G}} = A^0_{\boldsymbol{G}'} \tag{2.15}$$

where

$$M_{\boldsymbol{GG}'} = \frac{1}{S}\int_{u.c.} \exp\{\mathrm{i}[(\boldsymbol{G}-\boldsymbol{G}')\cdot\boldsymbol{R} + (k_{Gz}-k_{G'z})\zeta(\boldsymbol{R})]\}\,\mathrm{d}\boldsymbol{R} \tag{2.16}$$

and

$$A^0_{\boldsymbol{G}'} = -\frac{1}{S}\int_{u.c.} \exp\{-\mathrm{i}[\boldsymbol{G}'\cdot\boldsymbol{R} + (k_{G'z}-k_{iz})\zeta(\boldsymbol{R})]\}\,\mathrm{d}\boldsymbol{R} \tag{2.17}$$

where S denotes the unit cell area.

As one can see from (2.15), the diagonal elements of the (Hermitian) matrix $M_{\boldsymbol{GG}'}$ are all equal to unity. It can be shown that the order of magnitude of its off-diagonal elements is (for a one-dimensional corrugation) given by

$$M_{mn} \sim \frac{\pi}{2}\frac{\zeta_m}{a}\tan\theta_i \qquad m \neq n \tag{2.18}$$

where ζ_m denotes the maximum corrugation amplitude and a is the lattice constant. It means that, in cases where $\zeta_m \leqslant 0.1a$ and the angle of incidence is small ($\theta_i < 45^\circ$), they can be neglected so that (2.15) becomes

$$A_{\boldsymbol{G}} = A^0_{\boldsymbol{G}'}. \tag{2.19}$$

This is the so-called eikonal approximation (Garibaldi *et al* 1975), from which the diffraction probabilities can be readily calculated by simply evaluating the Fourier transform of a phase factor, as prescribed by (2.17). The eikonal approximation is not necessarily restricted to cases where the diffraction is weak, but its range of convergence is slightly smaller than for the GR method. Neglect of the off-diagonal terms in (2.15) corresponds to a neglect of multiple scattering events. As a consequence, the eikonal approximation does not satisfy the unitarity condition (2.14), but even under conditions where it gives poor unitarity, the relative strengths of the diffraction intensities can be quite close to that of an exact calculation. By performing an alternative derivation of the eikonal approximation, Garibaldi *et al* (1975) have developed kinematic factors which help to satisfy unitarity when using (2.17). We cite here the expression which was proven to give the best results for intensity calculations within the eikonal approximation:

$$A_{\boldsymbol{G}} = \frac{1 + \cos\theta_i \cos\theta_{jl} - \sin\theta_i \sin\theta_{jl} \cos(\phi_i - \phi_{jl})}{\cos\theta_{jl}(\cos\theta_i + \cos\theta_{jl})} A^0_{\boldsymbol{G}'} \tag{2.20}$$

where $A^0_{\boldsymbol{G}'}$ is given by (2.17) and the angles have been chosen according to (2.4) and (2.5). It should be made clear that interference between trajectories originating at different impact parameters is effectively included in formula (2.17). What is not included is multiple scattering and, consequently, interference between trajectories corresponding to single scattering and trajectories corresponding to multiple scattering, although there is, strictly speaking, no simple correspondence between multiple scattering in 'reciprocal lattice space' and classical multiple scattering in true position space. It can be shown that the approximation introduced by (2.19) corresponds to neglect of the contribution of evanescent waves ($k_G{}^2 < 0$), which belongs to G vectors outside the Ewald sphere. The unimportance of evanescent waves has a remarkable nontrivial consequence for surface structural investigations using atomic beam diffraction: the diffraction intensities of $\zeta(\boldsymbol{R})$ and $-\zeta(-\boldsymbol{R})$ are the same as long as multiple scattering is negligible (Engel and Rieder 1982). For surfaces with a mirror symmetry plane in which $\zeta(\boldsymbol{R}) = \zeta(-\boldsymbol{R})$ it means that from an analysis of diffraction intensities with the eikonal approximation, one cannot decide which of functions $\zeta(\boldsymbol{R})$ or $-\zeta(\boldsymbol{R})$ describes the real surface profile. In such cases, further calculations with the GR or RR′ methods (which do take into account the occurrence of multiple scattering) must be performed in order to distinguish the effects of opposite corrugations.

Because of the close relationship between the structure factor of kinematic diffraction theory in standard three-dimensional crystallography and the eikonal approximation described above, it is straightforward to transfer the concept of Patterson synthesis to HAS structural studies, as first proposed by Cantini *et al* (1979). Within the hard-wall approximation, the Patterson function is equivalent to a correlation function of surface heights in the surface electron density. The power of the Patterson method for He diffraction has been demonstrated by Gross *et al* (1991), who showed that the existence of two hydrogen atoms in the (2 × 2)H–Ni(111) unit cell as well as their mutual distances can be directly visualized by the Patterson function derived from experimental diffraction intensity data. This method has been more recently applied by Curson *et al* (1997) to determine the (3 × 3) structure formed by silane adsorbed on Cu(111) below 165 K.

2.3.5. The problem of data inversion. Whereas the methods discussed in the previous sections dealt with the problem of obtaining diffraction intensities for a given corrugation function $\zeta(x, y)$, usually one faces the inverse problem of determining $\zeta(x, y)$ from a set of measured spectra. A direct inversion of the experimental data is not possible, due to the fact that the measured intensities do not contain information on the phases of the scattered waves. Therefore, the trial-and-error approach must be adopted. Assuming for the corrugation function the Fourier series

$$\zeta(\boldsymbol{R}) = \tfrac{1}{4}\sum_{\boldsymbol{G}} \zeta_{\boldsymbol{G}} \exp(\mathrm{i}\boldsymbol{G}\cdot\boldsymbol{R}) \tag{2.21}$$

with the number of possible parameters $\zeta_{\boldsymbol{G}}$ reduced according to the symmetries of the unit cell, the best-fit coefficients can be determined by varying their amplitudes until optimum agreement between the measured $P_{\boldsymbol{G}}^{\mathrm{exp}}$ and the calculated intensities $P_{\boldsymbol{G}}^{\mathrm{calc}}$ is reached. The degree of agreement is jugded by using reliability factors (R-factors) which, as in the case of LEED, can be defined in many different ways. The one usually adopted reads

$$R = \frac{1}{N}\sqrt{\sum_{\boldsymbol{G}}(P_{\boldsymbol{G}}^{\mathrm{exp}} - P_{\boldsymbol{G}}^{\mathrm{calc}})^2} \tag{2.22}$$

where N denotes the number of beams G measured and the intensities are normalized to the specular beam (note that in this way all intensities are weighted equally). It is important to note that, by modelling the corrugation function as a Fourier series, data analyses can be performed entirely free of any model assumptions on the surface structure. However, for some problems it is more reasonable to start from a model structure which is expected to resemble the real one on physical grounds. Such a procedure is usually adopted in modelling hydrogen adlayers, where the substrate is described by a Fourier series and the hydrogen atoms by Gaussian hills (see for example Rieder 1992, Farías *et al* 1997c, d).

2.4. Rainbow scattering

The previous sections have been devoted to the description of different methods to calculate diffraction intensities. However, in most practical cases it is useful to have, prior to any calculation, a rough estimation of the maximum corrugation amplitude ζ_m in order to know which of the calculation methods is more suitable for the problem under consideration. Such an estimation can be easily made by considering a general feature of atom–surface scattering which is naturally explained by the HCW model, namely the surface rainbow effect.

The phenomenon of surface rainbow, a pair of strong maxima in the classical scattering probability as a function of scattering angle, was described theoretically by McClure (1970) who named it and studied it extensively by classical calculations (see also McClure 1972a, b). Historically, the name comes from optics, where rainbows originated from the presence of an extremum in the scattering angle of light rays from rain drops as a function of the impact parameter, leading to a large amount of light scattered at that angle. In atom–surface experiments, surface rainbows were first observed for the scattering of Ar (Smith *et al* 1969), Ne and Xe from LiF(001) (Smith *et al* 1970). Garibaldi *et al* (1975) have shown that rainbow scattering has a strong quantum correspondence which suggests that the maxima can be qualitatively analysed in a classical way. A strictly wave-like feature of rainbow scattering, however, is the supernumerary rainbow which may occur between the rainbow maximum and the specular beam for strongly corrugated surfaces. It arises when the phase shift between trajectories with the same scattering angle but from different impact parameters within the unit cell approaches 2π, and leads to the appearance of an oscillating

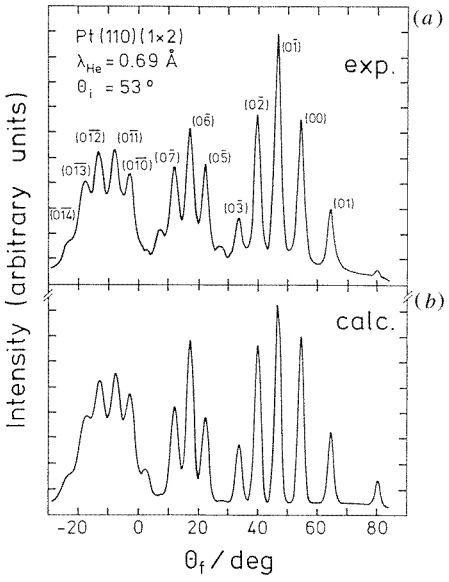

Figure 3. (*a*) The surface rainbow as seen in a He-diffraction spectrum. The envelope modulating the beams $(0\bar{1}0)$ to $(0\bar{1}4)$ represents the analogon of the classical rainbow. The oscillating structure made of alternating weak and intense diffraction peaks between the (00) and the rainbow pattern corresponds to the supernumerary rainbow, as described by Garibaldi *et al* (1975). The results of close-coupling calculations with a realistic potential are shown in (*b*). From Kirsten *et al* (1990).

pattern where intense and weak diffraction peaks alternate exactly. The appearance of both (principal and supernumerary) quantum surface rainbows in a He-scattering experiment is illustrated in figure 3 for the case of the missing-row reconstructed Pt(110)–(1×2) surface.

The diffraction envelope corresponds to the classical cross section for specular scattering from a hard wall whose shape is described by the corrugation function $\zeta(x)$. It is straighforward to show that the rainbow maximum arises from the point of inflection $\mathrm{d}^2\zeta(x)/\mathrm{d}x^2 = 0$ and that a maximum occurs at a scattering angle corresponding to the slope $\mathrm{d}\zeta(x)/\mathrm{d}x \equiv \zeta_x'(x)$ at the inflection point (Greene and Mason 1978). Thus, the angular displacement of the rainbow maximum from specular is $\Delta\theta_{rb} = \theta_{rb} - \theta_i = -2\arctan\zeta_x'(x)$. For a one-dimensional corrugation of period a and maximum amplitude ζ_m the simple relation

$$\zeta_m = \frac{a}{\pi}\tan\left(\frac{\Delta\theta_{rb}}{2}\right) \tag{2.23}$$

is obtained. For the example illustrated in figure 3, the angular distance from the envelope maxima to the specular beam can be estimated in $\Delta\theta_{rb} \sim 65^\circ$. By means of (2.23), the maximum corrugation can be estimated in $\sim$1.6 Å, which is very close to the value $\zeta_m = 1.5$ Å derived from a close-coupling fit to the data (Kirsten and Rieder 1989, Kirsten *et al* 1990).

As already mentioned, McClure (1970, 1972a, b) performed extensive calculations of classical scattering using realistic soft potentials. A more simplified classical analysis was carried out by Klein and Cole (1979a, b), who modelled the particle–surface interaction by a hard-wall potential with an attractive square well. This simple analysis showed that refractive scattering in the attractive well should cause a decrease in the separation between the rainbow maxima with increasing incident energy, as observed for the systems Ne/(1×2)–Au(110) (Engel and Weare 1985) and Ar/2H–W(100) (Schweizer and Rettner 1989).

A simple but quantitative semiclassical analysis of helium diffraction data based on the locations of supernumerary rainbows has been developed by Avrin and Merrill (1994) and also by Guantes *et al* (1995, 1996). The latter authors have recently predicted a new classical singularity which is closely related to rainbow scattering, the so-called skipping

singularity (Miret-Artés *et al* 1996b). This singularity should manifest as a rainbow peak with a final angle of $\pi/2$ (i.e. particles travelling parallel to the surface) but for impact parameters which in general differ from those corresponding to the classical rainbow. If observed experimentally, the skipping singularity would therefore provide direct evidence for the onset of classical chaos in elastic atom–surface scattering (see also Borondo *et al* 1994).

Rainbow structures are characteristic of highly corrugated systems, like stepped metal surfaces and reconstructed semiconductor surfaces, whereas the existence of intense specular scattering indicates a smooth corrugation, typically observed from low index metallic surfaces. This suggests that the transition from a semiconducting to a metallic surface should be easily detected with helium diffraction. A good example of this is provided by the growth of K on Si(100) at 150 K. Experiments performed by Foulias *et al* (1995) showed that, while the ratio of specular to first-order diffraction peak intensity is comparable to that of clean Si(100) up to 0.5 ML, the intensity ratio changes by more than one order of magnitude above 1 ML, indicating that the magnitude of the surface corrugation resembles very much that of a low-index metallic surface. Since HAS is sensitive to just the outermost electron density of the surface, the process of surface metallization must be localized in the K overlayer and not in the substrate (Foulias *et al* 1995). A similar behaviour was also observed for the order–order transition near 1050 K on Ge(111) (Lange *et al* 1995).

In closing this section, we mention that calculations by Gerber and co-workers predict the appearance of rainbow effects in the scattering from single adsorbates and substitutionally disordered mixed monolayers, as discussed in more detail in section 3.5.

2.5. The giant cross section for diffuse scattering

So far, we have introduced the mathematical background which allows structural analyses of ordered surfaces by means of He diffraction. The aim of this section is to present briefly the physical reasons which make thermal energy atom scattering (TEAS) a powerful tool to investigate disordered surfaces, as well as the related formalism in its simplest form. The method consists basically of monitoring the specular reflected He intensity I from a surface as it is exposed to adsorbate species. The nature of the interaction between adatoms as well as their lateral distribution on the surface is then easily obtained from an analysis of this adsorption curve. As it will become apparent, a minimum of theoretical complication is enough to describe quantitatively most of the results presented in section 4. For a detailed description of this subject, the reader is referred to the book by Poelsema and Comsa (1989).

The high sensitivity of TEAS to study disordered surfaces arises from the large cross section for He diffuse scattering of individual adatoms and defects. This makes TEAS an ideal method to detect very low coverages down to $\sim$0.001 ML. An example is illustrated in figure 4 for the CO/Pt(111) system (Poelsema *et al* 1982a). Note the dramatic attenuation of the relative He specular intensity I/I_0 as a function of CO exposure, even at very low coverages (I_0 is the specular intensity at zero coverage). The coverage scale has been calibrated in an independent experiment. Although this unusual sensitivity of He scattering has been known for many years, it was only after the cross section was studied systematically by Poelsema *et al* (1982a, 1983a) that TEAS became a reliable tool to investigate disorder at surfaces. In view of the specular beam profile, experiments performed by Poelsema *et al* (1982b) have shown that it is not affected by the presence of adsorbates, i.e. the peak heights can be taken as a measure of the peak intensity. The starting point to rationalize the physics behind an adsorption curve consists of defining a total cross section for diffuse

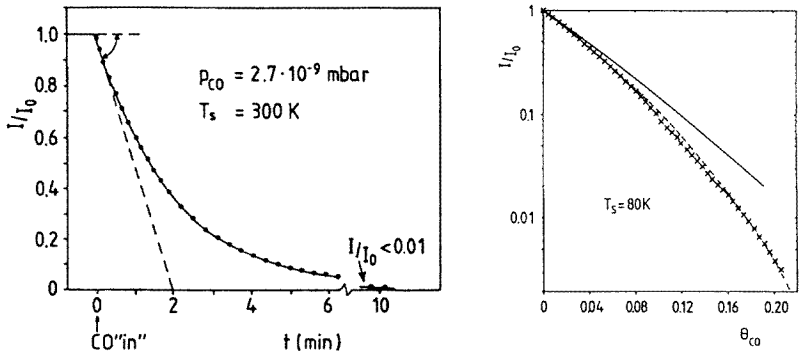

Figure 4. Left: relative He specular intensity as a function of CO exposure on Pt(111) ('adsorption curve'). Right: fit of experimental data assuming a lattice gas distribution (equation (2.26), full line) and a lattice gas with exclusion of occupation of nearest-neighbour sites with $m = 3$ (equation (2.27), broken line). After Poelsema and Comsa (1989).

scattering Σ by

$$1 - I/I_0 = n\Sigma = n_s\Theta\Sigma \tag{2.24}$$

where $\Theta = n/n_s$ and n, n_s denote the number of adsorbate and substrate atoms per unit area, respectively. Equation (2.24), valid for isolated adsorbates at very low coverages, states that the specular scattered intensity I arises exclusively from the substrate areas not covered by adsorbates, each of which scatters diffusively over an area Σ. Note that this definition is restricted to cases where specular scattering is the only coherent scattering observed. Xu *et al* (1988) and Armand *et al* (1996) have extended (2.24) to the case of periodic corrugated surfaces by including all diffraction beams. A more general expression for Σ is given by (Poelsema *et al* 1982a, 1983a)

$$\Sigma = -\frac{1}{n_s} \cdot \frac{\mathrm{d}(I/I_0)}{\mathrm{d}\Theta}\bigg|_{\Theta=0}. \tag{2.25}$$

This means that the value of Σ for a certain species is determined by the initial slope of the adsorption curve. Hamburger and Gerber (1995) have demonstrated that the operational definition given by (2.25) is in fact identical to the standard formal definition of quantum scattering theory. Note that (2.25) requires knowledge of the initial sticking probability s_0, since the dependence of I/I_0 on coverage is needed. In the case of CO/Pt(111), using the known value $s_0 = 0.84$ at 300 K one obtains $\Sigma_{CO} = 123$ Å^2, corresponding to a 63 meV He beam incident at $\theta_i = 40°$. Other values of cross sections are listed in table 1.

The large value obtained for Σ_{CO} is very similar to the CO gas phase cross section ($\sigma_{CO} = 85$ Å^2), suggesting that the same kind of forces (i.e. attractive dispersion forces) are responsible for the diffuse scattering of adsorbed CO. The conclusive proof has been obtained by measuring the dependence of Σ_{CO} on the incident particle velocity for He and H_2 beams (Poelsema *et al* 1982a, 1983a). These curves exhibit the same 'glory scattering' known from the gas phase scattering (Butz *et al* 1971), demonstrating in consequence that the origin of the large cross section of adsorbed CO must be ascribed to a deformation of the attractive part of the He–surface potential. This effect is illustrated schematically in figure 5(*a*). The repulsive contour at 63 meV is shown by the full curve, whereas the cross sections of adsorbed CO (Σ_{CO}) and gas phase CO (σ_{CO}) are represented by broken and dotted semicircles, respectively. Most particles traversing the broken large semicircle will be deflected off the specular direction (left-hand side of figure 5(*a*)), leading consequently

Table 1. Some cross section (Σ) values determined by TEAS. E_i is the beam energy and θ_i the angle of incidence.

Adsorbate	Surface	Σ (Å^2)	E_i (meV)	θ_i (deg)	Reference
H	Fe(110)	3.5	63	45	Kurz and Hudson (1988)
D	Fe(110)	3.4	63	45	Kurz and Hudson (1988)
O	Ni(110)	32	35	35	Wilsch and Rieder (1983)
CO	Ni(110)	93	35	35	Wilsch and Rieder (1983)
CO	Pt(111)	123	63	40	Poelsema *et al* (1983b)
NO	Pt(111)	100	63	40	Croci *et al* (1994)
Xe	Pt(111)	120	63	40	Poelsema *et al* (1983c)
CO	Rh(111)	120	63	45	Peterlinz *et al* (1991)
O	Rh(111)	62	63	45	Peterlinz and Sibener (1995)
CO	Ni(100)	170	63	45	Berndt *et al* (1990)
C_2H_4	Cu(100)	114	18	45	Graham *et al* (1996a)
Na	Cu(100)	120	12	48	Graham and Toennies (1997)
NaCl	NaCl(100)	80	30	45	Duan *et al* (1992a)
KBr	NaCl(100)	200	27	45	Duan *et al* (1992b)
KBr	RbCl(100)	60	30	45	Safron *et al* (1993)
Ag	Pd(100)	109	16	64	Vandoni *et al* (1994a)

to the steep intensity drop observed experimentally (figure 4). The refractive effects are less important for a dense ordered overlayer, since the overlap of the adsorbate cross sections leads to the appearance of a quasihard-wall potential and therefore to diffraction effects (figure 5(*b*)). According to this sketch, Σ should strongly depend on the angle of incidence θ_i and the beam energy E_i. Experiments performed by Poelsema *et al* (1983b) have shown that, in first approximation, Σ follows a $\cos\theta_i^{-1}$ behaviour, which can be explained by simple geometrical ('shadowing') effects (Poelsema and Comsa 1989, p 20). The way in which the van der Waals forces determine the large cross section for diffuse scattering has been treated theoretically by Gumhalter and Lovric (1986), Jónsson *et al* (1984a, b) and more recently by Levi and Passerone (1994) using a perturbation theory approach. An interesting result of the multiple scattering calculations performed by Jónsson *et al* (1984a, b) is that the specular intensity decreases exponentially with coverage for random adsorbates, whereas a linear dependence is obtained for islands. In general, Σ decreases with increasing beam energy, so that care must be taken when comparing Σ values measured at different scattering conditions. The dependence of Σ on energy has been calculated for cylindrically symmetric convex and concave shape functions by Hamburger and Gerber (1995) using the sudden approximation. These authors have also developed an inversion procedure for determining the shape function of an adsorbate from specular intensity measurements, which has been applied to fit experimental data for Ag on Pt(111) (Hamburger *et al* 1996). Calculations performed by Yinnon *et al* (1988a) have shown that $\Sigma(E_i, \theta_i)$ is quite sensitive to the adsorbate orientation with respect to the surface. In particular, the calculations suggest significant differences for the adsorption of O_2 molecules parallel and perpendicular to Pt(111) (Petrella *et al* 1989). These results indicate that important geometrical information can be extracted from the single defect cross section $\Sigma(E_i, \theta_i)$, as discussed in more detail by Gerber *et al* (1992) and Hamburger and Gerber (1995). Another important application of the energy dependence of the scattering cross section appears to be the measurement of the fractal dimension of disordered submonolayers, using the method developed by Hamburger *et al* (1996) (see also Hamburger and Lidar 1996).

The high sensitivity of TEAS to the presence of adsorbates suggests an obvious

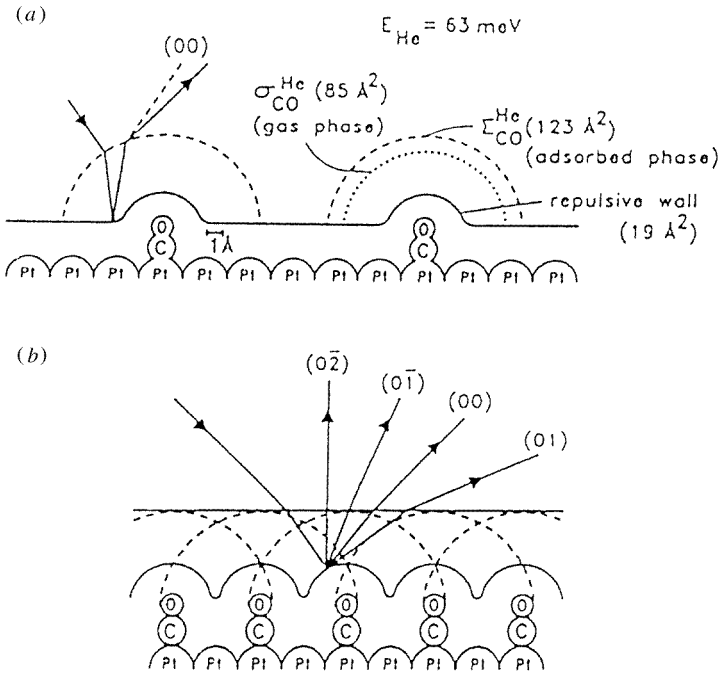

Figure 5. (*a*) Schematic drawing of isolated (low-coverage) CO molecules on Pt(111). The full curve represents the hard-wall potential corresponding to a room-temperature He beam. The broken and dotted semicircles correspond to the the cross sections of adsorbed CO (Σ_{CO}) and gas phase CO (σ_{CO}), respectively. (*b*) The overlap of the adsorbate cross sections in a dense ordered phase gives rise to a quasihard-wall potential, i.e. to the appearance of diffraction effects. Adapted from Poelsema *et al* (1983b).

application: its use as a probe of surface coverage. In fact, it has been shown that a continuous and reproducible determination of surface coverage down to ∼0.001 ML can be achieved with TEAS. A complete description of this method as well as of some related applications (measurements of isotherms, isobars, relative changes of sticking probability) is given in the book by Poelsema and Comsa (1989).

Before closing this section, a warning concerning the experimental determination of adsorbate cross sections is in order. Experiments performed by Verheij *et al* (1985) have shown that the scattering cross section of a step row can be viewed as an additional ∼10 Å broad band along the step row. Therefore, if adsorbates can migrate to defect sites, their cross sections will overlap with those of the steps leading to a Σ value much smaller than the correct one (Poelsema and Comsa 1989, p 40). This extreme sensitivity of helium scattering to the presence of defects on the surface makes TEAS a unique method to study diffusion on surfaces, as discussed in more detail in section 4.1.

2.5.1. The overlap approach. An immediate nontrivial consequence of the large size of Σ is that, even at low coverages, the overlap of the cross sections of the individual adatoms is not negligible. This is in fact the physical origin of the departure of the adsorption curve in figure 4 from linearity, i.e. the effective cross section decreases with increasing overlap. The degree of overlap depends not only on the coverage but also on the actual

lateral distribution of the adsorbates. Therefore, the shape of the adsorption curve I/I_0 versus coverage contains crucial information on the lateral distribution of adsorbates. A very simple procedure for extracting this information has been developed by Poelsema and Comsa (1989) and is called 'the overlap approach', since it is based on the assumption that the cross sections overlap is simply geometrical. For perfectly diffuse scatterers randomly distributed on the surface, it can be shown that the relative specular He intensity is given by

$$\frac{I}{I_0} = (1-\Theta)^{\Sigma n_s}. \tag{2.26}$$

This is the so-called 'lattice gas formula'. In cases where the occupation of nearest-neighbour sites is forbidden, the corresponding lattice gas expression reads

$$\frac{I}{I_0} = (1-m\Theta)^{\Sigma n_s/m} \tag{2.27}$$

where $\Theta_m = 1/m$ is the maximum possible coverage for the system. Although it may appear that the 'lattice gas' conditions are too restrictive to be useful in practice, the experimental data are described remarkably well for a large number of systems (e.g. CO, NO, Xe, Kr on Pt(111), Ni(111), O/Rh(111)). Applications of the overlap approach to other important cases (in particular, to adsorbates with non-negligible reflectivity like hydrogen or vacancies) can be found in the book by Poelsema and Comsa (1989, pp 26–33). The validity of the overlap approach has been demonstrated theoretically by Yinnon *et al* (1988a) in the case of small vacancies clusters, and by Petrella (1990) in the case of an ordered array of CO clusters on Pt(111). However, the overlap approach was found to break down when applied to single adatom or vacancies pairs on a flat surface (Petrella 1992, Petrella and Cassidei 1993). Using the sudden approximation, these authors found that in certain cases the cross section for scattering by two defects could be *greater* than the sum of the individual cross sections (i.e. 'negative overlap' occurs). In terms of He–target interaction, the overlap approach breaks down because it takes into account the interaction of He with just one defect in the overlap region, neglecting the simultaneous interaction with the second one (Petrella and Cassidei 1995). These interesting results are expected to stimulate calculations beyond the overlap approximation in order to allow more detailed analyses of defects on surfaces by means of TEAS.

Deviations of a measured $I(\Theta)/I_0$ curve from (2.26) yield directly the nature of the adsorbate–adsorbate interaction: attenuation curves lying below (above) the lattice-gas curve are indicative for repulsive (attractive) interactions. This point is illustrated for the case of CO on Pt(111) in figure 4 (Poelsema and Comsa 1989). The experimental data points (crosses) lie well below the lattice gas curve (2.26) (full line), showing that the average overlap of the cross sections is less effective than for a noninteracting gas. This implies that the CO–CO interaction must be repulsive. One can learn more about the lateral distribution of CO adatoms by fitting the experimental data with (2.27), i.e. excluding occupation of nearest-neighbouring sites. In the case of a fcc(111) lattice, these conditions restrict the maximum coverage to $\Theta_m = \frac{1}{3}$. The curve calculated with $m = 3$ (broken curve in figure 4) reproduces very well the experimental data, despite the simplicity of the model. A good example of attractive interactions between mobile adsorbates is given by the Xe/Pt(111) system (Poelsema *et al* 1983c, 1985).

Finally, it is important to mention that TEAS applications are not restricted to smooth surfaces like the fcc(111) or bcc(110). This has been clearly demonstrated by the TEAS studies of H and CO adsorption on Fe(111) performed in the group of Bernasek (Bernasek *et al* 1992, Jiang *et al* 1993a, b). These results showed that, although the data interpretation

is a bit more complicated, the cross sections of H and CO are still large enough so that TEAS can be successfully applied on rough surfaces, as also demonstrated by the study on K/Cu(115) reported by Armand *et al* (1996).

2.5.2. Determination of step density. In a real surface, the specular intensity is dominated by interference between waves scattered from different terraces. In the specular direction, the phase shift $\Delta\Phi$ between two adjacent terraces is given by

$$\Delta\Phi = \frac{4\pi d}{\lambda}\cos\theta_i = 2\pi n \tag{2.28}$$

where λ is the He wavelength, d is the interlayer spacing, and n has integer values for constructive interference or in-phase condition (intensity maxima) and half-integer values for destructive interference or antiphase condition (intensity minima). The first observation of this effect has been reported by Lapujoulade and Lejay (1977) for a chemically etched Cu(100) surface (figure 6). The intensity oscillations as a function of angle of incidence are clearly seen. The position of the extrema corresponds to $d = 1.8$ Å in agreement with the interlayer spacing between (100) planes in bulk Cu, indicating that the steps are of monatomic height. The amplitude of the oscillations is related to the surface step density θ_d, so that it can be estimated by assuming statistical models for the step distribution. The case of scattering from a randomly stepped surface has been solved by Lapujoulade (1981) within a hard-wall model approach. This model not only reproduced well the intensity oscillations observed experimentally, but also predicted a broadening of the diffraction peaks which should be maximum for destructive interference and almost zero when the in-phase condition is applied. This complementary behaviour of beam profile and intensity has been observed by Poelsema *et al* (1982b). The fit obtained with the randomly stepped model and $\theta_d = 0.01$ is illustrated by the full curve in figure 6(a). This is a simple way to determine the step atom density, i.e. the mean terrace width with TEAS. The sensitivity of this method is limited by the transfer width of the instrument w; the absence of oscillations in the rocking curves implies that the average terrace width is larger than $10w$ (Poelsema and Comsa 1989). For adsorption of gases on surfaces, (2.28) can also be used to determine the effective islands height, as done for CO deposited at low coverage ($\Theta \sim 0.2$) on Cu(100) by Ellis *et al* (1995).

A more exact determination of θ_d and even an estimation of the terrace width distribution can only be obtained from a detailed analysis of the peak shapes upon antiphase conditions. This has been done by Verheij *et al* (1985) for a randomly stepped Pt(111) surface, which was prepared by high-temperature ion bombardment. The density of steps θ_d on this surface has been determined using a 'facet ensemble' analysis (Verheij *et al* 1984) of the specular peak shape measured under antiphase conditions. An interesting result obtained with this method is that any model surface which reproduces correctly the antiphase peak shapes has, in very good approximation, the same step density as the real surface. This has been demonstrated by comparing simulations based on the random step models of Lapujoulade (1981), Lu and Lagally (1982) and Henzler (1978). Once θ_d is known, it can be used to determine the cross section for diffuse scattering from steps. Assuming that it has the shape of a strip of width D along the step edge contour, the intensity scattered from a rough surface upon in-phase conditions can be written as (Verheij *et al* 1985)

$$\frac{I}{I_0} = (1 - DS)^2 \tag{2.29}$$

where S is the length of the step edge per unit area and I_0 is the specular intensity for $S \sim 0$. From a comparison of the intensities measured before and after sputtering on the

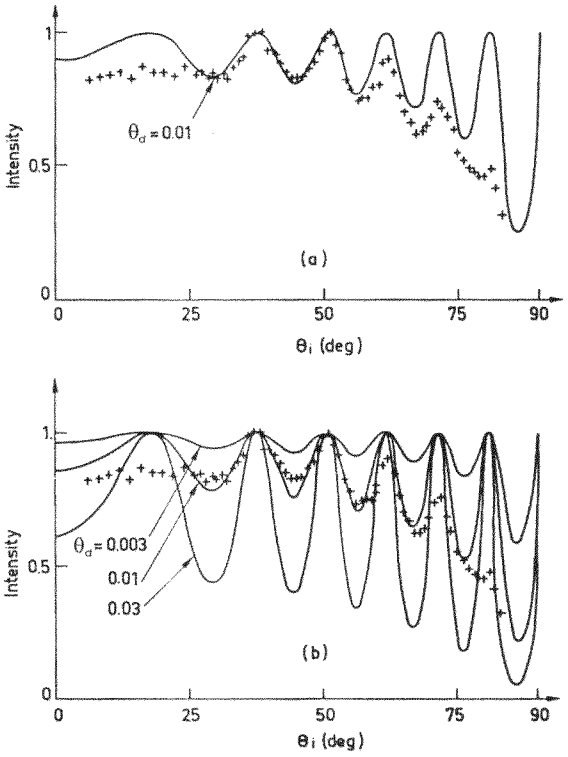

Figure 6. Intensity of the specular peak (corrected for Debye–Waller effects) versus angle of incidence for an etched Cu(100) surface. The He beam energy is 63 meV. Crosses denote experimental data (Lapujoulade and Lejay 1977). The full curves are fits modelling the distribution of terrace widths with (*a*) an isotropic model and (*b*) a rectangular decoupled model. In (*b*), curves corresponding to different step densities θ_d are shown. From Lapujoulade (1981).

same surface, a value $D = 12 \pm 2$ Å was obtained on Pt(111) (Verheij *et al* 1985). A similar value ($D = 13$ Å) has been reported for steps on Cu(100) by Sánchez and Ferrer (1987) and for Pd clusters deposited on MgO(100) (Henry *et al* 1993), so that $D \sim 10$ Å can be considered a typical value associated with diffuse scattering from steps. The method described above can be more generally applied to prepare *in situ* surfaces with a given step density in the range $0.001 < \theta_d < 0.15$ (Poelsema and Comsa 1989, pp 62–71).

Equation (2.29) can be also used to determine the island density at a given coverage Θ. In the case of two-dimensional compact islands, $S \sim \beta\sqrt{\Theta n}$, where β is a shape factor and n is the island density (Rosenfeld *et al* 1995, see also Xu *et al* 1991). Thus, the quantity $(1-\sqrt{I/I_0})^2$ is proportional to n, whose *absolute* value could be obtained if D were known. This is not necessary, however, to estimate *relative* values of n at different temperatures, which are simply obtained by comparing the corresponding in-phase intensities (Rosenfeld *et al* 1995).

2.5.3. Rocking curves from small islands. An interesting effect is observed when recording rocking curves from small two-dimensional islands: the curves are shifted as compared with those recorded for large islands. Two different explanations of the same phenomenon have been recently given by two groups, so that further work is required in order to understand

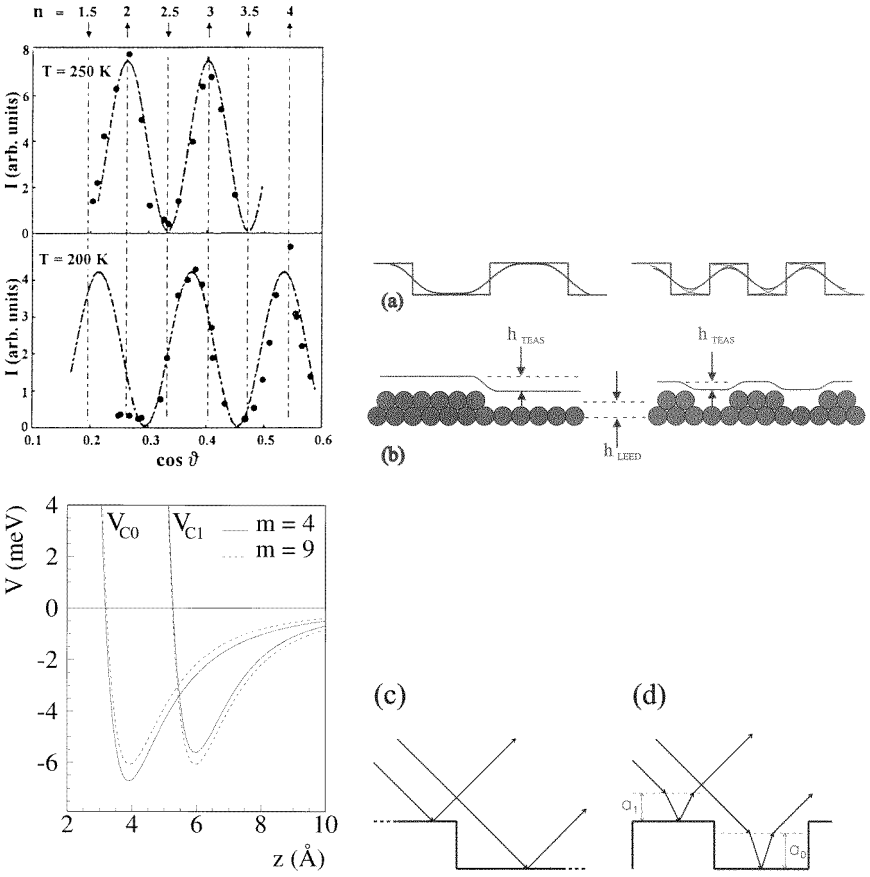

Figure 7. Top: Specular rocking curves recorded at 90 K after deposition of 0.5 ML Ag on Ag(100) at the indicated surface temperatures. The in-phase and antiphase scattering conditions corresponding to the bulk interlayer spacing are indicated by the up and down arrows, respectively. The explanations of this effect proposed by Bedrossian *et al* (1995) (*a*)–(*b*) and Terreni *et al* (1997) (*c*)–(*d*) are schematically illustrated (see text for details).

its physical origin. The first attempt to explain this effect has been reported by Bedrossian *et al* (1995) in a combined TEAS and SPA-LEED study of Ag islands grown on Ag(100). Figure 7 shows the rocking curves measured after deposition of 0.5 ML Ag at 250 and 200 K, where nucleation results in large (∼65 Å) and small (∼25 Å) island separations, respectively. The maxima and minima observed at 250 K agree well with the expected values calculated with (2.28) using the Ag bulk interlayer spacing ($d = 2.04$ Å), whereas an apparent reduction in the step height of 0.6 Å respect to the bulk value is deduced from the extrema recorded at 200 K. Since this contraction was not observed with SPA-LEED, it was concluded that it is caused by a smoothening of the electronic density profile probed by the He atoms (Smoluchowsky effect). This explanation is schematically illustrated in figure 7(*a*)–(*b*).

A very different explanation has been more recently given by Terreni *et al* (1997), based on a study of Fe islands grown on Ag(100) at 135 and 255 K, at which (similarly to the case of Ag on Ag(100)) small and large islands are formed, respectively. They concluded that the observed shift in the rocking curves is actually caused by refractive effects, due to

the fact that an incoming He atom experiences a different potential well in front of a small island or in front of the uncovered substrate†. This is illustrated for the simple case of a repulsive potential with different square wells in front of the adlayer (width a_0, depth D_0) and in front of the sublayer (width a_1, depth D_1) in figure 7(*c*)–(*d*). This means that (2.28) must be corrected for small islands, i.e. that the in-phase and out-of-phase interference conditions depend not only on the step height, but also on the size of the nucleated islands. Within a simple kinematic approach, it can be shown that the following equation must be used instead of (2.28) (Terreni *et al* 1997)

$$\Delta\Phi_W = \Delta\Phi + a_0(S_{0z} - S_z) - a_1(S_{1z} - S_z) \tag{2.30}$$

where $S_z = 2k\cos\theta_i$, $S_{1z,0z} = 2k(\cos^2\theta_i + D_{1,0}/E)^{1/2}$ and E is the kinetic energy of the incoming atom. The 'additional' phase difference in (2.30) can be rewritten in terms of a single free parameter δ such that: $a_0 = a(1+\delta)$, $D_0 = D(1+\delta)$, $a_1 = a(1-\delta)$ and $D_1 = D(1-\delta)$. A good fit to the experimental data is obtained assuming typical values for D and a, whereby the corresponding step heights are comparable at 135 K (1.76 Å) and 255 K (1.80 Å). This method was also applied to the rocking curves reported by Bedrossian *et al* (1995) for Ag on Ag(100), leading to step heights of 2.0 Å at 250 K and 1.90 Å at 200 K. Further support to this interpretation was obtained from calculations of He–surface potentials for the case of Ag square islands of $m \times m$ atoms grown on Ag at a coverage of 0.5 ML. The potential curves calculated at the centre of the islands (V_{C1}) and at the centre of the uncovered substrate (V_{C0}) for $m = 4$ and $m = 9$ are shown in figure 7. For $m = 4$, the well of V_{C0} is deeper and wider than the one of V_{C1}, confirming the conclusions discussed above on the basis of a kinematic approach.

3. Helium diffraction results

3.1. Experimental

An excellent description of the experimental demands for diffractive scattering from surfaces can be found in the two books edited by Scoles (1988, 1992). Apparatus used for HAS experiments can be classified according to their scattering geometries in two different groups: (a) 'fixed angle' systems, in which the angle between incident and outgoing beams is fixed and (b) systems which allow us to rotate the detector about two axes independently of the incident conditions. With the latter, all diffraction intensities can be recorded for a given scattering geometry, allowing an easier comparison with calculations and making this set-up the most favourable for structural studies. The major disadvantadge of this configuration is that it hardly allows for differential pumping of the detector, resulting in general in a smaller dynamical range of measured intensities as compared with the differentially pumped 'fixed angle' systems used in TOF experiments.

3.1.1. Coherence length and transfer width. The diffraction patterns obtained in an atom diffraction experiment result ultimately from the incoherent superposition of individual diffraction events, each produced by the interference of an incoming particle with itself. As the detectors are not sufficiently sensitive to detect single events, the experimental intensities are enhanced by the (incoherent) superposition of many individual diffraction events in a given time interval (Comsa 1979). The question which arises in interpreting such diffraction data is to what extent does the instrument itself and the surface perfection

† A similar explanation had been suggested in a previous TEAS study of Cu/W(110) by Xu *et al* (1991).

limit the widths of the diffracted wavepackets and consequently, the angular widths of the peaks $\Delta\theta_f$, which are in fact measured.

The concept of transfer width has been introduced by Park *et al* (1971) in connection with the problem of instrumental limitations in LEED experiments. It represents the minimum lateral dimension over which the surface must be perfect to give diffraction spots whose widths are limited only by the instrumental resolution. Comsa (1979) has derived an explicit formula for the transfer width in atom diffraction experiments which, as in the LEED case, depends on the energy spread in the incoming beam and the geometrical parameters of source and detector. The transfer width w is given by

$$w = \frac{\lambda}{\sqrt{(\Delta_\theta\theta_f)^2\cos^2\theta_f + (\sin\theta_i - \sin\theta_f)^2\overline{(\Delta E)^2}/E^2}} \tag{3.1}$$

where λ is the beam wavelength, θ_i and θ_f are the incident and exit angles as measured from the surface normal, Δ_θ represents the angular spread determined by source and detector, and $\overline{(\Delta E)^2}$ is the mean-square energy spread in the beam. Note that for $\theta_i = \theta_f$ the energy dependence disappears, indicating that the energy spread has no influence on the broadness of the specular beam. Large transfer widths can be obtained by minimizing the angular divergence in the beam and the beam diameter at the surface, as well as by using a small detector aperture and a large surface-to-detector distance. However, all of these steps will lead to a signal reduction at the detector; therefore, a compromise between transfer width and signal intensity must be taken.

3.2. Quantitative structural determinations from intensity analyses

In contrast to other techniques, HAS experiments often provide a number of conclusions about the structure of a surface without extensive diffraction calculations. For example, the maximum corrugation amplitude can be derived with relatively good accuracy directly from the position of the rainbow pattern in the experimental data (section 2.4). Therefore, the existence of missing-row reconstructions of the substrate or even minor changes in the corrugation amplitude with respect to the clean surface can be practically 'read off' from the spectra, as demonstrated by the examples presented in this section. The emphasis will be put on systems where HAS presents clear advantages in comparison with other techniques, such as adsorption of weakly bonded adsorbates. A complete update of all adsorbate structures detected with HAS is listed in table 2 (on metal surfaces) and table 3 (on isolator and semiconductor surfaces).

3.2.1. Clean metal surfaces. A comparison of corrugation amplitudes obtained with He, Ne and D_2 beams on clean metal surfaces is presented in table 5. Surface structural studies of clean metal surfaces with He and Ne have been reviewed by Rieder (1992, 1994) so we will not discuss them further here. Since then, several structural analyses on 'open' metal surfaces have been carried out. They include studies on Ni(511) (Kaufman *et al* 1987), the (1×2)–Rh(110) (Bellman *et al* 1993b), (1×2)–Au(110) (Cortona *et al* 1993) and (1×2)–Pt(110) (Cvetko *et al* 1995d) surfaces, Rh(311) (Apel *et al* 1996), the (1×2) missing-row reconstruction of Pd(311) (Farías *et al* 1997a) as well as on the Cu(211) and Cu(511) surfaces (Miret-Artés *et al* 1996a). A comparison of diffraction intensities calculated with both HCW and corrugated Morse potentials was performed for the Ni(511), Cu(211) and Cu(511) surfaces. These studies showed that corrugation amplitudes determined for HCW and soft potential have essentially the same shapes but differ in their maximum

Table 2. Structures detected with HAS for adsorption on metal surfaces. Incommensurate adlayers are denoted by 'inc.'.

Adsorbate	Surface	Structure	Coverage (ML)	Temperature (K)	Reference
H	Pt(111)	(1×1)	1	90–160	Lee *et al* (1983), Batra (1984)
	Ni(111)	(2×2)	0.5	100	Gross and Rieder (1991)
	Pt(100)	(1×1)	1	25	Romainczyk *et al* (1995)
	Ni(100)	(1×1)	1	100	Rieder and Wilsch (1983)
	Cu(100)	$p(2 \times 1)$,	0.5	170	Graham *et al* (1995, 1998)
		$(2\sqrt{2} \times 2\sqrt{2})R45^\circ$	1.25		
	Ni(110)	$c(2 \times 6)$, $c(2 \times 4)$	0.33, 0.50	100	Rieder (1983b)
		$c(2 \times 6)$, $c(2 \times 6)$	0.67, 0.83		Rieder and Stocker (1985c)
		(2×2), (1×2)	1, 1.5		
		(1×2) 'streaky'	1–1.5	100	Farías *et al* 1993
	Cu(110)	(1×4), (1×3)	0.25, 0.33	<80 K	Goerge *et al* (1993)
		(1×2), (1×1)	0.5, 1		
		(1×2)MR	0.5	>140	
	Rh(110)	(1×2)H	0.5	110	Parschau *et al* (1990)
		(1×3)H, (1×1)2H	0.33, 2	110	Parschau *et al* (1991)
	Ag(110)	$c(4 \times 4)$		100	Cantini *et al* (1989)
	Ni(311)	(1×1)	1	110	Rieder and Stocker (1986)
	Pd(311)	(2×1)H, (2×1)2H	0.25, 0.50	110	Farías *et al* (1996, 1997a)
		(2×1)3H, $c(1 \times 1)$H	0.75, 1		
	Rh(311)	(1×1), (1×3)H	1, 1.33	110	Apel *et al* (1995a, b)
		(1×2)H, $(1 \times 2)_{rec}$	1.5, 2		Farías *et al* (1997d)
	Ni(511)	(1×1)	1	100	Kaufman *et al* (1986)
O	Ni(100)	$p(2 \times 2)$, $c(2 \times 2)$	0.2, 0.50	110	Rieder (1983a)
					Barker and Batra (1983)
	Pd(100)	$p(2 \times 2)$	0.25	110	Rieder and Stocker (1985a)
	W(100)[a]	(2×1)	~0.3	300	Hinch *et al* (1987)
	Ni(111)	(2×2)	0.25	100	Gross and Rieder (1991)
	Rh(111)	(2×2), (1×1)	0.25, 1	40–250 K	Brault *et al* (1997)
	Ni(110)	(3×1), (2×1)	0.3–0.5	100	Engel *et al* (1984)
	Cu(110)	(2×1)	0.5	300	Lapujoulade *et al* (1980b, 1982),
					Kern *et al* (1991)
	Rh(311)	(2×1), (1×3)	0.5–1	110	Farías *et al* (1995)
	Pd(311)	(2×4)pg	0.5–1	110	Farías *et al* (1997b)
CO	Ni(110)	(2×1)	1	100	Parschau and Rieder (1991)
	Ru(0001)	$(\sqrt{3} \times \sqrt{3})R30^\circ$	$\frac{1}{3}$	100	Braun *et al* (1997)
		$(2\sqrt{3} \times 2\sqrt{3})R30^\circ$	$>\frac{1}{3}$	100	
		$(5\sqrt{3} \times 5\sqrt{3})R30^\circ$	$>\frac{1}{3}$	100	
silane	Cu(100)	(5×3)inc.	Cu_2Si	420	Graham *et al* (1992, 1994)
	Cu(111)	(3×3)	0.33	<165	Curson *et al* (1997)
Na	Cu(100)	$c(4\sqrt{2} \times 2\sqrt{2})R45^\circ$	0.125	50	Graham and Toennies (1997)
		$\begin{pmatrix} 3 & 0 \\ -2 & 2 \end{pmatrix}$	0.167		
		$p(4 \times 2)$	0.25		
		$(\sqrt{10} \times \sqrt{10})R18.4^\circ$	0.30		
		(4×1), $c(2 \times 2)$	0.37, 0.50		
H_2O	Pt(111)	$(\sqrt{37} \times \sqrt{37})R25.3^\circ$	<1	130	Glebov *et al* (1997a)
		$(\sqrt{39} \times \sqrt{39})R16.1^\circ$	2	130	
		(1×1)	~40	30	Braun *et al* (1998)
	$O(n \times 1)$/	$OH(1 \times 1), n = 2$	1	120	Canepa *et al* (1993a, b)
	/Ag(110)	$OH(1 \times m), n > 2$	$0 < \Theta < 1$	120	Canepa *et al* (1995a, b, 1997a)

[a] Stepped surface.

Table 2. (Continued.)

Adsorbate	Surface	Structure	Coverage (ML)	Temperature (K)	Reference
n-octadecanethiol	Au(111)	c(4 × 2)	1	30–100	Camillone *et al* (1993a)
n-alkane thiols	Au(111)	hexagonal	1	50	Camillone *et al* (1991)
docosyl-mercaptan	Au(111)	$(\sqrt{3} \times \sqrt{3})$R30°	1	35	Camillone *et al* (1993b)
	Au(100)	inc.	1	35	
	Au(110)	c(2 × 2)	1	38	
α-hexathiophene	Au(110)	$(T \times 4)$	1	375	Buongiorno Nardelli *et al* (1996a, b)
Cl	Ag(100)	c(2 × 2)	0.5	300	Cardillo *et al* (1983)
C_2H_4	Cu(100)	p(2 × 2)	0.50	50	Graham *et al* (1996a)
CH_4	Cu(100)	hex. inc.	0.432	53	Graham *et al* (1997)
CF_4	Cu(110)	(26 × 18)	<1	40	Diercks *et al* (1996)
		(2 × 18)	>1	40	
N_2	Cu(110)	HOC $\begin{pmatrix} 4 & 1 \\ 1 & 3 \end{pmatrix}$	1	20	Zeppenfeld *et al* (1997), Goerge *et al* (1995)
Xe	Cu(110)	(n × 2), n ⩾ 7	$0 < \Theta < 1$	20–70	Zeppenfeld *et al* (1996), Goerge *et al* (1995)
Ar	Pt(111)	p($n \times n$)HOC series	$0 < \Theta < 1$	25	Zeppenfeld *et al* (1992)
Kr	Pt(111)	(5 × 5)	∼1	25	Kern *et al* (1987)
Xe	Pt(111)	$(\sqrt{3} \times \sqrt{3})$R30°	$<\frac{1}{3}$	>60	Kern *et al* (1986a),
		inc.	$<\frac{1}{3}$	<60	Poelsema *et al* (1985)

amplitudes (typically, an error of 20–25% is made at energies corresponding to a room-temperature He beam). Whereas this error would be tolerable in deciding between two very different structural models, it is certainly significant if the relaxation of the surface atoms or modifications of the electronic structure at step edges are to be determined.

3.2.2. Adsorption on metal surfaces. We will begin our discussion with the HAS investigations of the H/Rh(311) adsorption system reported by Apel *et al* (1995a, b, 1996). This system had been previously investigated by LEED, TDS and work function measurements by Nichtl-Pecher *et al* (1991), who found a succession of (1 × 3)H, (1 × 2)H, (1 × 3)2H and $(1 \times 2)_{\mathrm{REC}}$ superstructures with increasing hydrogen exposure. A coverage of $\frac{1}{3}$ ML was attributed to the (1 × 3)H structure on the basis of TDS measurements, from which the initial sticking coefficient S_0 was concluded to have the very small value of ∼0.25. This unexpectedly low value contrasts with the obvious trend observed in the wealth of experimental data existent on H-metal systems, which indicate that S_0 values very close to unity are expected for 'open' surfaces, like the fcc(110), fcc(311) and bcc(211). Moreover, if the coverages proposed in the LEED study were accepted, serious difficulties arise when considering how the existence of only one adsorption site in the (1 × 3)H and (1 × 2)H phases can lead to the appearance of two and three desorption peaks in the respective thermal desorption spectra reported by Nichtl-Pecher *et al* (1991).

This situation was clarified in a series of HAS studies performed by Apel *et al* (1995a, b, 1996), who observed the formation of a well-ordered (1 × 1)H phase before completion of the (1 × 3)H phase. Figure 8 shows the development of in-plane spectra from Rh(311) with increasing hydrogen exposure at 110 K. The appearance of a (1 × 1)H structure, which requires a coverage of 1 ML, after exposure to ∼0.2 L demonstrates that the initial sticking

Table 3. Structures detected with HAS for different adsorbates on semiconductor and isolator surfaces.

Adsorbate	Surface	Structure	Coverage (ML)	Temperature (K)	Reference
clean	cleaved mica	(1×1)	clean	300	Brusdeylins and Schmicker (1995)
OCS	NaCl(100)	$(2 \times 1)/(2 \times 2)$	1	75	Glebov *et al* (1996)
					Picaud *et al* (1997)
C_2H_2	NaCl(100)	$(\sqrt{2} \times 3\sqrt{2})$R45°	$\frac{2}{3}$	90	Glebov *et al* (1997b)
C_2H_2	NaCl(100)	$(\sqrt{2} \times 7\sqrt{2})$R45°	1	80	
CO	NaCl(100)	(2×1), (1×1)	1	25–53	Schmicker *et al* (1991a)
CO_2	NaCl(100)	(2×1)	0.3	92	Liu *et al* (1992)
		$(2\sqrt{2} \times 2\sqrt{2})$R45°	1	73	
	NaCl(100)	(2×1)pg	1	80	Lange *et al* (1995)
		$c(2 \times 2)$	>1	55	
water	NaCl(100)	(1×1)	1	145	Bruch *et al* (1995)
	CaF_2(111)	$p(4 \times 4)$	0.375	130	Lehmann *et al* (1994)
	BaF_2(111)	(1×1)	?	130	Lehmann *et al* (1996)
bromohexane	KBr(100)	(1×2)	1	140	Hernández *et al* (1996)
water	MgO(100)	$c(4 \times 2)$	?	100	Ferry *et al* (1996)
		(3×2)	?	200	
CO	MgO(100)	$c(4 \times 2)$	1	36	Gerlach *et al* (1995)
		(1×1) latt. gas	<1	51	
CH_4	MgO(100)	$c(2 \times 2)$	1	50	Jung *et al* (1991)
CH_3Br	NaCl(100)	$(\sqrt{2} \times 3\sqrt{2})$R45°	low cov.	35	Robinson *et al* (1992)
		inc.	high cov.	35	
	LiF(100)	inc.	high cov.	35	
	C(0001)	inc.	1	35	Rowntree *et al* (1990)
	Xe/C(0001)	complex	1	35	
CH_3F	C(0001)	$(\sqrt{3} \times \sqrt{3})$R30°	1	35	Ruiz-Suárez *et al* (1988)
	Xe/C(0001)	$(\sqrt{3} \times 2\sqrt{3})$R30°	1	35	Rowntree *et al* (1990)
CH_3Cl	C(0001)	inc.	1	35	
	Xe/C(0001)	complex	1	35	
HCl	C(0001)	inc. hexagonal	1	35	Rowntree *et al* (1990)
Cl	C(0001)	inc. rotated	1	35	Liu *et al* (1989)
H	InSb(100)	(1×1)	1	300	Mason and Williams (1991)
	C(111)	(1×1)	1	<940	Schaich *et al* (1997)
K	Si(100)	$c(2 \times 4)$	1.25	150	Foulias *et al* (1995)
Cu	Si(111)	(5.55×5.55)inc.	1	300	Doak and Nguyen (1989)
Ga-rich	GaAs(100)	$c(8 \times 2)$, (6×6)	clean	350	Verheij *et al* (1995)
+ O ads.		(4×1), (6×6)	?	350	

coefficient is very close to unity, as expected from the arguments outlined above. The large rainbow structure present at ∼45° from the specular position already proves that the (1×1)H structure is much more corrugated than the clean surface. Further hydrogen exposure leads to a continuous decrease of the corrugation, as evidenced by the observed shift of the rainbow angle towards the specular beam.

Best-fit corrugations derived from experimental diffraction intensities for the two first adsorbed phases are shown in figure 9. The intensity analyses were performed with the GR method within the HCW model, which is well justified in view of the small corrugation amplitudes relative to the surface lattice dimensions (see section 2.3.2). The adatom configurations can be inferred directly from the grey-scale representation of the corrugations, in which the H-atoms correspond to the brightest spots. A comparison of the profiles

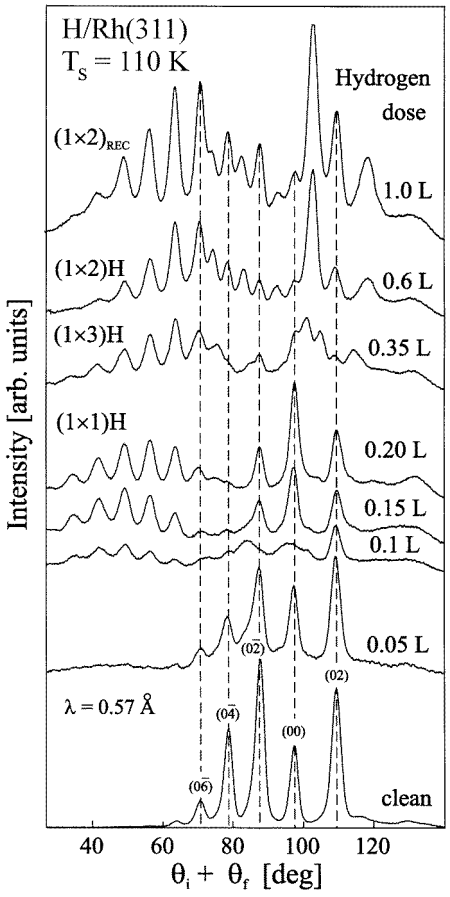

Figure 8. Development of the hydrogen phases on Rh(311) with increasing exposure at 110 K as observed with He diffraction. From Apel *et al* (1995a).

obtained for these phases with the one of the clean surface (not shown here) revealed an increase of the total corrugation amplitude by ∼0.3 Å as well as an appreciable modulation in the corrugation along the (111) facets, which immediately suggested H-chemisorption near to the threefold hollows (Apel *et al* 1995a). This was confirmed by performing surface charge density calculations at a density of 5×10^{-4} au (which corresponds roughly to the thermal beam energies used in the experiment) to reproduce the shape and amplitude of the corrugation experimentally determined as well as by the success in reproducing selective adsorption measurements using close-coupling calculations (Apel *et al* 1996). Also, an attempt was made to determine the H–Rh bond lengths in the (1×1)H phase. In view of the (1×3)H phase, a look at the corrugation profiles shown in figure 9 reveals that the maximum corrugation amplitude is very similar to the one of the (1×1)H phase (∼0.6 Å). This suggests that the (1×3)H unit cell is built up from three (1×1)H cells in addition to a fourth H-atom which is adsorbed in the wells between every third close-packed row, near to the fourfold hollows. Accordingly, the corresponding coverage is $\frac{4}{3}$ ML. The adsorption of a fourth H-atom between the first and second Rh layers causes a diminution of the work function, probably due to depolarization effects. The existence of two different H-species on the (1×3)H phase, strongly suggested by the presence of two binding states in the corresponding TDS data, has been recently demonstrated by HREELS measurements performed by Farías *et al* (1997d). These authors also presented a physical picture of the

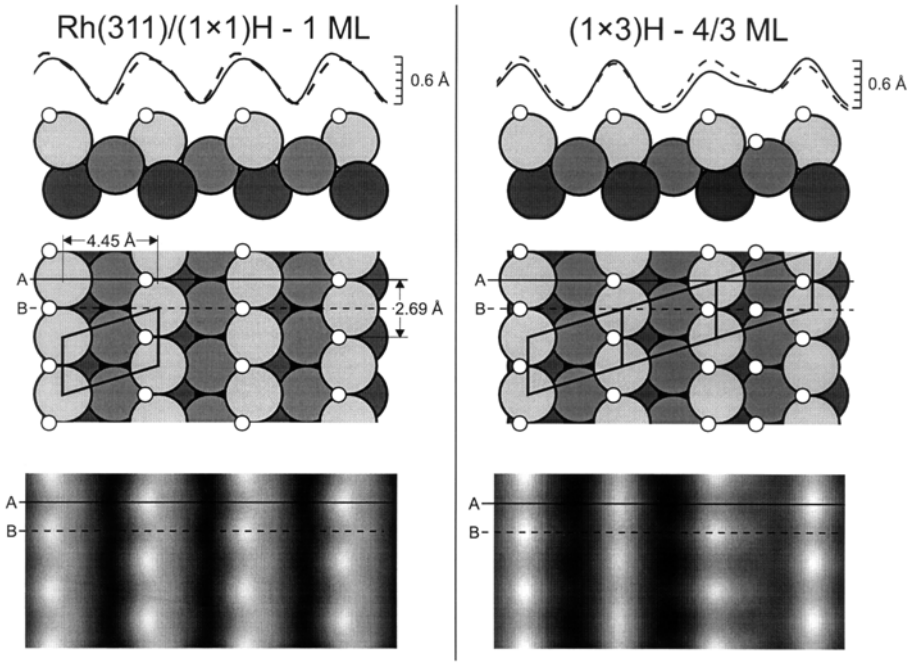

Figure 9. Grey-scale representation of the best-fit corrugation functions obtained for the (1×1)H and (1×3)H phases (bottom). The corresponding sphere models are also shown, as well as cuts along lines A (full line) and B (broken line). From Farías *et al* (1997d).

interaction of hydrogen with Rh(311) consistent with all available experimental data.

The results presented above suggest that detection of a (1×1)H adlayer by LEED is a very demanding task. A similar case is the H/Rh(111) system, on which Witte *et al* (1995) observed a (1×1)H structure with HAS which was not reported in previous LEED studies. Another good example of the high sensitivity of helium atoms to adsorbed hydrogen structures is given by the results reported by Allison and co-workers on H/Cu(100) (Graham *et al* 1995, 1998). The formation of two well-ordered overlayers was observed after exposure to hydrogen at 170 K—a $p(2 \times 1)$ at 0.5 ML and a saturated $(2\sqrt{2} \times 2\sqrt{2})R45^\circ$ structure—both of which were not reported in previous LEED studies. In view of the saturated structure, quantitative data analyses based on the eikonal approximation favoured a *p4g* clock rotation of 12° in the substrate and a hydrogen coverage of 1.25 ML, of which 0.75 ML occupy fourfold hollows and 0.5 ML are pseudobridge bonded (Graham *et al* 1995). Diffraction intensity analysis for the $p(2 \times 1)$ phase was performed within a close-coupling approach, from which adsorption on fourfold-coordinated sites was concluded (Graham *et al* 1998). An interesting feature of the helium diffraction data from the $p(2 \times 1)$ phase was the splitting of the half-order peaks, which indicate the presence of antiphase (2×1) domains within the hydrogen overlayer. The distribution of domain lengths was obtained from a quantitative spot-profile analysis of the half-order diffraction peaks by means of close-coupling calculations. An analysis of the coverage dependence of the diffraction intensities revealed that the high-coverage phase grows from the $p(2 \times 1)$ phase via an intermediate (1×1) phase. The presence of domain boundaries in the reconstructed phase was also concluded from the existence of additional broad peaks in the diffraction patterns (Graham *et al* 1998).

An attempt to determine the structure of the OH(1×1) phase on Ag(110) (formed after H_2O dissociation on the O(2×1)/Ag(110) surface) from He-diffraction data has been performed by Canepa *et al* (1993a). The corrugation function derived from intensity analysis clearly showed that this phase consists of OH rows aligned parallel to the close-packed rows of the Ag(110) substrate.

A combined HAS and SPALEED investigation of the domain structure of oxidized Cu(001) has been reported by Meyer *et al* (1997). This system consists of rectangular unit cells with a $(2\sqrt{2} \times \sqrt{2})$ structure, which can lead to the formation of eight different domains. Extensive eikonal simulations of the HAS data allowed us to conclude that this surface is covered mainly with small domains with a mean domain size of 32 unit cells, and that these domains have a random displacement distribution towards another which is peaked at a $[\frac{3}{2}, \frac{1}{2}, 0]a$ displacement, where a is the unit cell vector along [100]. These results illustrate the power of HAS to unravel complex structural details which extend over large surface distances.

We close this section with a discussion of the high-resolution HAS results reported by Glebov *et al* (1997a), who observed the formation of two well-ordered ice bilayers on Pt(111). Figure 10(a) shows a two-dimensional helium diffraction pattern recorded after covering ~80% of the surface area with D_2O island at $T_s = 130$ K. The sharpness of the diffraction peaks indicates the formation of large, well-ordered ice islands, while the very intense specular peak is caused by scattering from the remaining 20% of uncovered, highly reflective Pt(111) surface. The peak positions can be interpreted as two domains of a $(\sqrt{37} \times \sqrt{37})$R25.3° rotated overlayer structure, as shown in figure 10(b). Upon completion of the bilayer the ice lattice compresses further and rotates forming a $(\sqrt{39} \times \sqrt{39})$R16.1° structure. The corresponding diffraction pattern as well as the reciprocal space representation are shown in figures 10(c) and (d), respectively. It is interesting to note that the overlayer maintains an angle of 120° between lattice vectors, consistent with an undistorted hexagonal structure. No structural differences were observed between adsorbed D_2O and H_2O for both phases, which indicates that the structural properties of the ice bilayer are very similar to those of solid ice. A more detailed discussion of these results, including structural models for the two phases, can be found in the original work by Glebov *et al* (1997a).

3.2.3. Insulator surfaces. Helium atoms are especially interesting for studying adsorption on insulating surfaces because they do not affect the surface structure and also do not give rise to surface charging effects, in contrast to low-energy electron scattering whose use is problematic with most ionic surfaces.

HAS investigations of water adsorption on UHV cleaved $CaF_2(111)$ have revealed the formation of a well-ordered p(4×4) structure below 145 K (Lehmann *et al* 1994). In contrast to the case of water adsorption on metal surfaces, where solid ice structures are expected, these results demonstrated that water molecules form two-dimensional nanoclusters on $CaF_2(111)$. This conclusion was drawn from a quantitative analysis of the measured diffraction intensities. A grey-scale representation of the corrugation function is presented in figure 11. The pronounced maxima (bright patches) must be attributed to the adsorbate particles. The heights and the lateral extensions of these patches indicate the formation of two-dimensional water hexameres. The number six H_2O molecules per cluster was found to be consistent with the Bernal–Fowler–Pauling rules as well as with the results of molecular dynamics simulations reported by Wassermann *et al* (1994). These calculations predicted the formation of a $(2\sqrt{3} \times 2\sqrt{3})$ structure from hexameres, corresponding to a coverage of 0.5 ML. The observed p(4×4) structure with a coverage of 0.375 ML resembles very

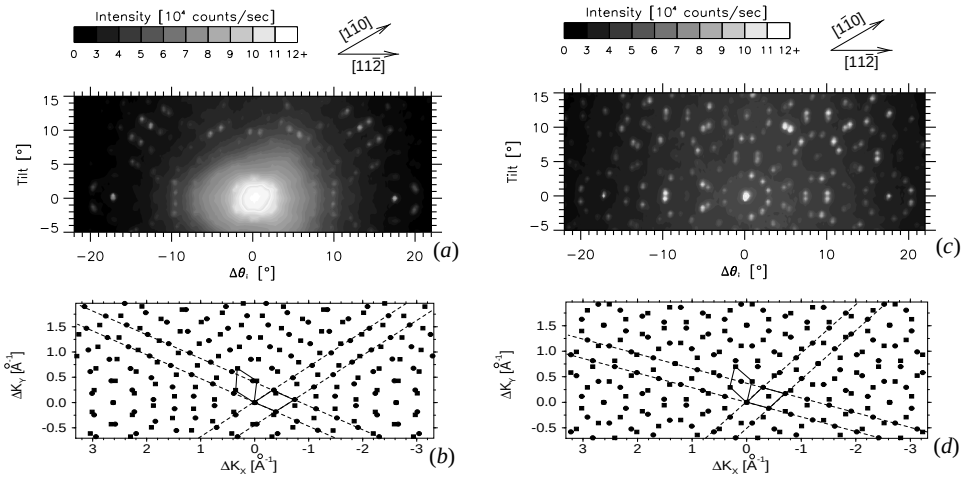

Figure 10. Two-dimensional helium diffraction pattern for an 80% coverage of the Pt(111) surface with D_2O islands (*a*) and for a complete bilayer (*c*). The incident helium energy is 22 meV and the surface temperature 130 K. Each diffraction pattern can be generated from two domains of an epitaxially rotated water overlayer whose reciprocal unit cells are $(\sqrt{37} \times \sqrt{37})$R25.3° and $(\sqrt{39} \times \sqrt{39})$R16.1° as shown in (*b*) and (*d*), respectively. The two different domains are shown by the full circles and squares in (*b*) and (*d*). From Glebov *et al* (1997a).

much the predicted one; the origin of this discrepancy is not clear. From inelastic He-atom scattering the bonding to the substrate was found to be much weaker than for water chemisorption on metallic surfaces, as proved by the low observed vibrational energy of 6 meV for the adsorbate vibration against the substrate (Lehmann *et al* 1994). The same authors have also investigated the influence of different surface defects on the adsorption behaviour of water (Lehmann *et al* 1995).

HAS investigations of alkali metal overlayers on graphite have been reported by Diehl and co-workers (Cui *et al* 1992, White *et al* 1994). No helium diffraction was observed from K, Rb and Cs overlayers, indicating that these surfaces exhibit very low corrugation amplitudes. The experimental upper limit of the ratio of the first-order diffraction intensities to the specular intensity was found to be 0.001, an order of magnitude smaller than expected from a superposition of atomic charge densities (Cui *et al* 1992). Good agreement with the experiment was obtained, however, with the corrugation function derived from density-functional theory calculations for K and Cs overlayers (White *et al* 1994).

HAS is also very well suited for the study of ordered physisorbed layers of polar molecules. A principal advantage of this technique is that the orientation of the adlayers with respect to the substrate can be determined in an absolutely nondestructive manner, as demonstrated by the studies reported by Scoles and co-workers. These authors have investigated the physisorption of CH_3F, CH_3Br, CH_3Cl, HCl and NH_3 on single-crystal surfaces of graphite as well as on Xe-precovered graphite surfaces (Ruiz-Suárez *et al* 1988, Rowntree *et al* 1990). Except for the NH_3/C(0001) system, all unit cell structures were found to be aligned along at least one of the high-symmetry directions of the substrate. This group has also reported on the physisorption of CH_3Br on NaCl(100) and LiF(100) (Robinson *et al* 1992).

The ability of HAS to determine the correct orientation of the CO molecules in the (1×1) phase on NaCl(100) has been numerically investigated by Carré *et al* (1996).

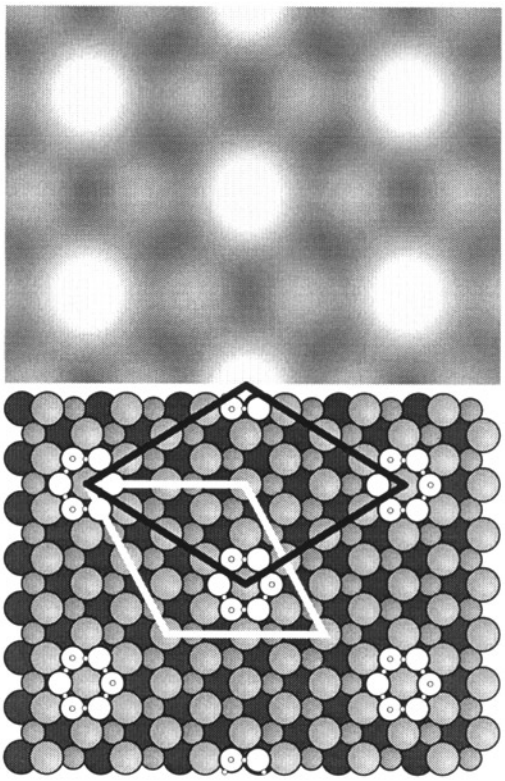

Figure 11. Top: grey-scale representation of the corrugation of the p(4 × 4)H_2O adsorbate structure on CaF_2(111) as determined from experimental diffraction intensities. Bottom: structural model with the water hexameres positioned around the top fluorines and forming a $(2\sqrt{3} \times 2\sqrt{3})$ structure (white lines) as predicted by Wassermann *et al* (1994); the observed p(4 × 4) unit cell is indicated by black lines. After Lehmann *et al* (1994).

By performing extensive three-dimensional wavepacket calculations for different scattering conditions, these authors showed that a distinction between the upright and bent (1 × 1)CO configurations can be made on the basis of He diffraction spectra provided that the He scattering dynamics is solved exactly. In particular, diffraction beam intensities were found to behave very differently as a function of the angle of incidence and beam energy for both CO orientations. The He–surface potential is, however, characterized by almost identical bound-state energies for the two configurations, so that they cannot be distinguished on the basis of measurements of selective adsorption resonances (section 3.4). These calculations, which could be easily extended to other molecular adlayers on insulators, are expected to encourage new experimental studies of such systems.

In concluding this section we mention that, whereas the clean (100) surfaces of the hitherto investigated alkali halides (like NaCl and LiF) exhibit peak-to-peak corrugation amplitudes which are in good agreement with the differences in the ionic radii of the surface atoms, the corrugation values of the oxides MgO(100) (Rieder 1982b) and NiO(100) (Cantini *et al* 1979) are appreciably smaller. This suggests that, because of the different bonding character, heavy charge redistributions take place at oxide surfaces.

3.2.4. Semiconductor surfaces. Cleaved semiconductor surfaces are known to reconstruct, resulting very often in the appearance of highly corrugated two-dimensional structures. From the point of view of He-diffraction, such systems not only cause the appearance of more diffraction beams in the experiment (requiring therefore better angular and energy resolutions) but also suggest that the problems under study cannot be solved by applying the computationally simple eikonal and GR methods, and that even the validity of the HCW model for the He–surface interaction potential should be questioned. As a consequence, only very few structural studies have been performed on semiconductor surfaces, and practically all of them were restricted to calculations based on the eikonal approach. Examples of this are the study on GaAs(110) by Cardillo *et al* (1981) and Laughlin (1982) and on Ge(100) by Lambert *et al* (1987). A structural determination of a semiconductor surface within the close-coupling approach still remains to be done. An additional complication is that the simple superposition of spherical atomic charge is substantially wrong for reconstructed semiconductor surfaces (Sakai *et al* 1986). An alternative procedure (the modified atomic charge superposition (MACS)) has been developed by Sakai *et al* (1986) and applied to the $(2 \times n)$/Si(100) reconstruction by Rohlfing *et al* (1988). We mention for completeness the study on the c(8×8) and (2×8) reconstructions of Si(100) by Barbier and Lapujoulade (1990). The validity of the Esbjerg and Nørskov ansatz (2.1) for a semiconductor surface has only recently been demonstrated by Buongiorno Nardelli (1996) in a density functional study of the interaction of He with the InSb(110) surface.

In this section, the recently reported quantitative analysis of the c(2×8) reconstruction of Ge(111) will be briefly discussed (Farías *et al* 1997c). The structure of this highly corrugated system had been studied with STM as well as by *ab initio* calculations, so that it is well suitable to test the reliability of the different approximation methods as well as the ability of the HCW approximation to reveal structural details. A very important result of this study was to show that, despite the large unit cell, the appreciable corrugation amplitude and the complexity added by the presence of three domains, calculations performed within the simple HCW model reflect all structural details of the c(2×8) reconstruction. The sensitivity of He-diffraction to the buckling observed between both rest atoms was demonstrated by model calculations performed with the eikonal approximation and the RR′ method within the HCW picture on the one hand and the close-coupled-channel (CCC) method with a realistic potential on the other.

The geometrical structure of the Ge(111)–c(2×8) surface is described by a simple adatom model, first proposed by Becker *et al* (1985) on the basis of STM measurements. This model is shown in figure 12 (bottom). The atoms placed at T_4 (top, fourfold-coordinated) sites are called adatoms and saturate 75% of the surface dangling bonds, leaving 25% of the surface atoms, the so-called rest atoms, unsaturated. As can be seen in figure 12, the c(2×8) structure contains alternating (2×2) and c(2×4) subunits, which leads to different local environments for each of the two adatoms and the two rest atoms within the c(2×8) unit cell. The four different dangling-bond states are labelled A_3, A_4, R_3 and R_4, where A and R stand for adatom and rest atom, respectively, and the indices refer to the sum of nearest and next-nearest dangling bonds. The fact that in the STM-study of Becker *et al* (1985) either the adatom or the rest atom was imaged, but not both simultaneously, leads to the conclusion that there is a complete electron transfer from the adatom to the rest atom, resulting in a fully occupied rest atom dangling-bond state and a completely empty adatom dangling-bond state. However, in a more recent STM study, Hirschorn *et al* (1991) could observe both rest atom and adatom dangling bonds simultaneously, which demonstrated that both kinds of dangling bonds are partially filled. Furthermore, they found that the two adatoms or the two rest atoms in a unit cell show significant differences in

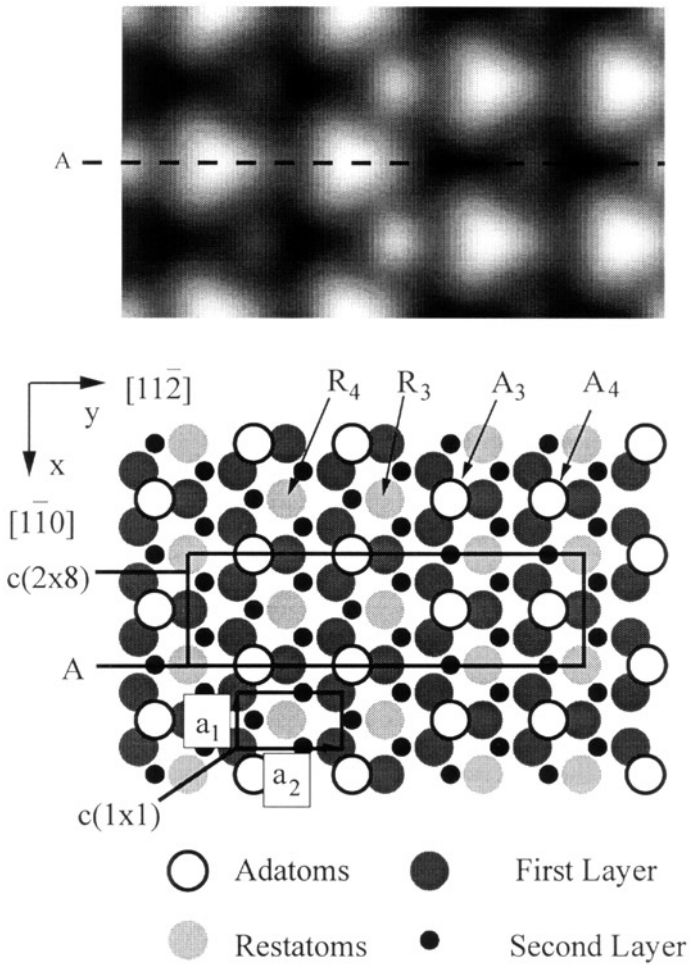

Figure 12. Bottom: top view of the adatom model for the Ge(111)–c(2 × 8) reconstruction. The lattice parameters of the rectangular (1 × 1) unit cell are $a_1 = 4.00$ Å and $a_2 = 4\sqrt{3}$ Å. See the text for details about the notation used in describing the two types of adatoms and rest atoms. Top: grey-scale representation of the best-fit corrugation function derived from diffraction intensity analysis (two rectangular unit cells are shown). Note the pronounced buckling between both rest atoms in the unit cell. From Farías *et al* (1997c).

apparent height depending on the image conditions, the effect being more pronounced for the rest atoms than for the adatoms. This buckling may reflect a geometrical inequivalence between both adatoms (rest atoms) as well as an asymmetric distribution of the surface electronic state density. In agreement with these results, *ab initio* calculations performed by Takeuchi *et al* (1992) showed that there is a small excess electron charge near the R_3-type rest atom relative to R_4, while no similar effect was seen for the adatoms.

Because of the great sensitivity of helium atoms to the total electron density distribution on the surface, it is interesting to ask if the asymmetries observed with STM could also be detected by means of He scattering. A look at the best-fit corrugation shown in figure 12 (top) demonstrates that this is actually the case. The presence of a pronounced buckling between both rest atoms is evident. This corrugation was obtained using the

eikonal approximation. The maximum corrugation amplitudes along $[1\bar{1}0]$ and $[11\bar{2}]$ are $\zeta_X \sim 1.10$ Å and $\zeta_Y \sim 1.50$ Å, respectively. The first of these values represents almost 15% of the corresponding lattice constant, suggesting that the problem under consideration could be outside the range of validity of the eikonal theory. Therefore, the results were checked by performing calculations with use of the RR′ method (García and Cabrera 1978), which represents the exact solution for a HCW interaction potential. The calculation of a unique intensity with this method requires the inversion of a matrix whose dimension M depends on the magnitude of the problem under consideration (for the c(2×8) structure, $M \sim 700$); this uses the RR′ method which is very time consuming and consequently inappropriate for trial-and-error searches in parameter space. However, due to the very good agreement obtained for both RR′ and eikonal methods, the use of the latter approximation could be well justified in this case. In view of the buckling between both rest atoms detected by HAS, the question arises as to what extent the observed asymmetries can be ascribed to a physical origin and not to the HCW approximation. This question was examined by calculating diffraction spectra for given symmetric and asymmetric one-dimensional corrugations using the CCC method with a realistic potential. Afterwards these spectra were fitted with eikonal using the same procedure applied for the c(2×8) structure. The error introduced by use of the HCW approximation was then estimated by comparing the best-fit corrugations obtained with eikonal with those used in the CCC calculations. As a result, it was concluded that the HCW assumption is not able to turn a symmetric corrugation into an asymmetric one or vice versa and thus the observed asymmetries between R_3 and R_4 must be attributed to a physical origin. A more detailed discussion of this system including a structural analysis of the high-temperature (1×1) structures of Ge(111) may be found in the original work by Farías *et al* (1997c).

3.2.5. Faceting of stepped surfaces. A subject which has received much interest in the past few years is the investigation of faceting of vicinal surfaces using HAS. In contrast to LEED, the large-angle scattered intensities in a HAS experiment are dominated by step-edge diffraction. Such intensities are not restricted to regions close to the reciprocal-lattice rods, but can be found at almost all kinematic conditions, which makes the identification of facets with HAS relatively easy. A detailed discussion of this subject as well as of the HAS form factors at different scattering conditions is given by Hinch *et al* (1990) and Hinch and Toennies (1990) (see also section 3.5).

One of the first HAS studies of vicinal surfaces was reported by Comsa *et al* (1982a, b), who showed that oxygen provokes a step doubling or faceting (depending on temperature) of Pt(997). A re-investigation of this system by Hahn *et al* (1994) demonstrated that the step-doubling transition is indeed caused by oxygen impurities, whereas the faceting transition is a property of the clean surface. The kinetics for the oxygen-induced step doubling and subsequent singling transformation of Ni(977) in the limit of very low coverages (<0.02 ML) has been recently studied by Niu *et al* (1996). The faceting and thermal stability of the Al(332) surface was investigated by Hinch *et al* (1990), who complemented their data with TOF measurements at high temperatures in order to separate inelastic scattering events. Other HAS investigations of faceting of metal surfaces include that of Avrin and Merrill (1992) on Ir(110) and the one performed by Schwenger and Ernst (1996) on the K-induced faceting and defaceting in Cu(115). Concerning semiconductor surfaces, the transition from double-step to single-step reconstruction of Si(1,1,17) as a function of temperature has been investigated by Barbier and Lapujoulade (1991).

3.3. The Debye–Waller factor

The theoretical methods for the calculation of diffraction intensities presented in section 2.3 assumed that the atoms of the lattice were at rest. However, both zero-point motion and thermal vibrations of the surface atoms lead to inelastic scattering of the incoming atoms. The principal observable effect of this is a thermal attenuation of the coherent diffraction intensities without a change of the peak shape. This problem is well known in neutron and x-ray diffraction from crystals, where the Debye–Waller factor relates the intensity $I(T)$ of a diffraction peak with the intensity I_0 from a lattice at rest by

$$I(T) = I_0 \mathrm{e}^{-2W(T)} \tag{3.2}$$

where $\exp[-2W(T)]$ is the Debye–Waller factor and

$$W(T) = \tfrac{1}{2}\langle(\boldsymbol{u}\cdot\boldsymbol{\Delta k_i})^2\rangle_T. \tag{3.3}$$

Here $\boldsymbol{u}$ is the displacement of a lattice atom from its equilibrium position, $\boldsymbol{\Delta k_i}$ is the momentum transfer in the scattering event and the outer brackets refer to a thermal average. The assumptions underlying these expressions are that the interaction in the scattering event is both weak and short in duration, which is well justified for neutron and x-ray diffraction. The situation is quite different for the scattering of thermal atoms from surfaces, since the collision times are long (comparable to phonon vibration periods), the incoming atoms may interact with several surface atoms simultaneously (the 'Armand effect' (Armand *et al* 1977)) and the atom–surface interaction is strong and long-ranged. As a consequence, the theoretical basis for a standard Debye–Waller factor in atom–surface scattering is not so firm as in neutron and x-ray diffraction from solids. However, and because the factorizable form (3.2) with $W(T)$ given by (3.3) describes many experiments rather well, considerable theoretical effort has been devoted to treating the inelastic scattering in approximations which produce the standard Debye–Waller factor. For the case of a fast collision with a hard lattice, the validity of (3.3) has been shown by Levi and Suhl (1979) on the basis of a semiclassical theory (see also Bortolani and Levi 1986). Similar results were obtained by Armand and Manson (1979) using a hard-wall model, and also by Meyer (1981) within the sudden approximation. Equation (3.3) can be further simplified by assuming that the momentum transfer parallel to the surface is zero. Although this is strictly valid only for the specular beam, it is a reasonable approximation for final angles not too different from the incident angle and even for high-order diffraction beams on 'open' surfaces like Ni(115) (Conrad *et al* 1985). So we can rewrite (3.3) as:

$$W(T) = \tfrac{1}{2}\langle u_z^2\rangle(\Delta k_z)^2 \tag{3.4}$$

where $\langle u_z^2\rangle$ is the average displacement of a crystal atom perpendicular to the surface. For a harmonic lattice (i.e. a Debye model of the solid) $\langle u_z^2\rangle$ is proportional to T at $T > \Theta_D$, where Θ_D is the surface Debye temperature. The effect of the atractive well near the surface is taken into consideration by the 'Beeby correction', which consists of replacing Δk_z by $\Delta k_z^* = (\Delta k_z + 2mD/\hbar^2)^{1/2}$, where m is the particle mass and D is the well depth (Beeby 1971). By doing this, we obtain the following simple expression for $W(T)$:

$$W(T) = \frac{3(\hbar^2\Delta k_z{}^2 + 8mD)T}{2Mk_B\Theta_D^2} \tag{3.5}$$

where M is the mass of a surface atom and k_B is the Boltzmann constant. This expression has been more recently derived by Manson (1991) in the semiclassical limit of a quantum mechanical description of inelastic scattering. For the specular beam, (3.5) can be easily expressed as a function of the incident beam energy E_i and the angle of incidence θ_i:

$$W(T) = \frac{12m(E_i\cos^2\theta_i + D)T}{Mk_B\Theta_D^2}. \tag{3.6}$$

This equation indicates that the strength of the diffraction intensities should be highest for grazing incidence, low incidence energy and low surface temperatures, in agreement with experiment. In general, the form of $W(T)$ given by (3.5) does not agree well with experiment in both the momentum *and* the temperature dependences; in particular, this means that physical conclusions based on a comparison of Θ_D values obtained from different surfaces must be taken with care. As expected, a full description of the thermal attenuation for real systems can be achieved only by a detailed investigation of multiphonon exchange, calculations which have been attempted by several groups. A general quantum mechanical theory describing the multiphonon inelastic scattering to arbitrarily high order in numbers of exchanged phonons has been developed by Manson (1994). A description of these theoretical methods lies beyond the scope of this review; a detailed discussion of the two most commonly used approaches (the so-called T-matrix and scattering spectrum formalisms) has been recently presented by Gumhalter (1996). In what follows, we summarize the most relevant experimental investigations of the atom–surface Debye–Waller factor as well as some related theoretical studies.

Experiments on hydrogen diffraction from LiF(100) by Hoinkes *et al* (1972, 1973) and from Cu(100) by Lapujoulade *et al* (1981b) as well as studies by Lapujoulade *et al* (1980a) on He and Ne diffraction from Cu(100) and on He diffraction from Cu(111), Cu(100), Cu(110), Cu(113), Cu(115) and Cu(117) (Lapujoulade *et al* 1983) have shown that the thermal dependence of various diffraction beams is well described by a Debye–Waller factor including the Beeby correction (3.5), although a too large value for the well depth was obtained for Ne diffraction ($D \sim 100$ meV). For the rougher Cu surfaces, a deviation from linear behaviour of $\ln I_{00}$ with T was observed above a threshold temperature, due to the increasing importance of anharmonicity effects (Lapujoulade *et al* 1983). A similar behaviour was reported for He diffraction from Cu(110) by Zeppenfeld *et al* (1989).

The He-diffraction data from Cu(100) and Cu(110) were satisfactorily reproduced (for different scattering conditions) by Armand and Manson (1984, 1988) using a perturbation series approach, in which an expansion of the scattering matrix is carried out in a distorted wave basis. Assuming that the coupling of the phonons occurs through exponentially repulsive potentials and allowing only this repulsive component to vibrate, Armand and Manson carried out phonon averages to all orders. An important result of these calculations was that the repeated single-phonon exchange processes give much larger contributions to the Debye–Waller factor than the multiphonon exchange arising from a single-vertex process (Manson and Armand 1987, 1988). These authors also proposed a resummation procedure in order to recover the effects of the multiphonon virtual exchange. Very good agreement with experiment was achieved for the scattering of He, H_2 and Ne from Cu(100) (Armand *et al* 1986, see also Armand 1989). Jackson (1988) developed a theory for the phonon inelastic scattering of light atoms from surfaces. It allows us to compute the reduced density matrix at any time and also gives detailed information on phonon excitations and absorption. The theory was shown to satisfactorily reproduce the experimental data for He/Cu(100). Within this approach, energy transfer was found to be sensitive to the steepness of the repulsive potential, incident kinetic energy and angle of incidence. Also, the 'Beeby correction' was examined and shown to be invalid (except at very low beam energies), i.e. the effect of varying E_i by a few meV was found to be considerably larger than of varying the well depth by a similar amount. Good agreement with experiment for the He–Cu(110) system was also reported by Miret-Artés (1995) using a new formulation of inelastic atom–surface scattering within the close-coupling formalism. In this formulation, the diffraction channels exhibit moving thresholds and are shifted (or 'dressed') in energy by an amount corresponding to the creation or annihilation of one or more phonons. The channels 'dressed' by a given number

of phonons are arranged in Floquet blocks, the number of which depends on the phonon approximation considered. Within the single-phonon approximation, Miret-Artés (1996a) was able to reproduce the temperature dependence of He-diffraction intensities from Cu(110) as well as the thermal attenuation of resonance line shapes from Cu(113). The role of the interaction potentials on the magnitude of the Debye–Waller factor on He–Cu(100) has been recently investigated by Šiber and Gumhalter (1997). These authors used the fully three-dimensional quantum model of inelastic He scattering from surfaces developed by Bilić and Gumhalter (1995). By combining several types of He–Cu(100) interaction potentials, whose attractive and repulsive components are both allowed to vibrate, with the substrate phonon density of states, a very good agreement with the experimental data was obtained without invoking any fitting parameters. In contrast, by taking the phonon cut-off wavevector Q_c as an adjustable parameter, good agreement with experiment was obtained with all model potentials (Šiber and Gumhalter 1997).

Other works on the validity of (3.5) include that of Asada (1979) on hydrogen and He scattering from Ag(111) and studies on He–Ag(111) (Horne *et al* 1980) and He–Pt(111) (Bortolani *et al* 1989). The calculations of the Debye–Waller factor from Ag(111) (Idiodi *et al* 1987) and Pt(111) (Bortolani *et al* 1989) were based on a three-dimensional formalism developed by Celli and Maradudin (1985), in which the phonon effects on the scattering are represented by an effective (optical) potential; explicit expressions for $W(T)$ were obtained within a low-order perturbation theory. Krzyzowski *et al* (1994) showed that (3.5) reproduces quite well He-diffraction data from the Pt(110)–(1×2) missing-row reconstruction in a wide range of surface temperatures. Similar results were reported for the scattering of H_2, D_2 and He beams from Ag(111) (Yu *et al* 1985), for D_2 scattering from Ni(110) and Cu(100) (Bertino *et al* 1997a, 1998b), also for H and D scattering from graphite (Iannotta *et al* 1985) and for He scattering from the CaF_2(111) and BaF_2(111) surfaces (Lehmann *et al* 1996). Several studies by Greene and co-workers demonstrated that the thermal attenuation of He beams diffracted from semiconductor surfaces is also well described by (3.5) (see the beginning of section 3.6.2 for references). For the scattering of He from Cu(100), Hofmann *et al* (1994) have measured the temperature dependence of the diffuse elastic peak, all single-phonon peaks and the multiphonon contribution over the range $100 < T < 1000$ K. A Debye–Waller behaviour was found for the inelastic Rayleigh and longitudinal resonance modes for temperatures up to 800 K.

As already mentioned, the measured diffraction intensities must be linearly extrapolated to $T = 0$ K in order to determine surface corrugation functions. The degree to which errors in this extrapolation affect the accuracy of the corrugation function determination has been investigated by Conrad *et al* (1985) for the diffraction of He from Ni(115). Measurements performed at different Δk_z values confirmed the applicability of (3.5) between 100 K and 300 K. Best-fit corrugations were calculated by inverting experimental data recorded at fixed angle of incidence, with and without the Debye–Waller correction (3.2). It was concluded that intensity corrections can be made for all diffraction peaks by measuring the $I(T)$ behaviour of the specular peak. A result of most practical importance was that surface corrugation functions can be accurately determined without Debye–Waller corrections for surface temperatures up to 300 K, if one assumes an error of $\pm 10\%$ in the peak intensities. Again, we emphasize that these results were obtained by analysing spectra measured at a *fixed angle of incidence* (Conrad *et al* 1985). A very interesting inversion procedure to determine the Debye–Waller factor from experimental data *during* the fitting process has been recently developed by Varga (1998) and applied to the He–LiF(001) system. Provided (3.2) and (3.3) hold, the method allows very efficient determination of the Debye–Waller factor from only one experimental set-up.

In contrast to the case of clean surfaces, only a few experimental studies have been devoted to test the validity of (3.5) for adsorbed layers. Lee *et al* (1983) have shown that the thermal attenuation of the specular and first-order He-diffraction beams from the (1×1)H/Pt(111) phase obey (3.5) for surface temperatures between 60 K and 200 K. Similar results have been reported by Lapujoulade *et al* (1982) for the He–(2×1)O/Cu(110) system between 100 K and 600 K. A Debye–Waller-like behaviour was also observed for a He beam specular scattered from the c(2×2)Cl/Ag(100) system (Becker *et al* 1983) and from the OH(1×1) phase on Ag(110) (Canepa *et al* 1993a). Schweizer and Rettner (1989) have shown that the thermal attenuation of He, Ne and Ar beams specularly reflected from 2H–W(100) is also well described by a Debye–Waller factor including the Beeby correction (3.5). These results were consistent with a surface Debye temperature of 400 K and well depths of 5, 20 and 40 meV for He, Ne and Ar, respectively (Schweizer *et al* 1991). The temperature dependence of a hydrogen atom beam scattered from a monolayer and bilayer of Xe on graphite has been measured by Ellis *et al* (1983, 1985). Equation (3.5) was found to describe well the data for the monolayer, which also agreed with calculations using an Einstein model. Similar results were obtained for He-diffraction from monolayers and multilayers of Ar, Kr and Xe physisorbed on Ag(111) by Gibson and Sibener (1988a, b) and Gibson *et al* (1988). Measurements on He–Cu(110) revealed that exposure to hydrogen at room temperature reduces the surface Debye temperature by 50 K, which was interpreted as evidence for a reduction of the binding of the Cu atoms in the top layer (Miyake *et al* 1997). Eikonal calculations for an oscillating soft wall were reported by Mahale *et al* (1987) and applied to the scattering of He from noble gas adlayers. A theoretical study of the scattering of He atoms by a dilute adlayer having a dispersionless Einstein mode has been performed by Manson (1988). For the case of ordered adlayers, Manson showed that the coherent elastic part has a thermal attenuation behaviour which very much resembles that of a Debye–Waller factor.

Another important manifestation of inelastic scattering is the thermal attenuation of line shapes under resonance conditions, a subject on which only few experimental studies exist. A simple method of applying a Debye–Waller factor to account for inelastic effects within a hard-wall potential was proposed by Hutchison (1980). This method has been extended to the case of scattering from soft potentials by Mantovani *et al* (1984) using the T-matrix formalism. A very important result of these calculations was that the thermal attenuation of the specular intensity is stronger under resonance conditions than away from a resonance. Armand *et al* (1989) developed a more general theory for treating inelastic effects in the presence of resonances, which is based on the distorted-wave formalism. By considering only one-phonon contributions, these authors were able to successfully reproduce the increase in resonance linewidths with temperature for Cu(115). However, the method has not yet been applied to reproduce the thermal attenuation of line shapes. Another very promising approach is the one proposed by Miret-Artés (1995, 1996a) on the basis of the close-coupling method. Line shapes were calculated at different surface temperatures for the He–Cu(113) system; excellent agreement was obtained at 70 K (only experimental curve available). This is clearly an area in which more experimental work is needed to make comparisons with theoretical predictions.

The validity of (3.5) for epitaxial thin films has been carefully analysed by Hulpke *et al* (1996) for the growth of Cs on Cu(111) and K on Ni(001). Measurements of the thermal dependence of the specular beam intensity for different coverages showed that (3.5) holds, and that the Debye–Waller factor strongly depends on the film thickness (Θ_D decreases with increasing film thickness). This behaviour was explained assuming that the misfit-induced stress in the film surface is reduced when the number of deposited layers increases. Similar

results were reported for the growth of rubidium on Ni(100) (Flach *et al* 1998).

In conclusion, the general form (3.2) with $W(T)$ given by (3.5) describes quite well most He and H_2 diffraction experiments from clean surfaces, although the $\Delta k_z{}^2$ dependence is experimentally less firmly established than the temperature dependence. Clearly, the considerable theoretical progress made in recent years on the quantitative understanding of temperature effects in atom–surface scattering makes more experimental work necessary. In particular, it would be interesting to investigate experimentally (i) the temperature dependence of resonance line shapes, at least for He/clean metal surfaces, (ii) the range of validity of the Δk_z^2 dependence and (iii) the extent to which a harmonic vibrations model describes well the thermal attenuation from adlayers.

3.4. Selective adsorption resonances

As mentioned in section 2.3.2, in cases where the incident beam energy E_i is comparable to D, the existence of the attractive well of the potential leads to the appearance of an important diffraction phenomenon called selective adsorption resonance (SAR), which was first observed by Frisch and Stern (1933). This effect is characterized by the sudden appearance of maxima (or minima) in the intensity of diffraction beams as a function of incident beam parameters. Lennard-Jones and Devonshire (1936) attributed these features correctly to resonant transitions of the incoming particles into bound states of the attractive potential. SAR measurements allow for a precise determination of bound-state energies in the atom–surface potential and constitute as a consequence a unique method for determining the laterally averaged interaction potential $V_0(z)$ experimentally (for a compilation of data on the $V_0(z)$ potential see Vidali *et al* 1991).

The kinematic condition for resonance into a bound state with binding energy $E_n < 0$ can be easily derived from the conservation of energy and parallel momentum, and is:

$$E_n = \frac{\hbar^2}{2m}[|\boldsymbol{k}_i|^2 - |\boldsymbol{K} + \boldsymbol{G}|^2]. \tag{3.7}$$

Here m is the particle mass, $\boldsymbol{k}_i$ is the wavevector of the incoming beam, $\boldsymbol{K}$ is its component parallel to the surface and $\boldsymbol{G}$ is the surface reciprocal vector giving rise to the resonance. Since the coupling occurs through diffraction channels, these resonances are called *diffraction-mediated selective adsorption resonances* (DMSAR). The energy released in the binding is made available to motion in the surface plane so that the parallel energy is greater than that prior to scattering. For a real crystal, these bound particles will ultimately be desorbed either by an elastic transition into some allowed diffraction channel, or by inelastic scattering from the lattice or surface defects. An increase of the elastic scattered intensity at resonance conditions is often observed at large parallel momentum transfer when measuring diffraction intensities as a function of angle of incidence for high-corrugated surfaces, suggesting that inelastic processes are not very important under these conditions. A good example of this is given by the (1×1)2H/Rh(110) and the (1×1)/Rh(311) surfaces (Kirsten *et al* 1991, Apel *et al* 1996, respectively).

According to (3.7), resonant scattering features can be determined by measuring the intensity of a diffracted beam (typically the specular one) as a function of either (1) the angle of incidence or (2) the azimuthal angle or (3) the incident beam energy, while keeping the other two parameters constant. From an experimental point of view, (1) is the easiest to apply and it is thus the most employed method. SAR investigations on insulators, clean metals and adsorbate systems up to about 1991 have been thoroughly reviewed by Hoinkes and Wilsch (1992). New experimental results since then include SAR studies on clean Rh(311) and the (1×1)/Rh(311) system by Apel *et al* (1996) (in the (1) mode),

the re-investigation of the Pt(110)–(1 × 2) surface by Krzyzowski *et al* (1995) (in the (3) mode), and the measurements on the (1 × 2)–Rh(110), (1 × 2)–Au(110) and (1 × 2)–Pt(110) surfaces by Tommasini and co-workers (Bellman *et al* 1993b, Cortona *et al* 1993, Cvetko *et al* 1995d, respectively) applying the (2) mode.

If the binding energies of at least two bound states are known, then the potential parameters can be determined. The two most common in use are as follows.

(1) The two-parameter Morse potential

$$V(z) = D(\mathrm{e}^{-2\alpha z} - 2\mathrm{e}^{-\alpha z}) \tag{3.8}$$

where D is the potential well depth and α is the range parameter. The energy levels can be computed by (Hoinkes 1980)

$$E_n^{\mathrm{Morse}} = -\left(\frac{\sqrt{2mD}}{\alpha\hbar} - n - \frac{1}{2}\right)^2 \frac{\alpha^2\hbar^2}{2m}. \tag{3.9}$$

(2) The two-parameter 9–3 potential

$$V(z) = \frac{3^{3/2}}{2} D\left[\left(\frac{\sigma}{z+z_0}\right)^9 - \left(\frac{\sigma}{z+z_0}\right)^3\right] \tag{3.10}$$

with D denoting the well depth, σ the reciprocal range parameter and $z_0 = 3^{1/6}\sigma$. The approximate energy eigenvalues are given by (Cole and Tsong 1977)

$$E_n^{9-3} = -D\left(1 - \frac{n+\frac{1}{2}}{L}\right)^6 \tag{3.11}$$

with $L = \frac{3.07}{\pi}\sqrt{2mD\frac{\sigma^2}{\hbar^2}}$ and $n = 0, 1, \ldots, n_{\max}$, where $n_{\max}$ is the next integer to $(L - \frac{1}{2})$. Other potentials commonly used are the Mattera potential (Mattera *et al* 1980) and the shifted-Morse-hybrid potential (Schwarz *et al* 1978), both of them with three free parameters. A more detailed description of model He–surface interaction potentials is given by Celli (1992). In view of the influence of the surface orientation on the potential shape, He-diffraction experiments performed by Perreau and Lapujoulade (1982b) on Cu(110), Cu(113), Cu(115) and Cu(117) showed that the energy levels, and consequently the potential well, do not depend significantly on surface crystallography. Similar results were reported for Rh(110) and Rh(113) by Apel *et al* (1996). Calculations by Peskin and Moiseyev (1992b) for the He–Cu(115) system have shown that nonspecular DMSA resonances are very sensitive to the presence of weak asymmetries in the surface corrugation, i.e. very different resonance features were obtained for scattering along or against the terraces. A similar effect was predicted by Hernández *et al* (1993) for DMSA resonances measured at rainbow conditions in the He–Cu(117) system.

Note that (3.7) is just a kinematic condition, i.e. the averaged potential is determined from the angular positions of the SAR features, without performing any intensity analysis. This relation was derived within the free-atom approximation (i.e. without considering the higher-order Fourier components of the potential) and is not expected to be valid for highly corrugated surfaces, where some periodic components of the potential may be significant compared with V_0 (Chow and Thompson 1976, see also Vargas and Mochán 1996, 1998). As a consequence, other approaches must be applied in order to determine the atom–surface potential. A direct inversion method for recovering the interaction potential from diffraction data using the sudden approximation was presented by Gerber and Yinnon (1980) and applied to the He/MgO(100) system by Yinnon *et al* (1986b). Another method consists in separating the potential into various terms of multibody contributions (taken

from gas-phase data), following the prescription of Chung *et al* (1985, 1986). Elastic close-coupling calculations are then compared with diffraction spectra and SAR measurements. The problem of the nonadditive three-body interactions in the He–Xe/C(0001) and He–Kr/C(0001) systems has been addressed by a number of groups (Hutson and Schwartz 1983, Bracco *et al* 1984, Larese *et al* 1985, Jónsson and Weare 1986, Schwartz 1986, Aziz *et al* 1989). A very impressive series of experiments on this subject has been reported by Gibson *et al* (1988). These authors performed diffraction and SAR measurements for Ar, Kr, and Xe physisorbed on Ag(111) on a layer-by-layer basis from 1 to 25 layers. An important result of all these studies was that the calculations are very sensitive to the form of the He–rare gas pair potential as well as to the presence of the triple-dipole term (see also Gibson and Sibener 1988a, b). A general iterative inversion procedure to determine the atom–surface interaction potential from diffraction data without separating the potential into several terms has been developed by Ho and Rabitz (1991, 1992) and applied to the He–Xe/C(0001) system. Vargas and Mochán (1996, 1998) have calculated the atom–surface band structure for several corrugated systems and analysed its implications for SAR studies. In particular, they proposed a method to correct the bond state energies determined with (3.7) which was showed to better reproduce previous experimental data on He/NaCl(001).

An alternative approach which accounts for the surface corrugation has been developed by Tommasini and co-workers. It is also based on close-coupling calculations of the diffraction intensities, where the He–surface interaction potential is modelled by a superposition of pseudopair anisotropic terms (Cortona *et al* 1992a, b). Results obtained for the (1×2)–Pt(110) surface are shown in figure 13. Good agreement with experiment was achieved with a potential whose well depth was strongly modulated in the direction perpendicular to the close-packed rows, reaching a minimum of -14.9 meV above the missing rows (the average value is ~ 8 meV). Maps of the electron density showed a substantial lateral spread of the electronic charge, as compared with the superposition of free atomic electron densities. A comparison with the data taken on (1×2)–Au(110) (also shown in figure 13) allowed the conclusion that the electronic densities and the shape of the potential well as seen by He atoms on both surfaces are almost identical. This approach has also been applied to the (1×2)–Rh(110) (Bellman *et al* 1993b) and the (1×2)–Au(110) surfaces (Cortona *et al* 1993).

DMSAR are not observed in the scattering from low-corrugation surfaces (like the close-packed metal surfaces) due to the weakness of diffractive coupling. Calculations by Hernández *et al* (1991, 1992) for the He–Cu(11n) systems (with $n = 0, 3, 5, 7$) suggest, however, that resonances could still be made visible on such surfaces by choosing special scattering conditions, which lead to the appearance of the so-called *critical kinematic* (CK) effect. This effect could be very helpful in determining potential wells of low-corrugated surfaces. The same can be said about the *focused inelastic resonances* (FIR) predicted by Benedek and Miret-Artés (1995), which can be considered the inelastic counterpart of the CK effect. The FIR effect has been recently observed by Benedek *et al* (1996) for the He–NaCl(001) system, whereas no experimental evidence has yet been reported for the CK effect in atomic scattering. In the case of diatomic molecule scattering, translational to rotational energy coupling provides another mechanism for the occurrence of SAR, which is then called *rotationally mediated* (RM) selective adsorption. The first observations of RM selective adsorption were reported by Sibener and co-workers for HD scattering from Pt(111) (Cowin *et al* 1981) and from Ag(111) (Yu *et al* 1982) as well as for H_2 and D_2 scattering from Ag(111) (Yu *et al* 1983). A detailed description of this subject is given in the review by Barker and Auerbach (1985); for completeness, we mention that numerical exact calculations for the scattering of HD from Pt(111) and Ag(111) were reported by Peskin and

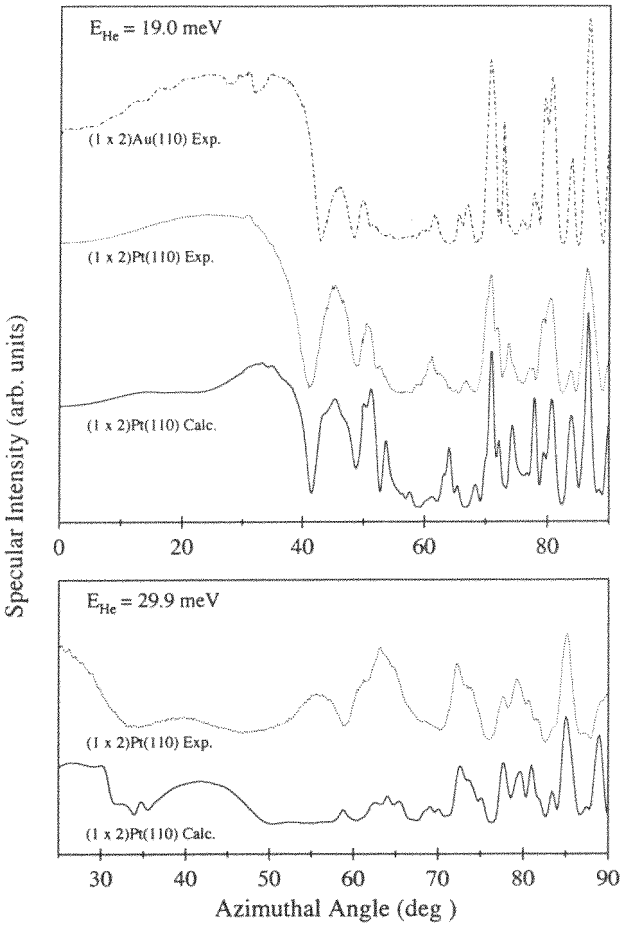

Figure 13. He-specular reflectivity measurements as a function of azimuthal angle for (1×2)–Au(110) and (1×2)–Pt(110) and incident beam energies of 19 and 29.9 meV. Calculated curves are also shown in the case of (1×2)–Pt(110). From Cvetko *et al* (1995d).

Moiseyev (1992a). The corresponding RMCK and RMFIR effects were recently observed by Bertino *et al* (1997c, 1998a) in the scattering of D_2 from Cu(001). Inelastic processes may also be involved in the transition into, as well as in the desorption from, bound states, leading to the appearance of *phonon mediated* (PM) selective adsorption and desorption (Lilienkamp and Toennies 1982, 1983). This subject is discussed in great detail in the review by Hoinkes and Wilsch (1992). A classification of the different elementary resonance processes as well as calculations of capture and desorption probabilities in the He diffraction from Cu(115) and Cu(117) was performed by Miret-Artés (1996b, 1993, respectively). More recently, Glebov *et al* (1997c) reported on *defect-mediated elastic resonances* (DER), in which the He atoms enter or leave bound states through elastic scattering from defects.

We close this section with a brief comment on the threshold resonances. These resonances are a general feature of diffraction systems and should appear whenever the initial conditions are such that a new diffraction beam just becomes visible (Cabrera and Solana 1974). These conditions correspond to $E_n = 0$ in (3.7), which already suggests that the name threshold resonance may be somewhat misleading, since no coupling with bound states is

involved. Since the intensity of the new beam increases from zero very steeply as a function of the incident angle (García 1978), conservation of flux suggests that such resonances should affect the intensity distribution of all diffraction beams. Calculations based on a hard-wall potential revealed that threshold resonances should be actually observable for highly corrugated systems (Cabrera and Solana 1974, García and Schlup 1982). However, this effect has not yet been observed in atom–surface scattering, suggesting that other factors may be important. This problem has been re-examined by Armand and Manson (1986) considering more realistic potentials in the scattering of H_2 from Cu(100). They found that if the repulsive part of the interaction potential is made realistically soft, threshold resonances become very weak and occur over an angular range which is too small, so that they were difficult to observe experimentally. The way in which threshold resonances could be enhanced by the simultaneous occurrence of the skipping singularity (see section 2.4) has been recently discussed by Guantes *et al* (1997). In particular, close-coupling calculations showed that these resonances should be easily visible in the diffraction of He from Cu(115). The relationship between SAR, trapping and chaotic scattering has been recently discussed by Borondo *et al* (1994).

3.5. Scattering from single defects and structurally disordered surfaces

Results obtained in recent years demonstrate that HAS is also a powerful tool for investigating structural disorder on surfaces. As described in section 2.5, the attenuation of the specular intensity by admolecules on a smooth surface is characterized by a giant cross section of the order of 100 Å^2. This attenuation is almost entirely due to small angle scattering (caused by long-range interactions in the He–surface system) and gives rise to a wealth of information on growth and diffusion studies, as discussed exhaustively in section 4. A second line in investigating defects on surfaces consists of looking at the small fraction of intensity scattered through larger angles, which results from short-range repulsive forces (Hinch 1988, 1989) and yields geometrical information on the surface defect. These large-angle elastic features are more difficult to observe experimentally because of their low intensities (typically 10^{-3}–10^{-4} of the specular intensity) and have been first observed by Lahee *et al* (1986a, b) from a stepped Pt(111) surface. From the theoretical point of view, one major difficulty in calculations of He scattering from disordered surfaces is that the problem involves a continuum of channels, since momentum changes are not restricted by a Bragg condition. As a consequence, the development of methods for treating these problems was necessary, the most important being the hard-wall approaches, the sudden approximation and quantum wavepacket (numerically exact) calculations. A more detailed description of these methods is given by Gerber *et al* (1992) and Manson (1992). The most relevant results achieved along this line of study will be presented in this section, as well as some interesting theoretical predictions which are expected to stimulate new experiments.

3.5.1. Scattering from step-edge defects and single adsorbates. The existence of characteristic nonspecular peaks in the elastic He scattering from isolated defects on a smooth surface has been first evidenced by wavepacket calculations performed by Gerber *et al* (1984) and also by hard-wall calculations reported by Heuer and Rice (1985). The oscillations in the angular intensity distribution predicted by these studies were then first observed by Lahee *et al* (1986a, b) from a randomly stepped Pt(111) surface and also for the case of isolated CO molecules on Pt(111) (Lahee *et al* 1987). These results are shown in figure 14. The only other previous application of He scattering for defect characterization is that of Schlup and Rieder (1986) who interpreted by hard-wall calculations a pronounced

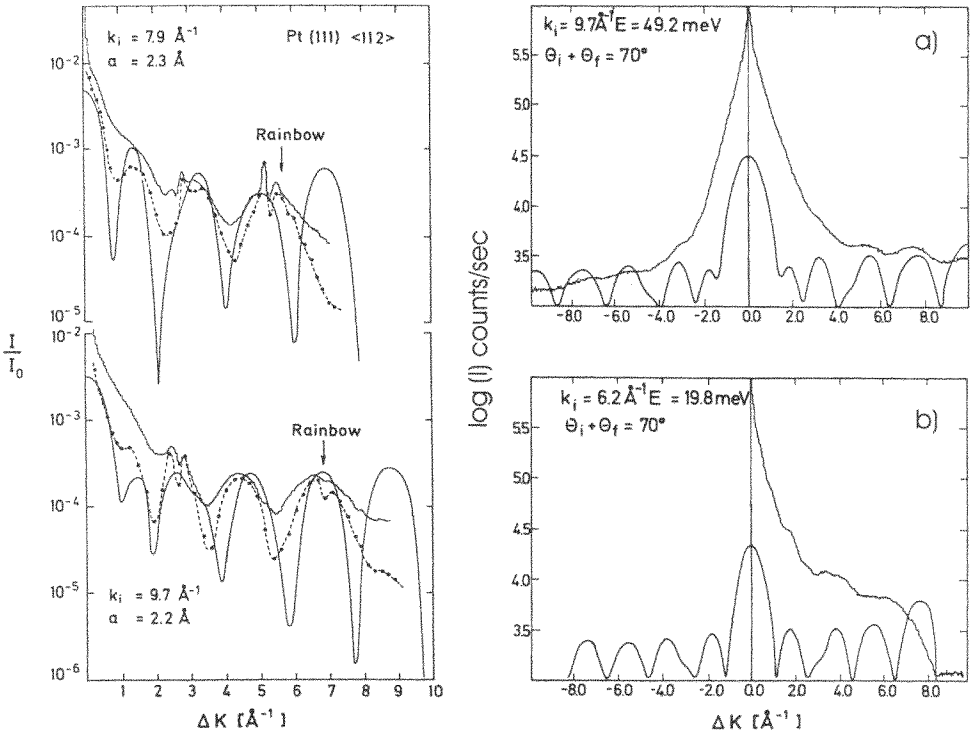

Figure 14. Left: comparison of theoretical angular distribution (full curve) and experiment (circles are elastic contribution only) for He atoms scattering from randomly stepped Pt(111). Right: angular distributions for two incident beam energies for scattering from isolated CO molecules on Pt(111). Theoretical fits obtained with a hard hemisphere model are also shown. Values of the hemisphere radius were 2.4 Å for (a) and 2.8 Å for (b). From Lahee *et al* (1986a, 1987).

triangular background in the vicinity of the specular peak for Ni(100)–c(2 × 2)O as originating from a random distribution of ∼15% empty oxygen sites.

The stepped Pt(111) surface (figure 14 (left)) was created by briefly sputtering the crystal at 600 K. A comparison of the total scattered intensity with the elastic contribution only (circles) confirmed that the observed oscillations arise from He atoms elastically scattered at steps. These modulated structures were initially explained by a model developed by Manson, in which the stepped surface was approximated by a hard, half-cylinder on a flat surface plane (Lahee *et al* 1986a, b). This problem can be solved analytically in the limit $k_i a \gg 1$, where a is the radius of the cylinder. As a result, the scattering amplitude can be written as the sum of two terms: a term describing the back-scattering (also called the illuminated face term) and a term which can be attributed to the mostly forward-scattered Fraunhofer diffraction. Since the contribution of the last term decreases with ΔK^{-2}, the oscillations observed at larger momentum transfer are mainly originated by the first term and its mirror interference, and are called reflection-symmetry interferences. The calculated angular distributions are also shown in figure 14. As can be seen, the most salient features in experiment are well reproduced by the calculations, providing support to the interpretation in terms of reflection symmetry interferences described above. The prediction by the theory of an additional peak not observed in the experiment is due to the fact that, unlike a half-

cylinder, a real step profile would produce a classical rainbow in the angular distribution. The rainbow positions expected for a step inclination of 30°† with respect to to the terraces are indicated by arrows in figure 14. In a subsequent study, Drolshagen and Vollmer (1987) carried out wavepacket calculations for soft potentials assuming a more realistic model for the step edge. The experimental distribution could be well reproduced by these calculations and included the correct rainbow maximum with the subsequent drop of intensity towards larger ΔK values; the largest slope in the step edge was found to be 31.75°. A similar study performed by Hinch *et al* (1989b) for Pt(111), Al(111), Cu(111) and Ni(001) has shown that the corresponding slopes lie between 34° and 43°. These authors were also able to observe, for Cu(111), asymmetric intensity distributions for positive and negative ΔK, which arise from scattering at downhill and uphill steps, respectively. Berndt *et al* (1990) have investigated the influence of CO adsorption on the large-angle diffraction oscillations recorded from a stepped Ni(001) surface. The peak positions were found to shift to larger ΔK values with increasing CO coverage, suggesting a change in step edge shape with adsorption. Further theoretical studies on diffuse He diffraction from steps have been reported by Hinch using the eikonal (Hinch 1988) and a modified sudden approximation (Hinch 1989). At this stage it is interesting to mention that similar studies on step edges have not yet been performed on semiconductor and ionic crystal surfaces. Finally, the 'fine-structure' features observed in experiment (see figure 14) were found to depend on surface preparation and thermal treatments (Hinch *et al* 1989b), and arise from step–step correlation effects (Hinch and Toennies 1990). These authors have also shown that steps produced by ion bombardment are not randomly directed, but tend to be oriented as the neighbouring step edges, i.e. to form microfacets of high step density.

Oscillations in the diffuse elastic intensity from single adsorbed molecules were first observed by Lahee *et al* (1987) for the case of CO on Pt(111). Measured angular distributions for two different incident energies are shown on the right panel of figure 14. These oscillations could be well reproduced by modelling the adsorbate with a hard hemisphere and the surface as a mirror. As for the case of a half-cylinder discussed above, this problem can also be solved analytically in the limit $k_i R_0 \gg 1$, where R_0 is the radius of the sphere; in this case, however, the Fraunhofer contribution decreases with ΔK^{-3}. Best-fit curves are also shown in figure 14. The good agreement with the experimental data demonstrates that the hard hemisphere model correctly describes the essential physics involved. Note that this model is not expected to successfully reproduce the data in the region close to the specular beam, in which the intensity is strongly influenced by the attractive potential. The slight decrease in R_0 with increasing incident energy is consistent with the expected increase in penetration of the He atoms.

These results have stimulated further theoretical studies, which were aimed to clarify the relation between rainbows and Fraunhofer peaks in the angular intensity distribution. The additional non-Bragg maxima were first interpreted by Gerber *et al* (1984) and Yinnon *et al* (1984) as rainbow effects due to the local corrugation caused by the adsorbate. Yinnon *et al* (1988b) found, on the basis of numerically exact and classical trajectory calculations, that peaks due to single- and double-collision rainbows should be present in addition to the Fraunhofer maxima. In typical scattering conditions, Fraunhofer peaks lie nearer to the specular peak, while rainbows occur at higher momentum transfer. These results have been confirmed by Carré and Lemoine (1994), who carried out exact calculations for the three-dimensional diffraction of He from isolated CO molecules on Pt(111). Scattering

† This value had been previously derived by Lapujoulade and Lejay (1977) in a hard-wall analysis of He-diffraction data from copper (113), (115) and (117) surfaces.

distributions were calculated at incident energies between 6 and 12 meV for two different sets of parameters defining the He–CO interaction potential. For both models, the Fraunhofer peaks were found to shift and change in intensity when going from two- to three-dimensional calculations, while rainbow peaks were found to remain almost unaffected. An interesting new result revealed by these calculations was the existence of a threshold energy of 8 meV for the single-collision rainbow. An analysis of the energy dependence of the interference peaks confirmed that: (1) the positions of Fraunhofer peaks remain at fixed ΔK values as the incident beam energy is changed and (2) the rainbow peaks shift to larger ΔK values with increasing incident beam energy. Finally, Carré and Lemoine (1994) proposed that the structures observed by Lahee *et al* (1987) (shown in figure 14) may well have been due only to rainbows, instead of to Fraunhofer diffraction. To clarify this situation, Graham *et al* (1996b) performed a new series of experiments for CO on Cu(001) and incident beam energies between 9.4 and 100 meV. Since the ΔK positions of all observed peaks were found to remain stable in the mentioned energy range, they were attributed to Fraunhofer interferences. On the basis of the good fit obtained with a hybrid eikonal calculation, all observed intensity oscillations were interpreted in terms of reflection symmetry interferences, with no evidence for rainbow structures. At present, the origin of this discrepancy with the theoretical studies of Yinnon *et al* (1988b) and Carré and Lemoine (1994) is not clear. We want to point out, however, that a rigorous comparison between experiment and the mentioned calculations is not possible because the calculations are performed for fixed (mostly, normal) incidence, while in the experiments the incident and final angles are related (usually by $\theta_i + \theta_f = 90^\circ$). The CO/Cu(001) measurements of Graham *et al* (1996b) were recently compared with exact quantum mechanical calculations for a hard hemisphere on a hard flat surface (Choi *et al* 1997). The expected increase of the hard hemisphere radius with decreasing incident energy was determined, in contrast to the inverse trend obtained from hybrid eikonal calculations (Graham *et al* 1996b). The influence of the potential softness and the defect shape in the angular intensity distributions has been investigated by comparing wavepacket calculations with hard-wall results by Drolshagen and Vollmer (1987).

An interesting effect predicted by Yinnon *et al* (1988b) is the occurrence of trapping resonances induced by the presence of isolated adsorbates on surfaces. The He atoms are trapped after hitting an inflexion point on the repulsive wall of the adsorbate, and exit the surface after collision with a second adsorbate. This effect, called rainbow-enhanced trapping, leads to the appearance of additional maxima in the angular intensity distribution and has not yet been observed experimentally, although a closely related effect (DER) was recently reported by Glebov *et al* (1997c).

3.5.2. Substitutionally disordered mixed monolayers. Surfaces which are random or partly random mixtures of two components constitute an important type of disordered systems. The utility of He diffraction for exploring such surfaces was first investigated by Gerber and Yinnon (1991) in a theoretical study of He diffraction from a surface percolation lattice, i.e. a surface that is a periodic, substitutionally random mixture of two components. Angular intensity distributions and lifetimes of scattering resonances were calculated for a Xe + Kr monolayer with different Xe:Kr mixing ratios on a flat surface. The calculations were carried out using the sudden approximation, the validity of which was tested by comparison with wavepacket calculations (see, for example, Yinnon *et al* 1986a, 1988b). The interaction between the scattered atom and the surface was built up as a sum of pairwise He/Xe and He/Kr potentials, which were taken from gas-phase data. As a result, new intensity maxima

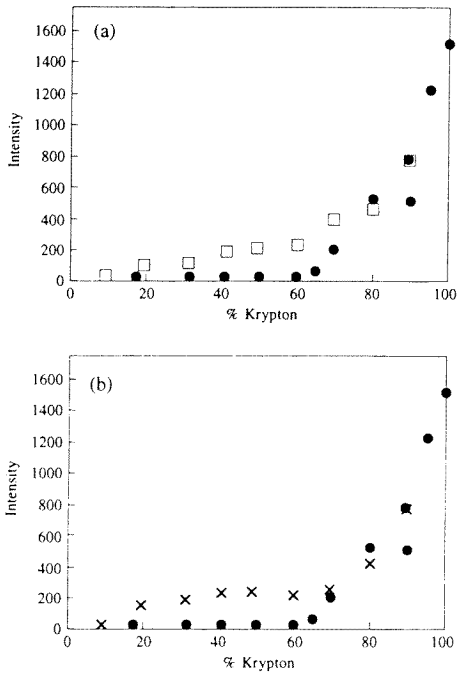

Figure 15. Experimental (●) and theoretical intensities (□, ×) of the (1, 0) diffraction peak versus Xe:Kr mixing ratio. (*a*) □: theoretical results for a structure in which the Xe is nearer to the surface plane than Kr. (*b*) ×: theoretical results for the structure where the Kr atoms lie nearer to the surface plane than Xe atoms. From Yanuka *et al* (1993).

were found at non-Bragg positions, which were identified as Fraunhofer peaks and 'disorder rainbows', since they are entirely due to substitutional disorder. The intensities of these rainbow peaks and, in part, also the positions depend on the Xe:Kr mixing ration of the adlayer, so that they may provide very detailed information on the disordered structures involved. The intensities of the disorder rainbows were estimated at 10^{-4}–10^{-5} of the specular intensity. In view of selective adsorption resonances, it was found that they are sharply sensitive to the percolation thresholds for the mixed monolayer. This effect as well as the disorder rainbows has not been observed experimentally up to now.

The structure of mixed Xe + Kr monolayers on Pt(111) has been further explored in a joint theoretical–experimental study performed by Yanuka *et al* (1993). The approach taken was based on the following three points: (i) Monte Carlo simulations of the structures of the mixed monolayers, (ii) He diffraction calculations from these structures and (iii) comparison with experimental results. Both Monte Carlo simulations and experiment showed that mixed Xe + Kr monolayers are periodic for all Xe:Kr concentration ratios; the lattice constant was found to vary linearly with the Xe:Kr ratio. A very important finding from the Monte Carlo simulations was that the Xe + Kr mixture forms an almost ideal substitutionally disordered system (i.e. the probability of having a Xe or Kr atom at any given site depends only on the concentration ratio, and is independent of the identity of the neighbouring atoms). The fair agreement between the theoretical intensities obtained from these structures and the experimental diffraction intensities for the (1, 0) and the (2, 0) Bragg peaks strongly suggests that the Xe + Kr monolayers have indeed a random substitutional disorder. The results corresponding to the (1, 0) diffraction peak are shown in figure 15. Note that comparable fits are obtained with models which differ only in the relative distance of the Xe and the Kr atoms from the Pt(111) surface, suggesting that the experiment is most sensitive to the lateral structure of the mixed monolayer.

3.5.3. Structurally disordered adlayers. A further step towards establishing He diffraction as a powerful tool in the investigation of surface disorder and epitaxial growth has been made by Gerber and co-workers. A first theoretical study by Hamburger *et al* (1995) demonstrated that compact clusters can be easily distinguished from diffusion-limited aggregates in He-scattering experiments. Calculations performed for compact Pt heptamers on a flat surface have revealed the appearance of characteristic signatures of structure in the angular intensity distributions, mainly rainbow and Fraunhofer peaks, which are absent in the angular distributions from diffusion-limited aggregates. It was also shown that the distribution of adsorbate heights above the metal surface can be easily extracted from an analysis of the specular peak attenuation as a function of incident energy. A Fourier analysis of the observed cross section oscillations yields the height distribution (Hamburger *et al* 1995).

In a more recent theoretical study, Yinnon *et al* (1997) have investigated the sensitivity of the He angular intensity distributions to three basic classes of disordered adlayers: translationally random adsorbates, translationally random compact islands and fractal/dendritic submonolayers. It was shown that a distinction between them can be made on the basis of the different scattering features that characterize the different types of disorder. A comparison with experimental He diffraction data was made for the case of a submonolayer of Ag at 50% coverage on Pt(111). The scattering intensities were calculated using the sudden approximation. The He/Ag adlayer interactions were represented by a sum of pairwise potentials, while the He/Ag adatom interaction was determined by fitting calculated single-adatom cross sections to experimental data over a large range of incident energies. The experimental data are represented by the circles in figure 16; the asymmetry between positive and negative ΔK is a consequence of the scattering geometry, and is thus not reproduced by the calculations. A comparison with the simulations allows one to rule out the fractal and randomly adsorbed adatom models (figures 16(*a*) and (*b*), respectively): the former due to a lack of peak structure for $\Delta K > 3$ Å^{-1}, the latter due to the poor agreement in peak positions. In contrast, fair agreement with the experimental data is achieved with a compact clusters model (figure 16(*c*)); in particular, the peaks near to the specular and the positions and broadening of the Bragg peaks are correctly reproduced. The model consisted of a set of hexagonal islands of two different sizes (seven and nine Ag atoms in diameter) mixed in a ratio 1:4 at 50% coverage. The quantitative agreement with the experimental data can be improved by using a more refined structure to model the adlayer. This was done by Yinnon *et al* (1998), in what turned out to be the first detailed atomic level structure determination of a disordered surface by He diffraction. These results demonstrate that He diffraction is also capable of performing a crystallography of disordered surfaces.

3.6. Phase transitions

The extreme sensitivity of He atoms to different surface phenomena demonstrated in this section suggests a natural extension of this technique to study phase transitions in two dimensions. Work performed by several groups has shown that temperature-induced changes of surface morphology can be determined with great accuracy by measuring the evolution of peak widths and heights. In particular, one of the most clear successes of HAS is to have demonstrated the occurrence of roughening transitions on stepped surfaces. Two excellent reviews about this subject have been recently written by Lapujoulade (1992, 1994), so we will not discuss it further here†. The same can be said of the commensurate–incommensurate

† We should mention here the HAS investigations on the deconstruction and roughening transitions on Pt(110)–(1×2) by Cvetko *et al* (1994c) and Krzyzowski *et al* (1994), as well as the energy-resolved HAS study of Cu(115) by Ernst *et al* (1995), which were published after completion of the last review by Lapujoulade (1994).

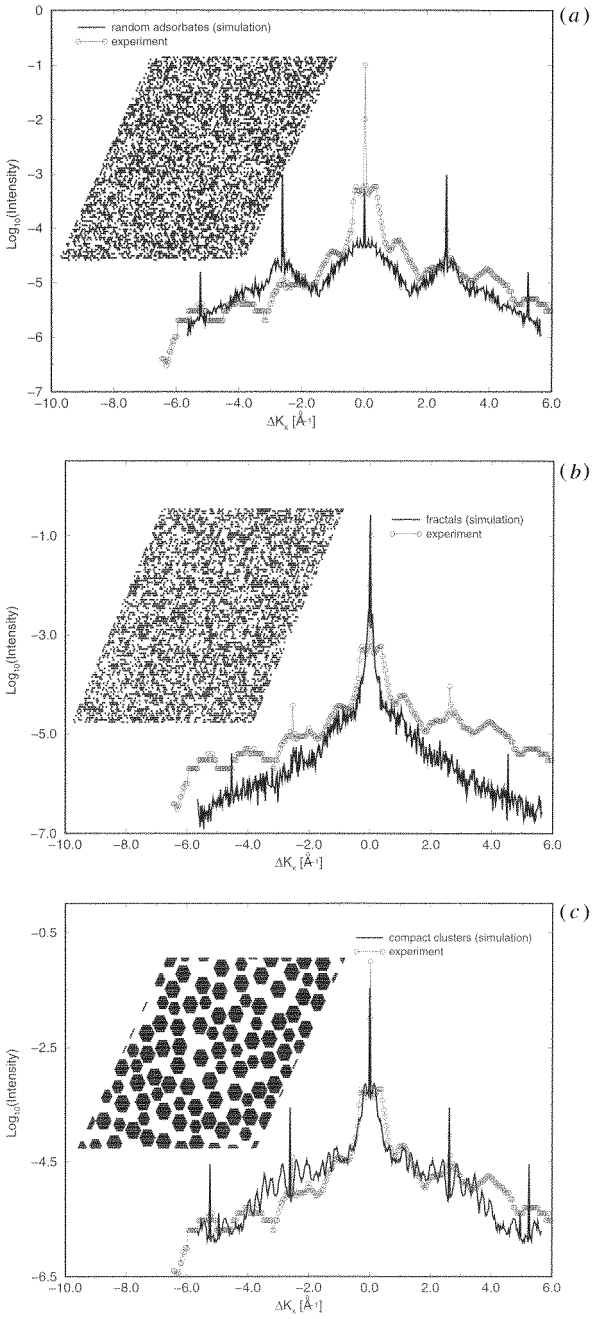

Figure 16. A comparison between experimental (circles) and theoretical (full curves) angular intensities for He scattered from a Pt(111) surface with 50% adsorbed Ag atoms in different disorder classes: (*a*) translationally random atoms, (*b*) fractal islands, (*c*) size-dispersed compact islands. Inset: typical configurations in each of the disorder classes. The orientation of the scattering plane is along the $[11\bar{2}]$ direction in real space. Experimental surface temperature is 38 K and the He beam energy is 21.6 meV. Only the elastically scattered intensity is shown. From Yinnon *et al* (1997).

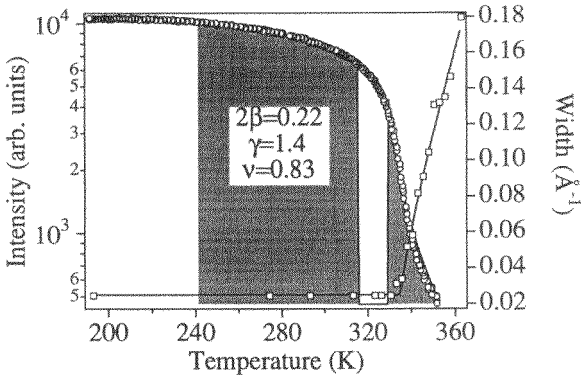

Figure 17. Experimental $(\frac{1}{3}, \frac{1}{3})$ HAS peak intensity (circles) and width (squares) as a function of temperature measured from the CO($\sqrt{3} \times \sqrt{3}$)R30° phase on Rh(111). The fitting curves are indicated as full lines. The white area beneath the intensity best-fit curve at 320 K corresponds to the temperature range $[-a, a]$ in which the finite-size effect affects the critical behaviour. From Over *et al* (1997b).

transition of rare gases on Pt(111) (Comra *et al* 1992) and the reconstructions observed on clean Au(111) and W(100) surfaces, which have been reviewed by Kern and Comsa (1989). Therefore, we shall limit ourselves to review HAS studies of order–disorder and order–order phase transitions, a field which in our opinion has received much less attention.

3.6.1. Order–disorder transitions. Most HAS investigations of order–disorder phase transitions on surfaces have been reported by the group of Tommasini in Trieste. In this section, we will discuss the results concerning the temperature behaviour of the Rh(111)–CO($\sqrt{3} \times \sqrt{3}$)R30° system, which have been reported in a combined HAS and LEED study (Over *et al* 1997b). The method consists basically of measuring temperature-dependent He peak intensities and profiles of fractional-order beams, from which the critical exponents are obtained after fitting the experimental data with an appropriate model. For the mentioned adlayer, the data corresponding to the ($\sqrt{3} \times \sqrt{3}$)R30° to (1 × 1) order–disorder transition are shown in figure 17. The measurements were performed with an apparatus characterized by a fixed deflection angle of 110° and an angular resolution of 0.135°. The FWHM of the profiles were evaluated by using a Gaussian profile far below the critical temperature and a Voigt profile near and above T_c. The $(\frac{1}{3}, \frac{1}{3})$ diffraction peak broadening observed with increasing temperature was fitted by a power law of the reduced temperature $t = [(T - T_c)/T_c]^{\nu}$. The best-fit parameters were found to be $T_c = 330 \pm 5$ K and $\nu = 0.83 \pm 0.01$, in excellent agreement with predictions according to the 3-state Potts model ($\nu = \frac{5}{6}$). In view of the temperature dependence of the half-peak intensity shown in figure 17, it depends on both the critical behaviour of the transition and on the Debye–Waller attenuation. The last effect was determined by fitting the temperature dependence of the peak intensity in the low-temperature range. Finally, the corrected peak intensity was fitted using the expression:

$$I(T) = \begin{cases} A|t|^{2\beta} + B_-|t|^{-\gamma} + C_- & t < -a \\ D & |t| < a \\ B_+|t|^{-\gamma} + C_+ & t > a. \end{cases} \tag{3.12}$$

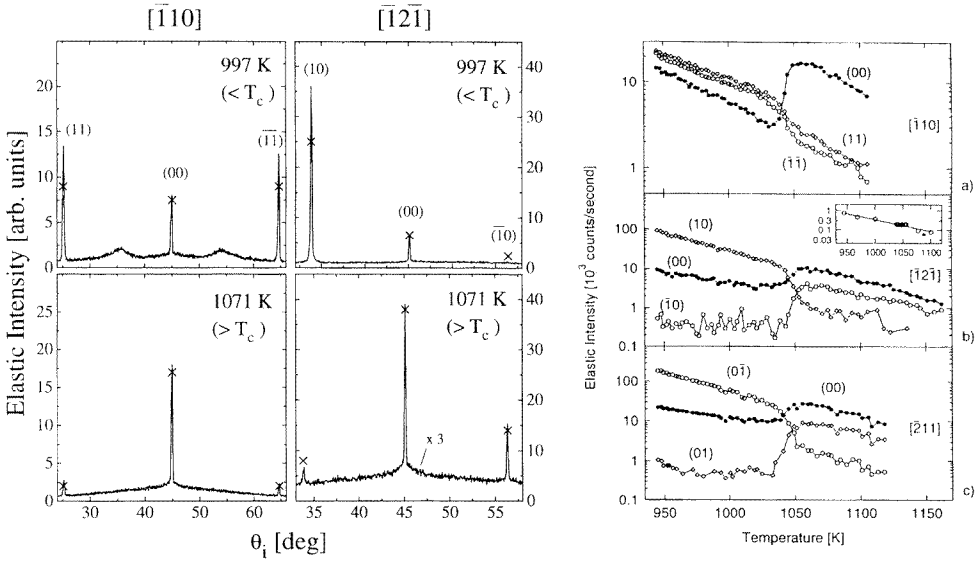

Figure 18. Left: angular distributions from He scattered from Ge(111) at temperatures below and above $T_c = 1050$ K; He energy is 22 meV. Right: temperature dependence of areas measured for the specular and first-order diffraction peaks shown on the left, scanned along three principal directions. The inset in (*b*) shows temperature dependence of incoherent elastic intensity measured at $\theta_i = 52.2^\circ$. From Meli *et al* (1995).

The temperature range in which finite-size effects alter the critical behaviour is indicated by the white area around 320 K in figure 17. It was found that the values of β, γ and T_c do not change for $a > 0.02$. The critical exponents $2\beta = 0.22 \pm 0.01$ and $\gamma = 1.2 \pm 0.3$ determined by the fitting procedure are in excellent agreement with the predicted values for the 3-state Potts model of $2\beta = 0.22$ and $\gamma = 1.44$.

A similar study reported by this group has revealed that the order–disorder transition of the Rh(111)–(2×2)O phase at $T_c = 280 \pm 5$ K falls into the universality class of the 4-state Potts model (Over *et al* 1997a), whereas the (2×2)p2mg to (1×2)O transition on Rh(110) belongs to the two-dimensional Ising class (Bellman *et al* 1993a). Further investigations of the Trieste group include a very detailed study of the transformation of the metastable (1×2)Rh(110) missing row reconstruction into the (1×1) equilibrium structure (Cvetko *et al* 1994b) as well as investigations of the disorder–order evolution of surface defects on InSb(110) (Cvetko *et al* 1994a, 1995a–c).

3.6.2. Order–order transitions. Structural phase transitions on semiconductors at high temperatures have been intensively investigated using HAS in the group of Greene. These experiments include studies of the phase transitions on the Ge(111) surface at 550 K (Ha and Greene 1989b), on the Ge(100) surface above 600 K (Meli and Greene 1994), as well as on the (111) and (100) surfaces of Si near 1000 K (Ha and Greene 1989a). The transitions observed on Ge(111) and Si(111) above 1000 K have been re-investigated in collaboration with the Toennies group using high-resolution HAS (Meli *et al* 1995, Lange *et al* 1997, respectively). In what follows we will describe in some detail the results reported for the order–order transition on Ge(111) near 1050 K (Meli *et al* 1995).

Figure 18 shows angular distributions of the elastic scattered intensity at temperatures

below and above $T_c = 1050$ K along $[1\bar{1}0]$ and $[11\bar{2}]$. The observation of only sharp, integral-order diffraction peaks above T_c demonstrates the persistence of long-range (1×1) order in the first bilayer. The occurrence of an order–disorder phase transition, as suggested on the basis of other experiments, can be clearly ruled out, since vacancy proliferation would lead to a strong attenuation of the specular peak and an increase in the incoherent scattered intensity which was not observed (see the inset in figure 18(*b*)). The fact that the fractional-order beams disappear at lower temperatures along $[11\bar{2}]$ than along $[1\bar{1}0]$ indicates that delocalization of the adatoms proceeds via correlated diffusion along $[1\bar{1}0]$. For increasing temperature, the diffraction peaks show the usual Debye–Waller exponential decrease due to thermal attenuation. This can be seen on the right panel of figure 18, where the intensities of some integer-order peaks along the main symmetry directions are shown as a function of temperature. With respect to the surface structure above T_c, the significant increase of the specular intensity is consistent with the metallization of the top bilayer observed in a previous EELS study (Modesti *et al* 1994). The presence of diffraction peaks suggests that the metallic state is localized at the surface; otherwise, a smoother surface would be expected, with spectra more similar to those seen in HAS studies of (111) metal surfaces. A quantitative analysis of the elastic intensities shown in figure 18 has been performed by Farías *et al* (1997c). An important result of this study was that the asymmetry reversal observed along $[11\bar{2}]$ for $T > T_c$ actually reflects the occurrence of a similar reversal in the structure of the surface, which cannot be reproduced by a simple reduction of the top bilayer spacing as previously suggested (Lange *et al* 1997).

The results shown in figure 18 demonstrate that, owing to its high-sensitivity and nondestructive character, HAS is especially well suited to investigate phase transitions at high temperatures. Another good example of this is provided by the diamond C(111)–(1×1)H surface, on which the transition to the hydrogen-free (2×1) π bonded chain structure was observed to occur at 990 K by HAS (Schaich *et al* 1997), well below the temperature of ∼1200 K determined in a previous LEED study by Hamza *et al* (1988). From an analysis of the temporal evolution of diffraction peak intensities for different substrate temperatures, Schaich *et al* (1997) were also able to determine the kinetic parameters for the hydrogen desorption process.

4. TEAS nucleation and growth studies

4.1. Diffusion and nucleation of adatoms on surfaces

4.1.1. CO/Pt(111): microscopic diffusion. As mentioned in section 2.5, the cross section for diffuse He scattering from a step Σ_{step} can be seen as a ∼10 Å wide strip along the step edge contour (Verheij *et al* 1985), whereas ∼100 Å can be considered a typical value of Σ_A for adsorbates. Therefore, if adsorbates can migrate and eventually stick to some defect sites, they will affect the reflectivity of the surface only with that fraction of Σ_A which has not overlapped with Σ_{step}. This fraction is in general much smaller than the nominal cross section Σ_A of the adsorbate determined on a defect-free surface. This is nicely illustrated in figure 19 (left) for the CO/Pt(111) system. Both adsorption curves have been measured at $T_s = 293$ K: (a) on a defect-free surface (×), (b) on one with a high defect density (□). Curve (b) exhibits a 'two-phase' behaviour: in the first phase, the CO molecules move from the (111) terraces (where they initially adsorb) to the step sites, where they bind more strongly and 'lose' a fraction of their nominal cross section Σ_A. When the defect sites become saturated, there is a crossover to the second phase, whose behaviour is similar to that of a defect-free surface. However, at $T_s = 107$ K (black

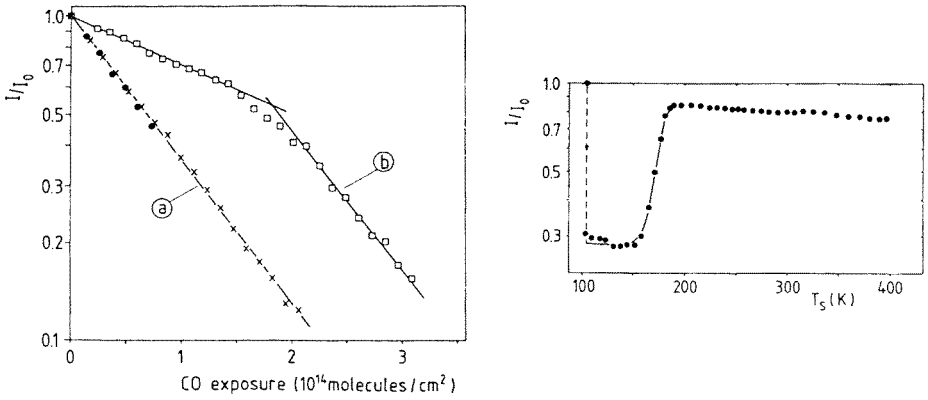

Figure 19. Left: relative He specular intensity as a function of exposure for CO/Pt(111). The data have been recorded with a 63 meV He beam incident at $\theta_i = 40^\circ$ on a 'perfect' surface (defect concentration ∼0.001) at $T_s = 293$ K (×), and on a surface with a high density of defects at $T_s = 293$ K (□) and $T_s = 107$ K (●). Right: Evolution of the relative He specular intensity as a function of temperature after deposition of ∼0.06 ML CO at $T_s = 107$ K on the surface with defects. ($I = I_0$ corresponds to the clean surface.) The data are corrected for Debye–Waller effects. From Poelsema *et al* (1982b).

dots in figure 19 (left)) the behaviour on the surface with defects is identical to that on the defect-free surface at $T_s = 293$ K. This demonstrates that the CO molecules have a very low mobility at $T_s = 107$ K, staying in consequence randomly distributed on the surface instead of migrating to defect sites. A new application of TEAS is suggested by these results: the *titration* of defects. This allows us to determine the step density on the surface from the position of the kink in curve (b). For example, assuming that one CO molecule is bound per step atom, a density of step atoms $\theta_d = 0.1$ is obtained. This procedure is very helpful when studying growth phenomena, as discussed in section 4.2.

The different behaviour observed on the surface with defects at $T_s = 293$ K and $T_s = 107$ K suggests a method to measure the surface migration of admolecules. The method consists of adsorbing a small number of CO molecules at a temperature low enough to ensure that they are immobile. Then the surface is heated linearly whereas the reflected specular intensity is monitored. As soon as the CO molecules become mobile, they migrate from terrace to step sites. Due to the overlap of Σ_A and Σ_{step} discussed above, a drastic increase of the specular intensity is observed: this corresponds to a vertical change from curve (●) to (□) in figure 19 (right). The onset of CO diffusion at ∼170 K is obvious. The fit (full curve) corresponds to a simple hopping model, from which an activation energy for diffusion of 7 kcal mol^{-1} is obtained (Poelsema *et al* 1982c).

4.1.2. CO/Pt(111): macroscopic diffusion. Diffusion of adsorbates over macroscopic distances on single-crystal surfaces can also be measured with TEAS using a new method recently developed by Croci *et al* (1993). Basically, molecules are deposited on a small spot on the sample and afterwards, the specular He intensity scattered from the same surface spot is recorded as a function of time. Diffusion of the adsorbed molecules outside of the measuring spot causes an increase of the specular intensity; from the shape of this curve, the diffusion parameters are easily obtained. Results of such an experiment for the CO/Pt(111) system are shown in figure 20. A small diaphragm of 0.5 mm diameter is placed near the surface and perpendicular to the surface, so that by choosing an angle of

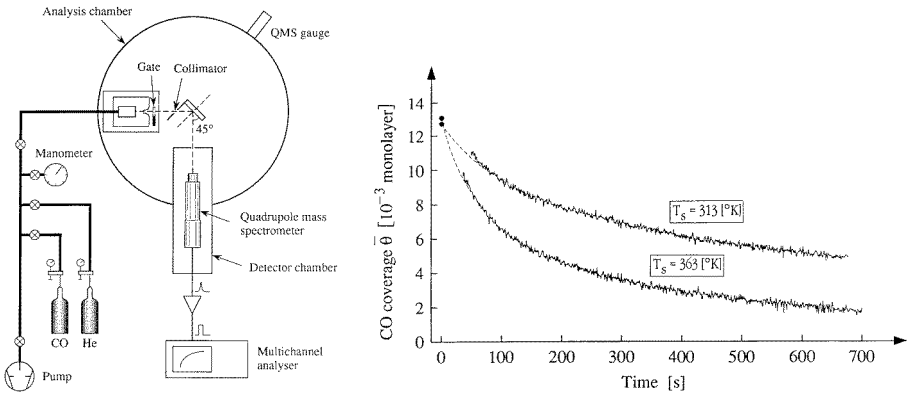

Figure 20. Left: experimental set-up used by Croci *et al* (1993) to measure macroscopic diffusion parameters. Right: evolution of a diffusion measurement at two different temperatures (note that the specular He intensity has been converted into CO coverage).

incidence of 45° only a small circular spot is seen by the He beam. Upon these conditions, a reference signal corresponding to zero CO coverage is recorded. The He beam is then shut down and seeded with ∼1% of CO molecules. Deposition proceeds by turning on the seeded He beam, which is turned off when the attenuation reaches the value corresponding to a coverage Θ_0 of 0.01 ML (the reflectivity versus coverage curve is calibrated in an independent experiment using the method described in section 2.5). Since the deposition time is short compared with the characteristic diffusion time t_D, the time at which the seeded beam is shut down can be taken as the time at which diffusion of the deposited molecules begins. The gas line is then quickly cleaned and the temporal evolution of the specular intensity is recorded with a pure He beam. Diminution of the average coverage $\bar{\Theta}(t)$ on the measured surface spot causes the observed increase of specular intensity (that this effect is not caused by desorption of CO molecules was checked in a control experiment). Similar measurements are performed for different surface temperatures between 273 and 373 K; two of these curves are also shown in figure 20. The experimental data for $\bar{\Theta}(t)$ at a given surface temperature are well reproduced by a simple model, from which an activation energy for diffusion of 6 kcal mol^{-1} is obtained. The method has been also applied to study the diffusion of NO on Pt(111); in this case, an activation energy of 11.8 kcal mol^{-1} is obtained (Croci *et al* 1994).

4.1.3. Diffusion of Cu on Cu(100). Another method to determine diffusion coefficients at surfaces using TEAS has been developed by Ernst *et al* (1992b). The approach relies on measuring the island number density as a function of surface temperature, a quantity which can be related to the migration coefficient using nucleation theory (Venables *et al* 1984). This method was first applied by Lagally and co-workers to study surface diffusion using STM (Mo *et al* 1991). In the case of TEAS, the number density of islands is determined by measuring diffraction beam profiles as a function of time at different temperatures. A series of angular distributions measured in the out-of-phase condition during deposition of Cu on Cu(100) are shown in figure 21. A special feature of these spectra is that, whereas the specular intensity decreases (as expected) with increasing coverage, additional diffraction peaks appear whose intensities increase with coverage. This effect is well known from previous LEED studies performed by Henzler and co-workers, which showed that the

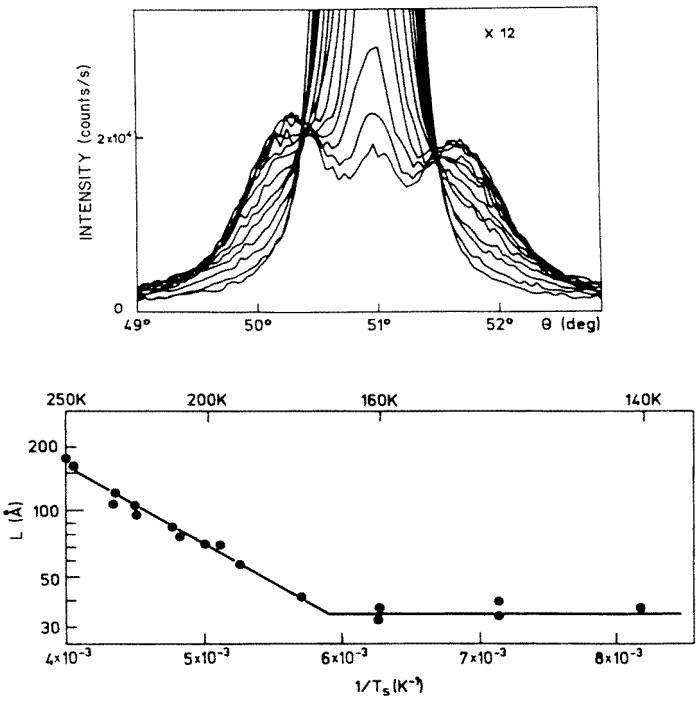

Figure 21. Top: angular distributions (taken in the out-of-phase condition) as a function of time during Cu deposition on Cu(100) at 210 K and a rate of 2700 s ML^{-1}. Each scan takes 104 s. $\theta_i = 51^\circ$ corresponds to the specular beam. Bottom: variation of the mean separation L between islands as a function of temperature. From Ernst *et al* (1992b).

angular position of these peaks can be associated to a characteristic length L on the surface (Hahn *et al* 1980). For the data shown in figure 21, note that the angular position of these peaks is independent of coverage up to 0.7 ML. Based on simulations performed within the kinematical approximation, the length L can be ascribed to the periodicity imposed by large islands formed at the beginning of the growth process, i.e. during the so-called transient regime (Ernst *et al* 1992b). L is related to the number density of stable nuclei N_x by $L = 1/[N_x]^{1/2}$. The relationship with the migration coefficient is given by (Venables *et al* 1984)

$$N_x = f(\Theta, i)R^p \exp(E_n/kT) \tag{4.1}$$

where R is the deposition rate, i is the number of atoms in the critical nucleus, $p = (i+1)/(i+3)$, $E_n = [E_i + (i+1)E_d]/(i+3)$, E_i is the binding energy of the critical nucleus, E_d is the activation energy for diffusion and $f(\Theta, i)$ is a function of coverage and specific material parameters. Figure 21 shows the dependence of L with inverse temperature. Experiments performed at fixed temperature showed that the characteristic length L varies as $R^{-1/4}$, indicating that $i = 1$; however, a re-investigation of this system by high-resolution LEED revealed that $i = 2$ at low-deposition flux (Zuo *et al* 1994; see also Brune 1998). Thus, with $p = \frac{1}{3}$ and using (4.1), an activation energy of $E_d = 0.42$ eV is finally obtained, which agrees well with the value of 0.40 eV determined previously from an analysis of step density using TEAS (de Miguel *et al* 1987) and is close to the value of 0.43 eV calculated within the effective-medium theory by Hansen *et al* (1991). An interesting feature of the method developed by Ernst *et al* (1992b) is that it is not even restricted to He-scattering, but

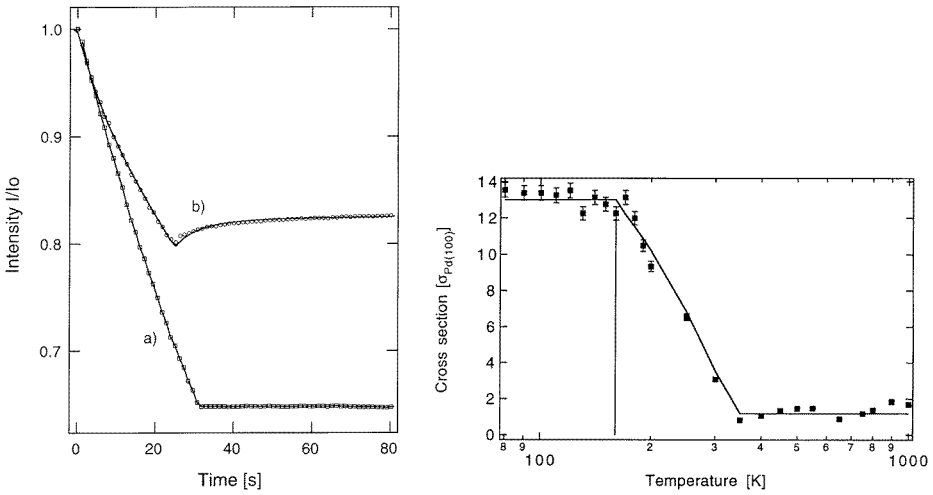

Figure 22. Left: He specular intensity from Pd(100) during the deposition of Ag atoms on a surface at 80 K (curve (a)) and 215 K (curve (b)). The Ag flux is started at $t = 0$ and stopped after ∼30 s. Right: cross section for diffuse scattering as a function of surface temperature. After Félix *et al* (1995) and Vandoni *et al* (1994a).

may also be applied with other surface diffraction techniques as demonstrated by the high-resolution LEED measurements of Zuo *et al* (1994). Determination of diffusion constants based also in (4.1) have been reported by Rosenfeld *et al* (1995) for Ag on Ag(111). In this case, however, the island density at different temperatures was determined by means of (2.29). Cvetko *et al* (1995a, b) have more recently applied this method to study the nucleation and growth of vacancy islands on InSb(110) during low-energy ion bombardment. They have shown that the models developed for the case of growth by deposition also apply to the inverse growth processes. In the case of InSb(110), the critical nucleus for nucleation of vacancy islands is a single dimer; the corresponding activation energy for diffusion was found to be $E_d = 1.14 \pm 0.06$ eV. A study of the time evolution of vacancy islands formed by ion bombardement showed that islands grow according to dynamical scaling during the sputtering process, while the statistical distribution of terraces changes gradually during the recovering at fixed surface temperature (Cvetko *et al* 1995c).

4.1.4. Diffusion of Ag on Pd(100). Another novel application of TEAS has been recently developed by Monot and co-workers. It enables us to study the dynamics of nucleation and growth of metals on metals, and in particular the determination of surface diffusion parameters. In this section we will discuss briefly the results obtained for the Ag/Pd(100) system (Vandoni *et al* 1994a, Félix *et al* 1995, 1996). Deposition curves as a function of time are shown in figure 22 (left) for two different surface temperatures. The Ag flux is started at $t = 0$ and stopped after ∼30 s (which corresponds to a coverage of 0.02 ML). One sees that the specular He intensity remains constant from this time on in curve (a) (recorded at 80 K) whereas an intensity increase is seen in curve (b), recorded at a higher surface temperature. This points to a higher mobility of the adatoms at 215 K, leading to the formation of larger clusters and therefore to an increase of the reflected He signal. This point is even more evident in figure 22 (right), where the cross section for diffuse scattering is plotted as a function of the deposition temperature. These values were determined from

the initial slope of different deposition curves using (2.26), and are expressed in units of the Pd(100) unit cell ($\sigma_{\mathrm{Pd(100)}} = 7.56$ Å^2). The constant cross section below 160 K indicates that, in the timescale of the experiment (∼10 s), the surface morphology does not change with temperature. In section 4.1.5 we will show that much can be learnt about the first steps of nucleation and growth of Ag adatoms from an analysis of deposition curves in this region. Obviously, measurements between 160 and 250 K are essential to determine diffusion parameters. Quantitative information is obtained by calculating I/I_0 at a given surface temperature using (Poelsema and Comsa 1989, Vandoni *et al* 1994a)

$$\frac{I}{I_0}(\Theta) = \left[1 - \sum_i \sigma_i n_i(\Theta) - \sigma_{\mathrm{step}} n_{\mathrm{step}}(\Theta)\right]^2 \tag{4.2}$$

where n_i is the number of clusters containing i atoms and n_{step} is the number of atoms condensing on steps. The corresponding cross sections σ_i and σ_{step} are obtained assuming that the overlap approach discussed in section 2.5.1 is valid and that the Ag adatoms only occupy fcc adlayer sites on Pd(100) (this is well justified since the growth of Ag begins with two epitaxial monolayers (Félix *et al* 1996)); σ_1 is defined as the 'lattice gas' cross section, i.e. the value measured at low temperatures and very low coverages. The crucial point to evaluate I/I_0 from (4.2) is the calculation of the cluster size distribution $n_i(\Theta)$. This is done by using a rate equation approach for the n_i up to a size $i = 6$, which is justified at low coverages. The mobility of adatoms and clusters is modelled by a simple hopping model. The experimental data are finally fitted by varying the hopping frequencies ν_i. In the case of Ag/Pd(100) and assuming that clusters larger than the dimer are immobile, excellent agreement with the experiment is obtained with ν_1 and ν_2 as the only free parameters (full curves in figure 22). From an Arrhenius plot of $\ln\nu_1$ versus $1/T_s$, an activation barrier for diffusion of adatoms $E_{d1} = 0.37 \pm 0.03$ eV is obtained, the corresponding hopping frequency being $\nu_0 = 8 \times 10^9$ s^{-1}. This value of E_{d1} compares well with $E_{d1} = 0.42$ eV obtained by molecular dynamics calculations (Sanders and DePristo 1992). An important result of these studies is that the dimer has a much lower mobility than the monomer; ν_2 was found to be about 30 times smaller than ν_1. For a more detailed description of the method, the reader is referred to the original works by Félix *et al* (1995, 1996).

More recently, this group has also applied TEAS to the characterization in real time of Ag_7 clusters deposited on Pd(100) (Vandoni *et al* 1994b, 1996). The method consists basically of measuring the change of the cross section Σ as a function of temperature for deposition of clusters of different kinetic energy. A comparison with Σ values for isolated Ag atoms and compact Ag_7 clusters provides evidence for fragmentation and damage creation on the surface.

4.1.5. Neighbour-driven mobility of Ag on Pd(100). The method just described has also been applied to the study of the very first steps of nucleation and growth of metal on metals. To do that, the whole shape of a deposition curve at very low coverages is modelled by simulating the size distribution of the adatoms with a nucleation model. We will illustrate the principle of the method with the system Ag/Pd(100). Vandoni *et al* (1994a) and Félix *et al* (1996) have shown that the deposition curves obtained at temperatures below the threshold of adatom mobility (160 K) cannot be fitted with the lattice-gas formula (2.26). Attempts to simulate these curves have been made by using two different models. The first one is the so-called *transient mobility model*, which postulates that the incoming atoms convert their thermal energy into kinetic energy parallel to the surface and then perform n random steps until they cluster. Monte Carlo simulations show that six random hops are nedeed in order to fit the experimental data. This large value of n is unrealistic, indicating

that another mechanism must influence the mobility of the Ag adatoms. This mechanism is revealed by fitting the experiment using the *neighbour-driven mobility model* (Vandoni *et al* 1994a), which assumes that the potential around an adatom or cluster is modified so that all incoming adatoms landing within this 'capture zone' move to form a dimer or enlarge the cluster. Very good agreement with the measurements is obtained by assuming a 'capture zone' of one unoccupied lattice site, i.e. a zone of ∼6 Å around an adatom. This *neighbour-driven mobility* is very similar to the one reported by Wang and Ehrlich (1993) for Ir clusters on Ir(111), although in the case of Ag on Pd(100) a single adatom seems to be sufficient to modify the potential seen by an incoming adatom. From the point of view of the applications of TEAS, an interesting result is that much insight into microscopic processes can be gained by modelling deposition curves, which are easily measured.

4.1.6. Nucleation and growth of Pd on MgO(100). A powerful method to study the nucleation and growth of three-dimensional metallic clusters on a crystalline substrate by means of TEAS has been developed by Henry *et al* (1993) in recent years. The method enables us to monitor *in situ*—under UHV and in real time—the nucleation and growth kinetics of the metal clusters. The only additional information needed is the final size distribution of the clusters, which is determined in an *ex situ* transmission electron microscopy (TEM) measurement. This method represents an enormous progress compared with classical TEM nucleation studies, which always require a new sample to record a single data point. In what follows, the results obtained for the deposition of Pd clusters on MgO(100) at different temperatures will be discussed. Figure 23 shows the attenuation of the diffracted (11) beam as a function of time during the growth of Pd clusters at 160 and 290 °C. The (11) beam is monitored instead of the specular to be sure that no coherent contributions from the Pd clusters are recorded. Two regimes are clearly seen in these curves. The first regime corresponds to a nucleation and growth period. The change of the slope after 100 s indicates that the saturation density of clusters n_s has been reached; from this point on, only cluster growth occurs. According to the definition of the cross section (2.24) and assuming that the cluster shapes are squares of side $D(t)$ (as observed with TEM), the attenuation A(t) of the (11) beam is

$$A(t) = 1 - I(t)/I_0 = n(t)[D(t) + 2\delta]^2 \tag{4.3}$$

where $n(t)$ is the time-dependent density of clusters and δ the width of the diffuse scattering band around the clusters. From a TEM measurement of the final deposit, n_s and the corresponding D_s are determined; thus, using (4.3) the value of δ could be estimated: ∼10 Å. It was found that this value does not depend either on the temperature (in the range 127–370 °C) or on the cluster size. The growth law is then easily derived by inversion of (4.3); the result is shown in figure 23(*c*). One sees that the mean size of the clusters follows the power law $D(t) = D_0 t^p$. The fits shown in figure 23 were obtained with $p = 0.27$, very near to $\frac{1}{3}$ which is the value predicted for three-dimensional growth by capture of migrating adatoms. Finally, the nucleation kinetics is obtained from (4.3) by assuming that the previously derived growth law is also valid at the beginning of condensation. The results are also shown in figure 23(*b*). The data are better fitted with a point defect nucleation model (full curves in figure 23) than with a random nucleation model (Meunier and Henry 1994). Finally, we note that the n_s and D_s values could be in principle determined from an analysis of the specular intensity as a function of time taking into account the reflectivity of the Pd clusters, as described by Poelsema and Comsa (1989). This example shows nicely how TEAS can be successfully applied to the quantitative study of nucleation and growth of metals on ionic crystals. Both the nucleation and growth rates are obtained in

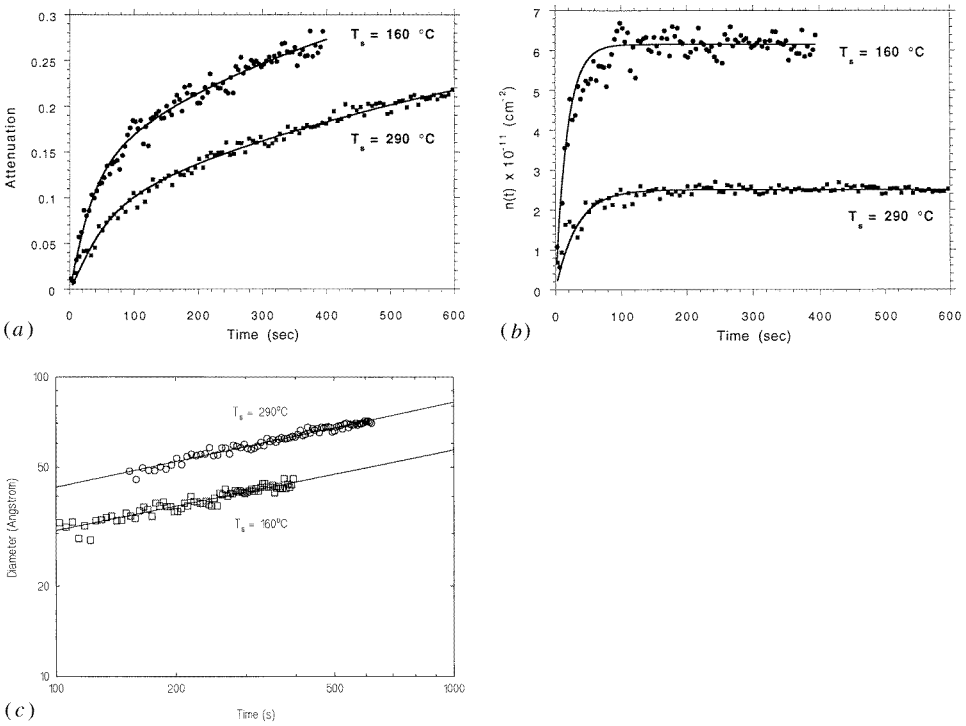

Figure 23. (*a*) Attenuation of the (11) diffraction beam during the growth of Pd clusters on MgO(100) at 160 and 290 °C. The full curves correspond to the best fit obtained with (4.3). (*b*) Nucleation and (*c*) growth kinetics of Pd clusters on MgO(100) at 160 and 290 °C. The full curves correspond to the best fit with analytical laws (see text). From Meunier and Henry (1994).

a single experiment, which represents an enormous improvement compared with classical TEM nucleation studies in which every data point must be measured with a new sample (see also Henry and Meunier 1996).

4.1.7. Dynamical scaling. Further interesting investigations of the growth of Cu on Cu(100) have been reported by the Saclay group (Ernst *et al* 1992c, 1994). An important result was the observation of dynamical scaling in spinodal decomposition in a two-dimensional system. The system was realized by adsorbing 0.5 ML Cu on Cu(100) at 100 K, i.e. at a temperature where thermally activated diffusion is inhibited. The surface temperature is then rapidly raised and held at a higher value, at which the kinetics of domain growth is monitored by measurements similar to those depicted in figure 21. Analyses performed for different temperatures revealed that the morphology of the system evolves in a self-similar form, i.e. that the functional form of domain pair correlations does not change with time (Ernst *et al* 1992c). Such a behaviour has been also observed for the growth of Pb islands on Cu(100) by Vidali and co-workers (Li *et al* 1993, Zeng and Vidali 1995). In a later experiment, the growth exponents associated with the dynamical scaling hypothesis have been determined (Ernst *et al* 1994). It was found that the width of the interface w grows as $w \propto t^{\beta}$ with $\beta \sim 0.5$ at 200 K and $\beta \sim 0.25$ at 160 K, whereas the correlation length ψ parallel to the surface scales as $\xi \propto t^{\beta/\alpha}$ with $\alpha \sim 1$. Similar experiments

performed by Zeng and Vidali (1995) for Pb on Cu(100) showed that $\beta \sim 0.3$ until 40 ML, changing to $\beta \sim 0.05$ for larger coverages and $\alpha \sim 1$. For Cu on Cu(100), an analysis of step correlations revealed that 'pyramid-like' structures appear on the surface, whose sides are composed of (113) and (115) facets for deposition at 160 and 200 K, respectively. This instability had been predicted by new growth models, which take into account an asymmetry in the vertical and horizontal mobility of adatoms originated by an excess energy barrier to diffusion at step edges. Further details can be found in the original work by Ernst *et al* (1994) and references therein. More recently, this group has also reported experimental evidence for the existence of a Bales–Zangwill instability during homoepitaxial step flow growth on Cu(115) and Cu(1,1,17) (Schwenger *et al* 1997).

4.2. Growth of thin films

The first application of TEAS to investigate metal-on-metal growth has been reported by Gómez *et al* (1985) for the system Cu/Cu(100). As in the case of RHEED, the method is based on the observation of diffraction intensity oscillations as a function of coverage. Although RHEED is perhaps the most widely used technique in MBE studies, it is known that the interpretation of the results is usually complicated by the existence of multiple scattering processes. In this sense, a major advantage of TEAS is its high sensitivity to step distributions on the topmost surface layer, which allows a simple interpretation of the data. The evolution of the defect density during growth is revealed by in-phase measurements of the specular beam (as defined in section 2.5.2), whereas the interference between terraces is revealed by the out-of-phase data. In addition, both in-phase and out-of-phase peak intensities are reduced by diffuse scattering due to defects on the surface. A more detailed discussion on the different information which can be gathered from the in-phase and out-of-phase oscillations has been given by Poelsema *et al* (1992) and Xu *et al* (1991). In the case of heteroepitaxial systems, Hulpke *et al* (1996) have recently shown that a damping of the oscillations may not only be caused by accumulation of defects on the surface, but also by thermal attenuation caused by the layer-dependent Debye–Waller factor (see also the discussion at the end of section 3.3).

Some useful formulae are those derived for the two extreme cases of ideal two- and three-dimensional growth within the kinematic approximation. For the case of ideal two-dimensional growth, the specular intensity measured upon out-of-phase condition is expected to vary as (Poelsema and Comsa 1989)

$$\frac{I}{I_0} = (1 - 2\Theta)^2 \tag{4.4}$$

where Θ is the coverage of the growing layer. Despite the fact that an ideal two-dimensional behaviour does not exist on real surfaces (except for the step flow regime), two-dimensional like growth can be inferred from the observation of intensity oscillations as a function of deposition time. In the case of ideal three-dimensional growth (i.e. growth where interlayer mass transport is hampered), it can be shown that the uncovered fractional areas of the growing layers have a Poisson distribution. The corresponding attenuation of the specular intensity is given by (Poelsema and Comsa 1989)

$$\frac{I}{I_0} = \mathrm{e}^{-4\Theta}. \tag{4.5}$$

where Θ denotes the total coverage of the growing layers. This means that a monotonic decay of the specular intensity is expected for three-dimensional like growth. A good example of the different behaviours observed for two- and three-dimensional growth is

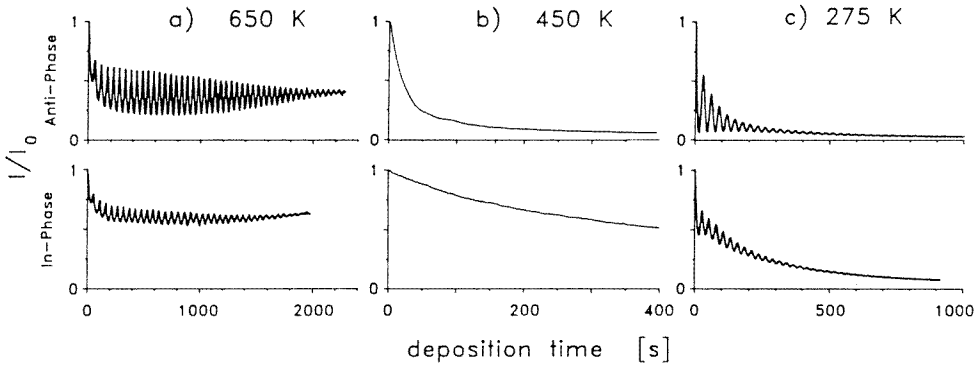

Figure 24. Temporal behaviour of the antiphase (upper curves) and in-phase (lower curves) normalized He-specular peak height during Pt deposition. The deposition rates are 0.018 ML s^{-1} in (*a*) and (*b*), and 0.037 ML s^{-1} in (*c*). From Poelsema *et al* (1992).

given by the homoepitaxial growth on Pt(111), as shown in figure 24. At 650 K, the observed oscillations reveal two-dimensional growth, whereas three-dimensional growth can be inferred from the intensity decay observed at 450 K. More interesting is the high-temperature 're-entrant' layer-by-layer growth below 340 K, which has been actually discovered by TEAS (Kunkel *et al* 1990, Poelsema *et al* 1991).

Actually, (4.4) and (4.5) were derived by Poelsema and Comsa for the case of layer-by-layer removal during ion bombardment, the inverse process of epitaxial growth. Oscillations of the antiphase peak height as a function of ion fluence during sputtering have been first observed on Pt(111) by Poelsema *et al* (1984). More recently, results obtained on InSb(110) and InSb(100) have been reported by Cvetko *et al* (1995a–c) and (1996), respectively. Besides the natural extension to the study of crystal growth, two new applications of TEAS have been derived from these results: (a) a simple and accurate method to determine sputtering yields and (b) a procedure to prepare *in situ* surfaces with any desired defect density. These subjects are treated in great detail in the book by Poelsema and Comsa (1989), and will not be further discussed here.

It is our intent to review in this section all investigations of thin films growth made using TEAS up until now. A list with all studied systems is presented in table 4. It is clear that, due to obvious space limitations, only a few systems can be discussed exhaustively. Some representative examples are described in the following sections.

4.2.1. Cu on Cu(100). In their pioneering work, Gómez *et al* (1985) studied the nucleation and growth of Cu(100) from its vapour (see also de Miguel *et al* 1987). Using an antiphase scattering geometry, intensity oscillations of the specular beam have been observed, although in a limited temperature range (between 265 and 365 K). These oscillations demonstrate layer-by-layer growth via nucleation and formation of islands on terraces. However, the fact that the amplitude of the oscillations decreases with increasing coverage indicates that the layer-by-layer growth is not perfect, i.e. growth of a new layer begins before the previous one is completed. At $T > 365$ K, no change in the specular intensity was observed, indicating that the step density remains constant within the transfer width of experiment (500 Å). This suggests that above this temperature the diffusion of deposited adatoms is so fast that they are captured by pre-existing steps (step flow mechanism), as confirmed by Monte Carlo simulations of the growth process (de Miguel *et al* 1988b). Another important result of

Table 4. Growth studies performed with TEAS.

System	Temperature (K)	Remarks	Reference
Cu/Cu(100)	265–365		Gómez *et al* (1985), de Miguel *et al* (1988a, b)
	100–400	dynamical scaling	Ernst *et al* (1992a, c)
Co/Cu(100)	387–500	+ LEED study	de Miguel *et al* (1989)
	270–418	+ UPS, neutron diffraction	de Miguel *et al* (1990)
Pb/Cu(100)	300–600	heat of vaporization	Sánchez *et al* (1987)
	150–400	quantum size effects	Zeng *et al* (1994)
Hg/Cu(100)	150–300	up to 1 ML	Li *et al* (1992)
Na/Cu(100)	50–330	+ phonon measurements	Benedek *et al* (1994)
K/Cu(100)	120–373	+ isotherms	Reichmut *et al* (1994)
Fe/Cu(100)	220–420		Arnott *et al* 1992, Dastoor *et al* (1992)
silane/Cu(100)	173–650		Graham *et al* (1992)
Pb/Cu(1,1,11)	130–600		Goapper *et al* (1996)
Pb/Cu(111)	140	quantum size effects	Hinch *et al* (1989, 1991)
	40–200	+ phonon measurements	Braun and Toennies (1996, 1997)
	303-413		de Beauvais *et al* (1996)
Cu/Cu(111)	110–400		Dastoor *et al* (1994)
	100–450	manipulated growth	Rosenfeld *et al* (1995) Wulfhekel *et al* (1996b)
	300–500	surfactant-assisted growth	Camarero *et al* (1998)
Cu/Co/Cu(111)	300–500	surfactant-assisted growth	Camarero *et al* (1994)
Ni/Cu(111)	125–425	manipulated growth	Wulfhekel *et al* (1996a, 1998)
silane/Cu(111)	130–250	chemis. and alloy formation	Curson *et al* (1997)
Cs/Cu(111)	25–225	+ phonon measurements	Hulpke *et al* (1996)
Pb/Cu(110)	343	Pb lattice gas	de Beauvais *et al* (1995)
Pt/Cu(110)	200–800	$\Theta_{Pt} < 0.02$ ML	Hugenschmidt and de Beauvais (1994)
Co/Cu(110)	350	surfactant-assisted growth	Tölkes *et al* (1998)
Fe/Ag(100)	135		Canepa *et al* (1997b)
Ag/Ag(111)	100–300	manipulated growth	Rosenfeld *et al* (1993, 1995)
Cu/W(110)	170–1000	quantification of defects	Xu *et al* (1991)
Ag/W(110)	170–800	+ structural analysis	Yang *et al* (1992)
Pt/Pt(111)	275–650	're-entrant' two-dimensional growth	Kunkel *et al* (1990)
Ag/Pt(111)	80–1000	submonolayer coverage	Becker *et al* (1993)
Cu/Pt(111)	340	+ STM study	Holst *et al* (1997a)
K/Ni(100)	30–100	+ phonon measurements	Hulpke *et al* (1996)
Rb/Ni(100)	50–90	morphology analysis	Flach *et al* (1998)
Co/Au(111)	50–700	alloy formation	Tölkes *et al* (1997a)
	300	morphology analysis	Tölkes *et al* (1997b)
Au/Au(1 × 2)	128–373	+ Monte Carlo study	Barbier *et al* (1994)
Cu/Si(111)	300	+ phonon measurements	Doak and Nguyen (1989)
Pb/Si(111)	100	+ RHEED and x-rays study	Schmicker *et al* (1997)
K/Si(100)	150	surface metallization	Foulias *et al* (1995)
Pb/Ge(100)	130	quantum size effects	Crottini *et al* (1997)
α-In/InSb(100)	300–520		Mason and Williams (1992)
InSb(110)	390–670	inverse growth	Cvetko *et al* (1995a–c)
NaCl/NaCl(100)	150–400		Duan *et al* (1992a)
KBr/NaCl(100)	223	+ phonon measurements	Duan *et al* (1992b)
KBr/RbCl(100)	180–220	+ phonon measurements	Safron *et al* (1993)
C_{60}/mica(100)	300	+ phonon measurements	Schmicker *et al* (1991b)
Pd/MgO(100)	450–600	+ TEM	Henry *et al* (1993)
FeO/MgO(100)	140–950	+ phonon measurements	Fahsold *et al* (1998)

this study was the demonstration that the hight of islands growing on a surface can be determined in a simple way using TEAS. This information can be extracted from measuring rocking curves, as described in section 2.5.2. By doing this, a value of $d = 1.80$ Å was obtained for the island height, which is identical within experimental error to the interlayer spacing of bulk copper. This shows that the growing islands are of monatomic height. Finally, the density of steps as a function of temperature was determined using the random step model of Lapujoulade (see section 2.5.2) by de Miguel *et al* (1988a).

In a subsequent investigation of this system with RHEED, oscillations of the specular peak intensity have been observed at room temperature, but also at 77 K (Egelhoff and Jacob 1989). To clarify this point, the growth of Cu on Cu(100) was re-investigated by Ernst *et al* (1992a) using TEAS. They were able to observe oscillations even for temperatures as low as 100 K, probably due to the better dynamical range of their experiment as compared with the one performed by Gómez *et al* (1985). In addition, they found that oscillations between 150 and 165 K are slightly stronger damped than at 100 K.

4.2.2. Pb on Cu(100). The first application of TEAS to the study of growth of an heteroepitaxial system (Pb on Cu(100)) has also been performed in the group of Miranda (Sánchez *et al* 1987). The most interesting result of this work was the determination of the heat of vaporization of Pb atoms from step to terrace sites. The experiment consisted of measuring the temperature dependence of the cross section Σ_{Pb} after deposition of 3×10^{-3} ML Pb, i.e. a coverage below saturation of the steps (a step density of 7×10^{-3} was estimated applying the method described for CO on Pt(111) in section 4.1.1). The result is an S-shaped curve: a value of $\Sigma_{Pb} \sim 30$ Å is obtained up to 400 K (due to adsorption on step sites), which changes to $\Sigma_{Pb} \sim 80$ Å at 600–700 K (indicating adsorption on the terraces). Using the Clausius equation, a value for the two-dimensional heat of vaporization of 0.4 ± 0.1 eV per atom is obtained. It should be mentioned that very different results have been reported in a TEAS study of Pb adsorbed on Cu(1,1,11), a (100) vicinal surface (Goapper *et al* 1996). It was found that, at 130 K, the Pb atoms are randomly adsorbed on the surface, whereas equilibrium between step edge and terrace adsorption occurs in the temperature range 150–250 K. This implies a much lower well depth for adsorption on steps, estimated to ∼60 meV. Finally, surface alloy formation above 250 K was concluded from the observed irreversible decay of the cross section.

Pb deposition at room temperature leads to the formation of ordered c(4 × 4), c(2 × 2) and c($5\sqrt{2} \times \sqrt{2}$R45°) overlayers (already observed in a previous LEED study (Henrion and Rhead 1972)) with coverages $\frac{3}{8}$, 0.5 and 0.6 ML, respectively. A unique feature of this system has been reported by Li and Vidali (1992). They observed a corrugation enhancement by a factor of 10 (compared with clean Cu(100)) after adsorption of ∼0.1 ML Pb at 410 K, i.e. at a coverage well below the formation of the first ordered Pb overlayer. The results were interpreted as caused by a redistribution of the Cu(100) surface charge density. Similar results were obtained upon Bi adsorption, whereas no change of the corrugation was observed with Hg.

The structure and melting of the room-temperature phases have been investigated by Sánchez and Ferrer (1989). Adsorption of Pb at 150 K leads to the appearance of two additional high-order commensurate phases: the $(\sqrt{61} \times \sqrt{61})\mathrm{R}\tan^{-1}(\frac{5}{6})$, with coverage 0.49 ML and 30 Pb atoms in the unit cell, and the $(5 \times 5)\mathrm{R}\tan^{-1}(\frac{3}{4})$ with a coverage of 0.64 ML and 16 Pb atoms in the unit cell (Li *et al* 1991, 1993). Both phases are metastable; upon heating above 300 K, they convert irreversibly to the phases observed by deposition at room temperature. A complete phase diagram for this system has been reported by Li *et*

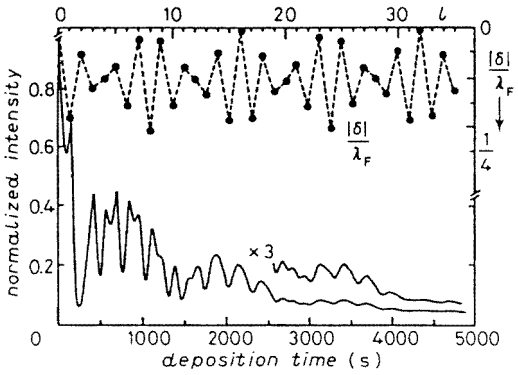

Figure 25. Intensity oscillations of the specular He beam (full curve) during deposition of Pb on Cu(111) at 140 K ($k_i = 3.36$ Å^{-1}), and the corresponding coverage dependence of the misfit δ defined in (4.6). The expected point of filling of the lth layer (assuming no quantum size effects) is shown in the upper scale. From Hinch *et al* (1989a).

al (1993). Transition in the growth mode from Stranski–Krastanov at 400 K to quasi layer-by-layer growth below 200 K was also clearly observed by recording deposition curves at different temperatures (Zeng *et al* 1994).

4.2.3. Pb on Cu(111): observation of quantum size effects during thin film growth. HAS investigations of the growth of Pb on Cu(111) have revealed, for the first time, the influence of quantum size effects (QSE) on thin film growth (Hinch *et al* 1989a, 1991). The intensity oscillations of the specular helium beam during Pb deposition at 140 K are shown in figure 25. Periods corresponding to single- and double-layer growths are clearly evident, in contrast to the damped, single-layer oscillations observed for deposition of Pb on Pb(111) (not shown here). These results are interpreted on the basis of a QSE which leads to an additional stabilizing influence on layers of certain thicknesses. The physics involved in this effect has been revealed by calculations made with a simple jellium model by Schulte (1976), which showed the appearance of oscillations in the electron density inside and outside the crystal with increasing layer thickness. These oscillations are attributed to changes in the occupation of quantized electronic energy levels. With increasing layer thickness, the levels decrease in energy and more levels fall below the Fermi energy. The onset of occupation of an additional level occurs at thicknesses $D = 0.5\lambda_F n$, where λ_F is the Fermi wavelength and n is an integer. As a result, a simple measure of the strength of the QSE is given by the misfit δ (Hinch *et al* 1989a)

$$\delta = \left| l d_0 - n\frac{\lambda_F}{2} \right| \tag{4.6}$$

where l is the number of layers, each of which is assumed to have the thickness $d_0 = 2.86$ Å (interlattice spacing of bulk Pb). The coverage dependence of the misfit (normalized to λ_F) is compared with the experimental curve in figure 25. Both curves correlate well for films thicker than 10 layers. Lead overlayers with a thickness corresponding to large δ values have a low reflectivity: for example, no evidence was found for the unstable 15 ML film. The correlation with the experimental curve is not as good for smaller coverages. This is a consequence of the fact that the δ values were calculated using bulk lead parameters, which are not expected to be applicable in the early stage of the film growth. A reasonably good fit of the experimental data reproducing all double- and single-layer growth regions was

obtained from a calculation of the specular intensity considering the influence of the QSE (Hinch *et al* 1989a). More recently, Braun and Toennies (1997) found that the apparent step heights as derived from drift spectra also oscillate with a period of 2 ML in the coverage range 3.5–8.5 ML lead. These curves could be well reproduced by a model calculation based on a quasifree electron gas confined in a potential well of finite depth. This demonstrates that a variation in the Fermi energy due to a QSE can lead to similar variation in the electronic density even far from the surface. The different sensitivity of x-rays, RHEED and HAS to detect the QSE has been investigated by Schmicker *et al* (1997) for the case of Pb on Si(111)(7×7). QSE have been also observed using HAS for Pb growth on Cu(100) at 150 K (Zeng and Vidali 1995) and for growth of Pb on Ge(100) at 130 K (Crottini *et al* 1997).

The growth of Pb on Cu(111) has been recently investigated by de Beauvais *et al* (1996) for substrate temperatures between 303 and 413 K, and by the Göttingen group for temperatures below 200 K (Braun and Toennies 1996). The last experiments revealed, in addition to the layer-by-layer growth previously reported in a LEED study (Meyer *et al* 1988), that a second monolayer can only be grown by codeposition of lead with 20% thallium at 95 K (no layer-by-layer growth was observed for pure thallium). Thallium seems to reduce the interaction between the Pb overlayer and the substrate, leading to a relaxation of the Pb monolayer; this explanation was favoured by complementary measurements of phonon dispersion curves and slab calculations (Braun and Toennies 1996). Pb deposition at substrate temperatures between 303 and 413 K (de Beauvais *et al* 1996) leads to: (a) the formation of a disordered surface alloy for coverages $\Theta < 0.21$ ML and (b) the appearance of a nonalloyed p(4×4) structure above this coverage through a first-order transition. A very interesting result of this work was the observation of an additional specular intensity decrease after Pb deposition was stopped, indicating that equilibrium was not reached during Pb deposition in the temperature range studied. Equilibrium conditions were reached after 400 s at 373 K for coverages below 0.1 ML, and after 2 h at 413 K in the monolayer range ($\Theta = 0.56$). This fact may explain the different results obtained in a previous LEED study of this system (Meyer *et al* 1988).

4.2.4. Pb on Cu(110). Growth of Pb on Cu(110) has been studied by means of TEAS by de Beauvais *et al* (1991, 1992, 1995). This is the first system for which deposition curves along the two symmetry directions of the substrate have been measured. From a fit to the experimental data with (2.27) (using $m = 2$), one obtains cross section values of 77 and 91 Å along the $[1\bar{1}0]$ and [001] directions, respectively (de Beauvais *et al* 1991). The formation of c(2×2), p(4×1) and p(5×1) structures was observed after Pb deposition at room temperature, with coverages 0.5, 0.75 and 0.8 ML, respectively (these phases had been reported in a previous LEED study (Henrion and Rhead 1972)). In contrast to LEED, however, the TEAS results clearly demonstrate the formation of a lattice gas of Pb adatoms at low coverages followed by a two-level behaviour up to completion of the c(2×2) structure (de Beauvais *et al* 1995). These conclusions are supported by the results shown in figure 26. The intensity variation of the $(\bar{1}0)$ beam during Pb deposition at 343 K for two angles of incidence is shown in figure 26. This is the first-order diffraction beam along the close-packed rows, and is therefore not present in the spectra of the clean surface due to its low corrugation. For $\Theta < 0.2$ ML, the intensity increases as Θ^2 for both angles of incidence (see inset). Armand and Salanon (1989) have shown that this law is indicative of random adsorption on lattice sites, i.e. a two-dimensional lattice gas (a similar behaviour has also been reported for Pt deposition on Cu(110) by Hugenschmidt and de Beauvais

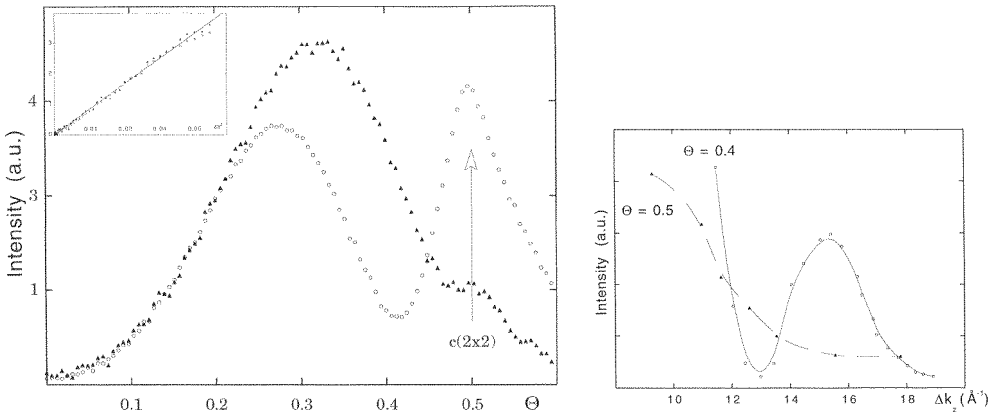

Figure 26. Left: intensity of the $(\bar{1}0)$ diffraction peak as a function of Pb coverage on Cu(110) for angles of incidence of 64.2° (○) and 36.9° (△). The inset shows that up to $\Theta \sim 0.2$ ML, the intensity follows a parabolic law. Right: rocking curves for the $(\bar{1}0)$ peak at $\Theta_{Pb} = 0.5$ ML and $\Theta_{Pb} = 0.4$ ML. The minimum and maximum in the last curve correspond to the scattering conditions of curves (○) and (△) on the left, respectively. From de Beauvais *et al* (1996).

(1994)). The $(\bar{1}0)$ peak intensity exhibits a strong dependence on the scattering conditions in the range $0.25 < \Theta < 0.5$ ML. The reasons are revealed by the rocking curves shown in figure 26: the oscillatory behaviour observed for $\Theta = 0.4$ ML demonstrates the existence of two levels on the surface, which are separated by a distance $h = 1.2 \pm 0.1$ Å. This value was interpreted assuming that in the lattice gas state, the Pb adatoms replace three Cu atoms from a close-packed row whereas the ones forming the c(2×2) phase occupy fourfold sites between two ridges. Evidence for the onset of the c(2×2) island formation at $\Theta \sim 0.3$ ML was found in a large increase of the FWHM of the $(\bar{1}0)$ peak under out of phase conditions. Further increase of the Pb coverage at room temperature results in the formation of a new lattice gas on top of the c(2×2) phase; when this lattice gas is compressed to about 0.1 ML, it contributes to the c(2×2)–p(4×1) first-order transition. The transition from this structure into the quasicompact hexagonal p(5×1) phase occurs by elimination of domain walls, with intermediate formation of p($n \times 1$) structures with $n = 9, 13, 14, 17, 19$ (de Beauvais *et al* 1991, 1992).

4.2.5. Fe on Cu(100). A further application of TEAS to the study of the early stages of growth in a heteroepitaxial system has been developed in the group of Allison (Dastoor *et al* 1992). It was shown that, because single scattering dominates helium interactions at low-corrugated surfaces, it is possible to extract information on the vertical distribution of growing terraces even when it is not possible to decompose the observed peak profile into a sharp, coherently scattered and a broad, incoherently scattered component. The method has been applied to the growth of fcc iron on Cu(100). Following the kinematic approach of Lent and Cohen (1984), the intensity scattered from a surface involving N exposed layers separated by steps of height d can be written as:

$$I(\boldsymbol{S}) = \delta(\boldsymbol{S}_\parallel)\left[c_0 + \sum_{l=1}^{N-1} 2c_l \cos(S_z l d)\right] + \sum_{l=1}^{N-1} F_l(\boldsymbol{S}_\parallel) 2c_l [1 - \cos(S_z l d)] \tag{4.7}$$

where $\boldsymbol{S}(\boldsymbol{S}_\parallel, S_z) = \boldsymbol{k}_f - \boldsymbol{k}_i$ is the scattering vector, the peak profiles $F_l(\boldsymbol{S}_\parallel)$ of the broad component are determined by the lateral step correlations and $c_l = \sum_{q=1}^{N-l} \Theta_q \Theta_{q+1}$, with Θ_i

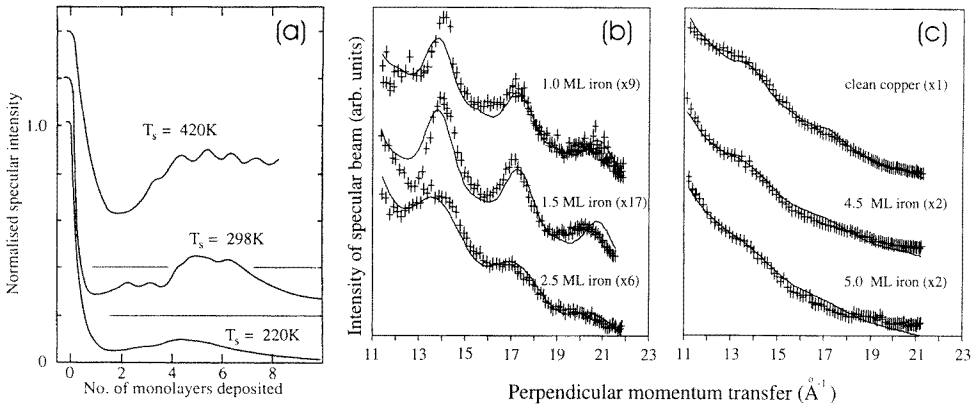

Figure 27. (*a*) In-phase scattered specular intensity during the growth of Fe on Cu(100) at different substrate temperatures. The angle of incidence is 52° and the He beam energy 63 meV. (*b*), (*c*) Scattered intensity along the specular lattice rod as a function of perpendicular momentum transfer. The full curves are fits using (4.8). From Dastoor *et al* (1992).

the coverage of the ith-exposed layer. After convolution with the response function of the detector, (4.7) can be rearranged to obtain the variation of the specular intensity ($\boldsymbol{S}_\parallel = 0$) with S_z (Dastoor *et al* 1992):

$$I(\boldsymbol{S}_\parallel = 0) = 1 + \sum_{l=1}^{N-1} \frac{a_l}{a_0} \cos(S_z l d) \tag{4.8}$$

where

$$a_0 = Ac_0 + \sum_{l=1}^{N-1} 2c_l B_l \qquad \text{and} \qquad a_l = 2c_l(A - B_l). \tag{4.9}$$

A and B_l are, respectively, the values of the sharp and broad components in the peak profiles measured at the specular position. In an ideal experiment, $A \gg B_l$, and the sharp component can be easily separated from the incoherently scattered one. In many cases, however, $A \sim B_l$ and therefore a conventional spot profile analysis is not possible. In such cases, an analysis of the data based in (4.8) provides a direct picture of the vertical growth morphology, as discussed below for the Fe/Cu(100) system (for which $A/B_l \sim 2$). In particular, note that the number of growing layers can be directly inferred from the number of terms in the Fourier series (4.8).

Growth curves recorded upon in-phase conditions during Fe deposition on Cu(100) at three substrate temperatures are shown in figure 27(*a*) (Arnott *et al* 1992). The low value of the specular intensity observed at 220 K indicates the presence of a large number of defects, and suggests that growth is diffusion limited. At room temperature, a minimum is observed at one monolayer, indicating also a high defect density. Note that this observation alone is sufficient to rule out layer-by-layer growth at 298 K. An improvement in the surface order takes place around 2 ML and 4 ML, as revealed by the increase in the specular intensity. Finally, a layer-by-layer growth is observed at 420 K for thicknesses beyond 3 ML, whereby Auger measurements reveal the formation of a surface alloy (Arnott *et al* 1992). More insight into the growth mode at 298 K is provided by an analysis of rocking curves recorded at different coverages. The results are shown in figures 27(*b*) and (*c*). The full curves are fits to the data with (4.8), using only two oscillatory terms. The fundamental period of the oscillations corresponds in all cases to single height atomic steps. The gradual

transition in the curve shape from a nonsinusoidal to a sinusoidal form can be clearly seen, indicating a transition from multilayer to layer-by-layer growth at ∼2 ML. A progressive increase in the mean step separation above 4 ML can also be concluded from the decrease in amplitude of the oscillations, in addition to the specular intensity increase observed for in-phase scattering. Note that initial bilayer as well as layer-by-layer growth can be ruled out from a qualitative inspection of the data: the bilayer model would lead to the appearance of a doubled frequency in the oscillations (which is not observed), whereas layer-by-layer growth would exhibit a single Fourier component, contrary to the observations below 2 ML.

A similar analysis has been applied more recently to the growth of Fe on Ag(100) by Canepa *et al* (1997b), whereby (4.8) has been generalized for the case of different step heights d and d' corresponding to the first and subsequent growing layers, respectively.

4.2.6. Growth of KBr and NaCl on NaCl(100). Alkali halides are known to be the prototypical ionic insulators, so that the study of growth on these systems can be considered as a first step before studying more complicated insulators, like the perovskites and high-T_c ceramics. Since TEAS presents some advantages over RHEED for investigating ionic insulators, we feel this is an area which should be further exploited in future TEAS studies. In what follows, we summarize the results reported by Duan *et al* (1992a, b) for the growth of NaCl and KBr on NaCl(100) and KBr on RbCl(100) (Safron *et al* 1993). In particular, we point out that these and the C60/mica(100) study reported by Schmicker *et al* (1991) are the only investigations of growth of insulators peformed up to date with TEAS.

NaCl(100) is a highly corrugated surface, which means that many intensive diffraction peaks are present in the spectra. This has two important implications for the experiment: (1) deposition curves can (and indeed should) be measured for several beams (in contrast to metals) and (2) the different growth stages can be characterized by stopping the deposition and measuring the angular distributions. In view of (1), for the deposition of vapour NaCl, Duan *et al* (1992a) were able to observe oscillations of the specular beam but also more than 15 periods in the oscillations of the first- and second-order Bragg peaks at 200 K. A good example of (2) is given by the growth of KBr. The spectra recorded after completion of the first six layers clearly show how the NaCl peaks diminish in intensity while the KBr peaks grow in intensity (Duan *et al* 1992b). In view of the KBr/RbCl(100) system, an interesting result is that the step height d of the first layer appears to be larger than for the subsequent layers, an effect whose origin could not be explained. With respect to cross section measurements on NaCl(100), a value of 80 Å was obtained for deposition of NaCl at 200 K; this value drops substantially above 250 K, indicating that island nucleation sets in. A larger value was found for KBr deposition at 223 K (200–250 Å), the origin of which was ascribed to KBr molecules oriented perpendicular to the surface. On RbCl(100), on the contrary, a smaller value of 60 Å was obtained for KBr adsorption.

Finally, we mention that in a more recent HAS study of NaCl(100), Höche *et al* (1993) have reported for the first time the occurrence of photon-stimulated layer-by-layer desorption.

4.2.7. Manipulated growth. We close our presentation of growth investigations by means of TEAS with a brief discussion of the results on growth manipulation reported by the group of Comsa (Rosenfeld *et al* 1993, 1995, Wulfhekel *et al* 1996a, b). Although the use of TEAS is not essential to obtain the desired growth mode, the fact that it allows *in situ* monitoring of growth whereas ion bombardment is applied has been of decisive importance for the developing of this method. The main idea of growth manipulation

consists of changing the growth parameters of a film *during* growth in order to obtain layer-by-layer growth in cases where three-dimensional growth is observed otherwise. This is achieved by creating an enhanced island density during the early stage of growth of each monolayer, which improves interlayer mass transport allowing thus the appearance of layer-by-layer growth. Two easy ways to produce an enhanced density of nuclei are: (a) by lowering the substrate temperature during the nucleation stage of each monolayer or (b) by bombarding the surface with low-energy ions during nucleation (Rosenfeld *et al* 1993, 1995). These procedures have been successfully applied to the homoepitaxial growth on Ag(111) (Rosenfeld *et al* 1993) and Cu(111) (Wulfhekel *et al* 1996b), as well as to the heteroepitaxial growth of Ni on Cu(111) (Wulfhekel *et al* 1996a, 1998). Results corresponding to Ag on Ag(111) are shown in figure 28. In figure 28 (top), the effect of changing the substrate temperature during monolayer growth can be seen. With increasing island density (corresponding to lower T_1), a transition from the monotonic decay of the specular intensity to a two-dimensional growth behaviour is clearly observed; the intensity maximum corresponds to deposition of 1 ML. The results obtained using a pulsed ion beam during nucleation in each layer are shown in figure 28 (bottom, curve b). Layer-by-layer growth is clearly seen, compared with three-dimensional growth observed with conventional growth (curve a) or during continuous ion bombardement (curve c). Similar results have been reported for the Cu/Cu(111) system (Wulfhekel *et al* 1996b, Rosenfeld *et al* 1995). Concerning this system, it should be mentioned that no intensity oscillations were observed during conventional growth between 100 and 450 K, in agreement with a previous TEAS study performed by Dastoor *et al* (1994) where the growth mode was found to change gradually from step propagation at 400 K to diffusion-limited growth below 300 K. These results are in contradiction to a previous SPA-LEED study (Henzler 1993), where oscillations were clearly resolved at 370 K (see Wulfhekel *et al* 1996b).

More recently, TEAS has also been applied to investigate surfactant-induced layer-by-layer growth. The first of such studies was reported by Miranda and co-workers, who showed that the structural quality of Co/Cu superlattices grown on Cu(111) can be much improved if the clean surface is precovered with a monolayer of Pb (Camarero *et al* 1994). For growth of Cu on Cu(111) at room temperature, the use of oxygen as a surfactant has been shown to induce weak He-intensity oscillations, although the quality of the resulting films was low (Wulfhekel 1996b). More recently, Tölkes *et al* (1998) have demonstrated that preadsorption of oxygen on Cu(110) at 350 K leads to layer-by-layer growth of a pseudomorphic fcc(110) cobalt film. Since diffraction is observed from this surface, more insight into the different growth stages could be gained by stopping deposition and measuring angular distributions, in a similar way to that discussed in the previous section for growth on NaCl(100) and RbCl(100).

5. Diffraction of other particles

5.1. Neon diffraction results

The first studies of Ne scattering from LiF(001) were performed by Smith *et al* (1970) and O'Keefe *et al* (1971), who observed that (at high surface temperatures) the angular distributions are dominated by a classical rainbow behaviour (see section 2.4). Attempts to extract atom–surface properties from an analysis of the rainbow patterns have been reported by McClure (1972a, b). The major experimental difficulties in observing Ne diffraction from solid surfaces are caused by: (i) the large inelastic contributions, which result from the fact that mainly bulk single-phonons are produced in Ne-scattering processes (in contrast

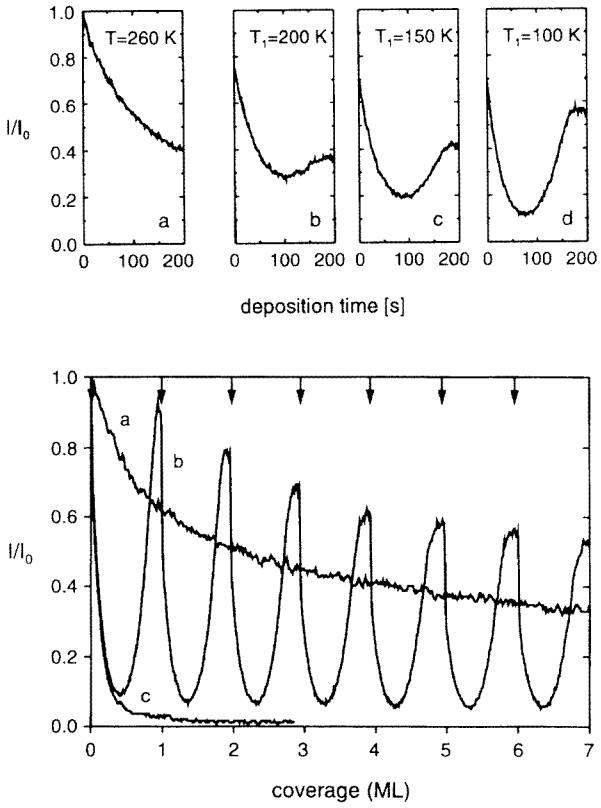

Figure 28. Top: evolution of the normalized antiphase He-specular intensity during deposition of Ag at a rate of 4.2×10^{-3} ML s^{-1} and a substrate temperature of 260 K on different prepared Ag(111) surfaces: (a) clean surface, (b–d) after predepositing 0.05 ML Ag at the indicated preparation temperature T_1. Bottom: Evolution of the normalized antiphase He-specular intensity during deposition of Ag on Ag(111) at 300 K: (a) continuous deposition at a rate of 4.7×10^{-3} ML s^{-1}, (b) same as (a) but in addition (at the times marked by the arrows) a short ion pulse was given (600 eV Ar^+), (c) same as (a) combined with continous ion bombardment. From Rosenfeld *et al* (1995).

to the case of He-scattering where surface Rayleigh modes predominate (Semerad and Hörl 1983)), (ii) the shorter wavelength (0.26 Å for a room-temperature beam), which makes higher angular and energy resolutions necessary in order to detect all diffraction beams and (iii) the enhanced sensitivity to defects due to the higher Ne polarizability as compared with He. As a consequence, Ne diffraction was first observed from highly corrugated surfaces, like LiF(100) (Williams 1971, Boato *et al* 1976b) and Cu(117) (Lapujoulade *et al* 1981a). Intensity analyses for LiF(100) gave similar corrugations for He and Ne with a slightly smaller amplitude for Ne (Boato *et al* 1976b). A quantitative evaluation of Ne-diffraction data for the stepped Cu(117) surface was not possible because of the complicated shape and large amplitude of the corrugation.

Ne diffraction from low-index metal surfaces was observed somewhat later by Rieder and Stocker (1984) and Salanon (1984). In surprising contrast to the LiF(100) results, on metals Ne yields larger corrugation amplitudes, suggesting that Ne diffraction may be more sensitive to structural details. Studies performed on the (110) surfaces of Ni, Cu, Rh,

Table 5. Comparison of corrugation amplitudes with well depths D corresponding to the interaction potentials of room-temperature He, Ne, and H_2/D_2 beams with different clean, unreconstructed metal surfaces. The values of the corrugation amplitude refer to the more corrugated surface directions. The D values have been derived from selective adsorption measurements, except for D_2/Ni(110) on which it was obtained from a Debye–Waller fit to the data.

	Corrugation (Å)			D (meV)		
Surface	He	Ne	H_2/D_2	He	H_2/D_2	Reference
Ni(111)	0.022	—	0.16	—	—	Hayward and Taylor (1986)
Ag(111)	0.022	—	0.08	—	32[a]	Mattera *et al* (1985)[b]
Cu(100)	<0.01	—	0.06	—	30.9[c]	Lapujoulade and Perreau (1983)[d]
Ni(110)	0.075	0.17[e]	0.09[f]	—	45[f]	Rieder (1982a)
Cu(110)	0.13[g]	0.21[h]	0.216	6.3[i]	21	Lapujoulade and Perreau (1983)[d]
Rh(110)	0.15	0.29	0.166[j]	8.5	—	Parschau *et al* (1989)
Pd(110)	0.24	0.42[e]	—	8.05	—	Rieder and Stocker (1983)
Ag(110)	0.27	—	0.11[k]	6.0	31.7[k]	Luntz *et al* (1982, 1983)
Ni(113)	0.177	0.30	—	—	—	Rieder (1989)
Rh(113)	0.27	0.47	—	8.4	—	Apel *et al* (1996)

[a] Yu *et al* (1985).
[b] See also Boato *et al* (1976a).
[c] Andersson *et al* (1988), see also Bertino *et al* (1997b, 1998a).
[d] See also Perreau and Lapujoulade (1982a, b).
[e] Rieder and Stocker (1984).
[f] Bertino *et al* (1997a).
[g] Gorse *et al* (1984).
[h] Rieder and Stocker (1985b).
[i] Extrapolated from Cu(113), Cu(115) and Cu(117).
[j] Cvetko *et al* (1996).
[k] Mattera *et al* (1985), Chiesa *et al* (1985).

Pd and the (113) surfaces of Ni and Rh (see table 5) revealed that Ne-derived corrugation amplitudes are about twice as large as those derived from He-diffraction. These experiments also showed that the repulsive potential experienced by Ne atoms is about twice as steep as that felt by He atoms. A very interesting observation, which strikingly demonstrates the enhanced sensitivity of Ne atoms towards details of the surface corrugation, was made on Ni(113) by Rieder *et al* (1985). Whereas with room-temperature He beams both in-plane and out-of-plane diffraction spectra appeared rather symmetric, the out-of-plane diffraction pattern obtained with Ne showed the expected pronounced asymmetry. Quantitative analyses of Ne diffraction intensities allowed us to conclude that a surface charge transfer takes place on Ni(113) from the (111) to the (100) microfacets, which smoothens the charge density along the (100) microfacets and leads to a more pronounced charge density variation along the (111) microfacets. In accordance with these results, the out-of-plane asymmetry observed with Ne became visible with He only at high incident energies ($\geqslant$180 meV (Rieder 1989)). This higher sensitivity of Ne to unravel structural details may play an important role for investigating alloy surfaces. Indeed, recent results on NiAl(110) (Farías *et al* 1998) show that both Ni and Al atoms are visible in the Ne-derived corrugations, whereas only the topmost Ni or Al atoms appear in the corrugation determined from He-diffraction data. Ne diffraction from the reconstructed (1×2)–Au(110) surface has been reported by Engel and Weare (1985). These authors performed a classical analysis of the rainbow scattering observed with Ne in the [001] azimuth and their angular shift with incident angle and energy,

which could be satisfactorily described using the model of Klein and Cole (1979a, b) (see section 2.4).

Ne diffraction was only very recently extended to investigations of adsorbate systems, and have up to now been restricted only to studies on hydrogen overlayers. The first Ne diffraction experiments were made with the high-coverage (2×1)H and (1×2)H phases on Ni(110) by Parschau *et al* (1993). Intensity analyses of diffraction spectra revealed that the corrugation amplitudes observed with Ne were again systematically larger than with He, although the increases were not as dramatic as for the clean surfaces. Further studies on the low-coverage hydrogen phases on Ni(110) and Rh(110) (Rieder *et al* 1993) opened up the possibility to search experimentally for evidence on anticorrugating effects in the interaction of He with metal surfaces, as proposed initially by Annett and Haydock (1984). These authors were the first to theoretically discuss an extension of the simple Esbjerg and Nørskov picture (2.1). According to their proposition, the repulsive part of the potential should read

$$V_{AH}(\boldsymbol{r}) = \alpha\rho(\boldsymbol{r}) + \beta \bigtriangledown^2 \rho(\boldsymbol{r}) - \nu\rho_u(\boldsymbol{r}). \tag{5.1}$$

Here, the first term is the Esbjerg–Nørskov leading repulsive term. The second term accounts for the inhomogeneities of the electron distributions and leads to a lateral smearing of the corrugation; it should be more pronounced for Ne than for He, but was shown to be generally very small. Most important is the third term, since it gives rise to the appearance of anticorrugating effects due to the hybridization of the orbitals of the incoming atoms with the unoccupied metal states and is thus proportional to the unoccupied density of states $\rho_u(\boldsymbol{r})$. This additional term reduces the total corrugation and can compensate and even exceed in special cases the first term in (5.1).

A simple physical picture of the influence of the third term in (5.1) can be obtained by observing that unoccupied states have essentially antibonding character with larger densities at the top positions of the surface atoms than at bridge or centre sites. Consequently, He atoms with their electronic ground state $1s^2$ will be more strongly attracted at top positions due to the large overlap between the He $1s^2$ orbitals and the surface wavefunctions of the unoccupied states than at centre positions, where the overlap is zero and the corrugation will thus be diminished. For Ne (ground state $2s^22p^6$), on the other hand, this 'anticorrugating effect' is expected to be smaller, because the $2p_x$ orbital counteracts the anticorrugating influence of the $2s^2$ orbital, leading to $\nu \sim 0$ for Ne in (5.1). For He/Ni(110) Annet and Haydock (1984) have determined the value of ν semiempirically by adjusting the corrugation amplitude perpendicular to the close-packed rows to obtain agreement with the one determined experimentally by Rieder and García (1982). As a result, they found that along the close-packed rows the anticorrugating contribution for Ni(110) leads even to a reversal of the corrugation, so that the corrugation maxima should correspond to short bridge sites of the close-packed rows. These results were questioned by Harris and Zaremba (1985), who performed local density calculations and found that the anticorrugating effects should be appreciably smaller. In response to this work, Annett and Haydock (1986) performed first principle calculations which supported their initial conclusions. Also, electronic surface states were shown to contribute to anticorrugating effects (Bertel 1996). More recent *ab initio* calculations reported by Petersen *et al* (1996, 1998) reproduced the corrugation amplitudes extracted from He and Ne experiments, including the anticorrugation effect for the Ne data. The different behaviour of the two probe particles is attributed to the different interaction of the He and Ne orbitals with the surface electronic wavefunctions at the Fermi level, not with the electronic density. For Rh and Ni(110) the wavefunctions of the $d_{3z^2-r^2}$ and d_{xz} states play the crucial role in the scattering process. Finally, *ab initio* calculations reported by Trioni *et al* (1998) have shown that anticorrugating effects may

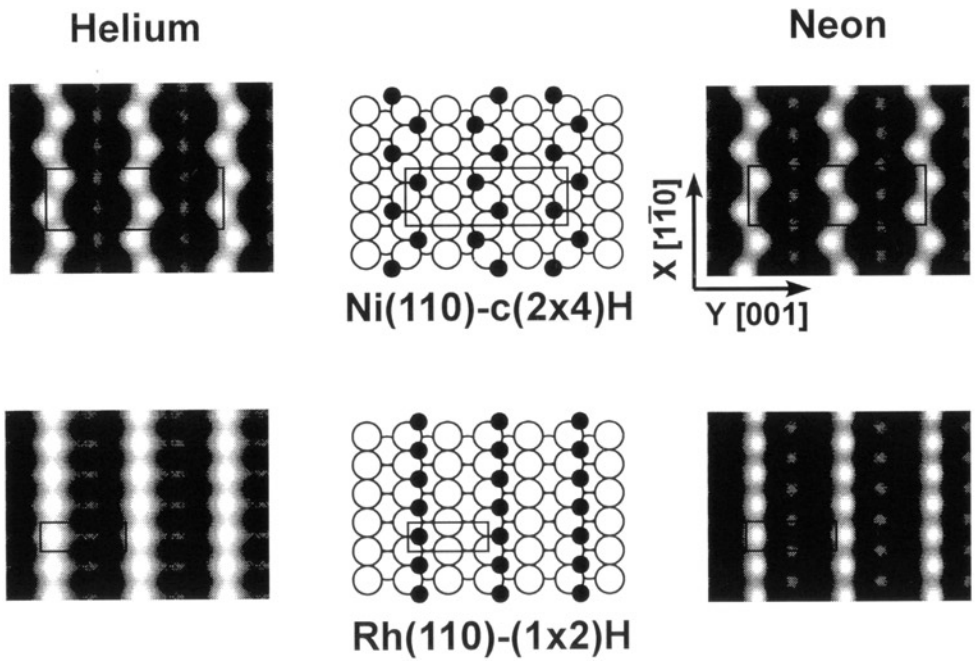

Figure 29. Sphere models of H phases on Ni(110) and Rh(110) together with grey-scale representations of the corrugation functions derived from He and Ne diffraction. In the sphere models large open circles denote metal atoms and small full circles denote H adatoms at the locations determined by LEED. The H atoms show up as the brightest spots in the grey-scale top views. Note that in the He-derived corrugations there occur less bright maxima between the H atoms along [001] on all H-free metal rows in disagreement with the true atom arrangements shown in the sphere models. In contrast to this, in the Ne-derived corrugations the metal maxima are shifted by $a_1/2$ along [1$\bar{1}$0] in agreement with the true surface structures. From Rieder *et al* (1993).

also be accounted for by the different polarizations of He and Ne (see also Montalenti *et al* 1996).

The experimental confirmation for anticorrugating effects in He–metal interactions was reported by Rieder *et al* (1993). These authors found systematic differences in the corrugations of partially H-covered (110) surfaces of Ni and Rh when determined with He and Ne diffraction: whereas in all Ne-derived corrugations the hills along the H-free close-packed metal rows correspond to underlying metal atoms, they are shifted to short-bridge sites in all He-derived corrugations. This situation is illustrated in figure 29 for the Ni(110)–c(2×4)H and Rh(110)–(1×2)H systems. For a detailed description of the fitting procedure the reader is referred to the original work (Rieder *et al* 1993). It is important to emphasize that the H-adatoms were needed in these analyses in order to 'mark' the threefold-coordinated sites, so that other areas of the corrugation could be properly assigned. A brief review on surface structural studies with He and Ne diffraction has been given by Rieder (1994). Finally, we mention the interesting attempt of Santoro *et al* (1998) of including the anticorrugation effect in the calculation of the He differential reflection coefficient for the inelastic scattering from Rh(111).

On the basis of the results reviewed above, it is clear that corrugation functions derived from Ne diffraction data deliver more faithful pictures of surface atom arrangements than

corrugations deduced from He diffraction; moreover, Ne 'sees' larger corrugation amplitudes for clean metals and H-adlayers on metals and may thus be more sensitive to structural details. This may be of special importance for investigating composed surfaces, as suggested by recent results on the alloy NiAl(110) (Farías *et al* 1998).

5.2. Argon diffraction results

Due to the larger mass of the Ar atoms, inelastic contributions are much stronger than in the case of Ne, and less structured scattering is obtained. First Ar scattering studies on LiF(100) already evidenced the existence of rainbow-like features in the in-plane angular distributions, with the rainbow angle smaller than in the case of Ne (Smith *et al* 1969, 1970). Structure in the angular distributions of Ar (and Ne) scattered from LiF(100) could be clearly resolved by LeGrand and Greene (1986), who used a velocity selector (resolution ∼3%) to filter out all but the nearly elastic scattering. This system was re-investigated by Vidali *et al* (1988) for incident energies between 89 and 350 meV and for a variety of polar and azimuthal incidence angles. A bilobular scattering pattern was observed for small incidence angles and along the direction of maximum corrugation on the surface, and a broad peak centred around the specular direction for higher angles of incidence. The data were interpreted using a classical single- and double-hit rainbow scattering model in which the surface was represented by a corrugated hard wall with an attractive well in front. The peak-to-trough corrugation of the hard-wall function was found to be $\zeta_m \sim 0.30$ Å, in good agreement with the one calculated using a potential based on the effective medium theory. This value is smaller than those estimated by Boato *et al* (1976b) for Ne/LiF(100) ($\zeta_m \sim 0.54$ Å) and He/LiF(100)† ($\zeta_m \sim 0.58$ Å).

In view of metal surfaces, angular distributions in Ar scattering experiments have been measured for Cu(110) (Rieder and Stocker 1985b) and Ni(511) (Aten *et al* 1987). On Cu(110), the existence of pronounced rainbow-scattering features was clearly observed in the in-plane spectra recorded along the [001] direction. As in the case of Ar/LiF(100), the rainbow angle as measured from the specular beam was found to be smaller than in the case of Ne scattering. A puzzling result of this study was the observation of out-of-plane diffraction-like features with Ar (as well as with N_2) whereas no out-of-plane diffraction was observed with He and Ne. The scattering of Ar from Ni(511) was investigated for a range of incident energies (between 63 and 273 meV) and surface temperatures with the primary goal of achieving a better understanding of the dependence of energy exchange on surface corrugation (Aten *et al* 1987). Lobular angular distributions consistent with direct inelastic scattering were observed with the beam incident along the weakly corrugated $[1\bar{1}0]$ azimuth, whereas rainbow scattering was observed in the in-plane angular distributions recorded in the direction perpendicular to the close-packed rows. Using expression (2.23) for classical rainbow scattering, the maximum corrugation amplitude was estimated to $\zeta_m \sim 0.36$ Å, somewhat smaller than the values of 0.62 and 0.50 Å derived for He/Ni(511) using a hard-wall potential and a corrugated Morse potential, respectively (Kaufman *et al* 1986).

In general, one expects quantum effects to be most important at long wavelengths—i.e. for scattering of light particles at low kinetic energies—and become increasingly less important for heavy particles. The first indication that wave character may be important even for such heavy species as Ar was reported by Schweizer and Rettner (1989), who observed sharp diffraction peaks in the scattering of Ar from 2H–W(100) for incident beam energies between 25 and 140 meV ($\lambda = 0.27$ Å and 0.12 Å, respectively) and

† More exact calculations based on a semi *ab initio* potential yielded a value of $\zeta_m \sim 0.50$ Å for He/LiF(100) (Celli *et al* 1985).

surface temperatures up to 200 K. Since the scattering plane was not oriented along a high-symmetry direction of the surface, the diffraction intensities could not be measured with sufficient accuracy, so that it was not possible to determine the surface corrugation function. The fraction of Ar atoms reflected elastically from the 2H–W(100) surface was estimated at ∼1% for the most favourable case studied, corresponding to $E_i = 27$ meV and a surface temperature of 90 K. The thermal attenuation of Ar, Ne and He specular beams exhibited Debye–Waller behaviour consistent with a surface Debye temperature of 400 K. For large incidence angles (e.g. $\theta_i = 60^\circ$) the angular distributions were observed to consist of a single quasispecular lobe which narrows substantially with increasing incidence energy. In contrast, for incidence angles close to the surface normal, a rainbow distribution was found with the angular separation of the two lobes decreasing with increasing energy. The latter may be explained classically by considering the effect of the attractive potential well, which refracts the incoming and outgoing atoms to different extents. The energy dependence of the rainbow angles could be well described using the model of Klein and Cole (1979a, b) (see section 2.4). This allowed the corrugation amplitude to be estimated to 0.03 Å, which is similar to values obtained for He and Ne diffraction from this surface, and the depth of the potential well to amount to 100 meV. The same model was also able to account for the increase in the width of the angular distributions of the inelastic scattering lobe with decreasing incident beam energy (Schweizer *et al* 1991). Due to the basic importance of these results which, however, left many questions open, it would be very desirable to obtain more experimental data for a wider range of scattering conditions.

5.3. Diffraction with H_2 and D_2 molecular beams

The diffraction of H_2 and D_2 molecular beams from surfaces is in principle quite similar to diffraction of He, the only major difference being the possibility of rotational-state transitions in the case of molecular scattering. This may occur via: (a) a pure elastic process, in which the incident molecules convert part of their translational energy into rotational energy, or (b) a dissipative process, which involves creation or annihilation of phonons. A detailed description of this subject can be found in the review by Barker and Auerbach (1985). For low-energy collisions and low surface temperatures, process (a) will dominate. This leads to the appearance of additional diffraction peaks in the angular distributions, which are called *rotationally inelastic diffraction* (RID) peaks. A very comprehensive review on diffractive scattering of simple molecules which includes a discussion on the issues relevant to molecular beam production has been presented by Mattera (1992). The position of a RID peak within an angular distribution can be obtained applying the Bragg condition (2.3) and the relation for conservation of energy, which reads

$$E_f - E_i = \Delta E_{\mathrm{rot}}. \tag{5.2}$$

Here, E_f and E_i are the final and incident beam energies, respectively, and ΔE_{rot} is the energy associated with a rotational transition. For H_2 (D_2) this energy is $\Delta E_{\mathrm{rot}} =$ 44.6 (22.4) meV for $j = 0 \rightleftharpoons 2$ transitions and $\Delta E_{\mathrm{rot}} = 74.3$ (37.3) meV for $j = 1 \rightleftharpoons 3$ transitions (Mattera *et al* 1985). Models to calculate the relative population of the different rotational levels for H_2 and D_2 nozzle beams have been proposed by Kern *et al* (1985) and Faubel *et al* (1994). In the case of H_2 and D_2 scattering from low-index metal surfaces, RID peaks manifest themselves usually as weak shoulders in the flanks of the elastic diffraction peaks. RID peaks could be clearly resolved in very few cases, such as in H_2 scattering from Ag(111) (Yu *et al* 1985) and in D_2 scattering from Ni(110) and Cu(100) (Bertino *et al* 1997a, 1998b, respectively), whereby the latter experiments are by far those with the best resolution. To illustrate this point, we show the D_2/Cu(100) results in figure 30.

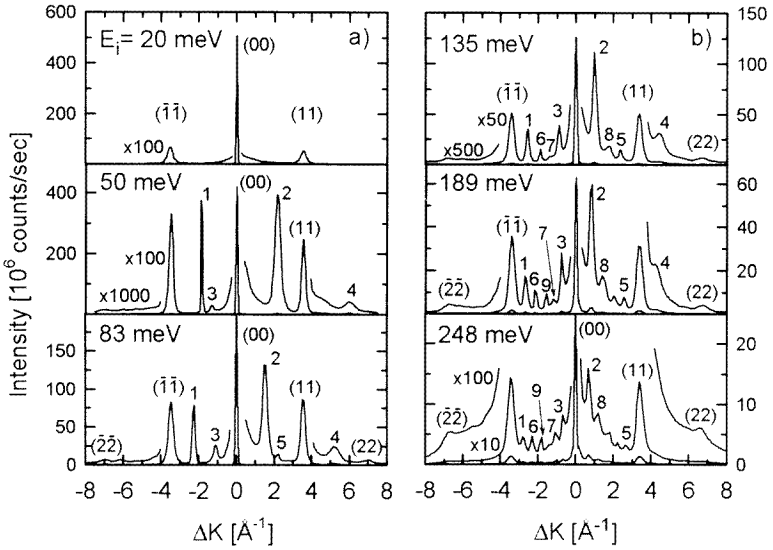

Figure 30. Angular distributions of D_2 scattered from Cu(100) along the [100] direction at a surface temperature of 60 K. The RID peaks are identified with numerical labels, which correspond to the transitions $j = 0 \rightleftharpoons 2$ (1–5), $j = 1 \rightleftharpoons 3$ (6–8) and $j = 2 \rightarrow 4$ (9). From Bertino *et al* (1998b).

In view of the methods to calculate RID probabilities, approximate calculations with different levels of accuracy have been reported. These approaches (usually tested with the H_2/LiF(100) system) include the eikonal approximation (Garibaldi *et al* 1976), the sudden approximation (Gerber *et al* 1980, 1981, Fitz *et al* 1981, Kouri and Gerber 1982, Schinke 1982a†, b), a semiclassical perturbation approach (Hubbard and Miller 1983), a distorted-wave treatment for subsets of the internal states (Whaley and Light 1984) and a nonperturbative method based on Gaussian wavepackets (Jackson and Metiu 1986). Like in the case of atom scattering, a big disadvantage of these approximations is that their range of validity is in general not known, making a comparison with exact close-coupling calculation necessary. Such calculations were performed by Drolshagen *et al* (1985) for H_2 scattering from LiF(100) and collision energies up to 0.7 eV, a much broader range than the one covered in the early (also exact) calculations reported by Wolken (1973b, c, 1975). A finite-temperature theory to calculate RID probabilities as a function of surface temperature was reported by Cruz and Jackson (1989). The surface was treated in a quantum mechanical fashion using the formalism developed by Jackson (1988). A Debye–Waller-like attenuation was observed for the scattering of H_2, HD and D_2 from Cu(100). This attenuation was found to increase with increasing molecular mass and kinetic energy, and to decrease as the peaks become more off-specular. Most of the approximations mentioned above assume that the coupling between rotational and diffraction probabilities is weak, so that both can essentially be treated independently. This assumption is well justified as long as the quadrupole moment of the molecule and the electrostatic field produced by the surface can be neglected, such as for example on metal surfaces (Kroes and Mowrey 1995a, b, Kroes *et al* 1995). More recently, Pijper and Kroes (1998) have shown that when quadrupole terms are included in the potential, large probabilities appear for transitions in

† This work includes a detailed discussion of rotational rainbows.

which the magnetic rotational quantum number m_j changes, which suggests a very promising method for obtaining polarized beams of H_2.

In general, the diffraction intensities for H_2 are larger than those for He and a two-dimensional corrugation is detected, also on highly anisotropic surfaces such as the fcc(110) ones. Good examples of this are provided by a comparison of H_2 and He diffraction from Ag(111) (Horne *et al* 1980), Cu(100) and Cu(110) (Lapujoulade and Perreau 1983), Ni(111) (Hayward and Taylor 1986), MgO(100) (Kolodney and Amirav 1985), Ni(110) (Robota *et al* 1985) as well as by the more recent results on D_2 diffraction from Rh(110) (Cvetko *et al* 1996), Ni(110) and Cu(100) (Bertino *et al* 1997a, 1998b). Although diffraction is usually stronger for H_2 than for He, this is never as large as predicted by the theory (see for example Darling and Holloway 1994). Possible origins of this discrepancy are discussed by Darling and Holloway (1995, p 1639). The large qualitative difference in the behaviour of H_2 as compared with He is a consequence of its larger polarizability, which gives rise to a stronger attractive interaction (Liebsch and Harris 1983). As a result, larger corrugation amplitudes and potential well depths D are usually measured by H_2 beams as compared with He beams, as illustrated by the values listed in table 5. One exception to this behaviour is the Ag(110) surface, on which a larger corrugation was observed with He than with H_2 (Mattera *et al* 1985), although a two-dimensional corrugation was sampled by the H_2 beam (see also Canepa *et al* 1991); the origin of this behaviour is not clear at present. A similar effect was observed on MgO(100) by Kolodney and Amirav (1985), who reported corrugation amplitudes of 0.16 Å and 0.11 Å along the [100] azimuth for He and H_2, respectively.

As first pointed out by Halstead and Holloway (1988), hydrogen diffraction measurements over a wide incident energy range should provide precise information regarding the positions of key topological features of the *reactive potential* within the unit cell, since molecules incident at different sites will be scattered through different angles. Diffraction experiments are thus expected to be complementary to sticking coefficient measurements (see for example Rendulic *et al* 1989, Rettner 1992, Rettner *et al* 1992a, b), which provide information on the chemisorption process averaged over the unit cell. The theoretical models used for describing the dynamics of molecular dissociation at surfaces has been recently reviewed by Darling and Holloway (1995). The studies of Holloway and co-workers (Halstead and Holloway 1988, Darling and Holloway 1990, 1992) and others (Gross and Scheffler 1996) are expected to stimulate new and more detailed hydrogen diffraction experiments to check the implications of the theory. Unfortunately, a serious experimental limitation concerns the high incident energies E_i required, which should be in the range of the activation barriers, i.e. between 200 and 500 meV. The situation is more complicated on very reactive surfaces, since—to prevent the buildup of a H-adlayer—they must be kept at high temperatures ($\sim$500 K), which results in a high inelastic background in the diffraction spectra. As a consequence, H_2 diffraction experiments were in the past restricted to low E_i values, the only exception being the study by Lapujoulade and Perreau (1983) on H_2 diffraction from Cu(100) for $76 < E_i < 297$ meV.

It was not until very recently that He and D_2 diffraction experiments were performed over a wide range of incident energies and with a resolution high enough to also allow investigation of RID peaks. The experiments have been carried out by Bertino and co-workers on Ni(110) and Cu(100), which can be considered as representative examples for systems with a low and a high barrier, respectively, to dissociative chemisorption (Bertino *et al* 1997a, 1998b, respectively). Diffraction of D_2 and He from the inert Cu(100) surface at 60 K was measured as a function of the incident beam energy in the range $20 < E_i < 250$ meV. Due to the high angular resolution (0.35°), a large number of RID peaks could be resolved in the D_2 spectra, as can be seen in figure 30. Diffraction

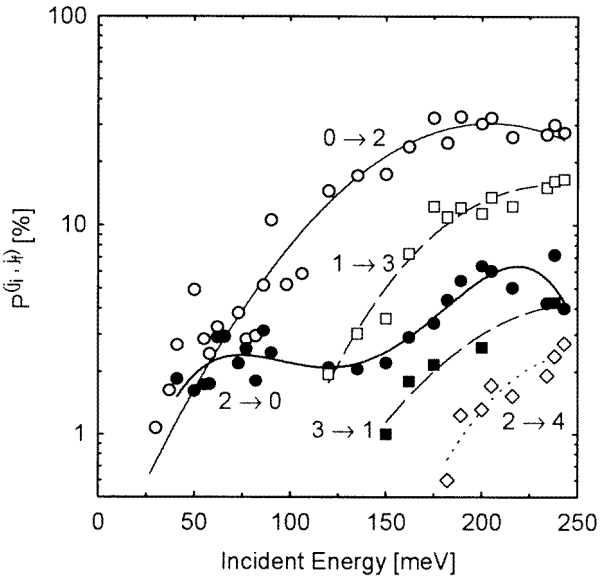

Figure 31. Rotational inelastic transition probabilities in the scattering of D_2 from Cu(100) as a function of incident energy. The lines are added as a guide to the eye. The surface temperature is 60 K. From Bertino *et al* (1998b).

reflectivities of the same order of magnitude were measured for He and D_2, whose temperature attenuation showed a Debye–Waller behaviour up to energies $E_i \sim 250$ meV. Concerning this point, it is interesting to mention that six-dimensional quantum dynamical calculations of H_2 scattering from Pd(100) performed by Gross and Scheffler (1996) have revealed that there is a substantial decrease of the scattered intensities as a function of incident energy also when the substrate atoms are kept fixed, i.e. without taking into account phonon excitations (see also Darling and Holloway 1992). Figure 31 shows as a function of E_i a plot of $P^{(j_i,j_f)}$, the ratio of the RID reflectivities for a given rotational transition $j = j_i \rightarrow j_f$ to the sum of the elastic and inelastic reflectivities. $P^{(j_i,j_f)}$ increases for all transitions (except for $j = 2 \rightarrow 0$) by about an order of magnitude between 50 and 200 meV. The enhancement of the RID probabilities with E_i may be interpreted as an indication of the influence of the dissociative chemisorption barrier, a behaviour also predicted by theoretical calculations (Nielsen *et al* 1995, Gross and Scheffler 1996). The data of figure 31 show, however, that high RID probabilities are also present at energies well below the dissociative chemisorption barrier.

The diffraction and RID peak intensities could be well reproduced using the eikonal approximation for molecular scattering (Garibaldi *et al* 1976). From the good agreement with experiment it was concluded that both elastic and inelastic diffraction probabilities can be accounted for by a hard-wall scattering mechanism, in much the same way as in the case of He diffraction (Bertino *et al* 1998b). Surprisingly, similar conclusions were obtained for D_2 diffraction from the highly reactive Ni(110) surface (Bertino *et al* 1997a). In this case, however, the RID probabilities were found to remain constant for $E_i > 70$ meV. This was interpreted as an indication of the presence of the interaction with the chemisorption potential at all incident energies, in agreement with theoretical calculations. In contrast to these results, an increase of the $j = 0 \rightarrow 2$ transition probability for E_i between 70 and 80 meV was observed in D_2 scattering from the reactive Rh(110) surface (Cvetko *et al* 1996).

One major merit of the experiments performed by Bertino *et al* was that they have determined, for the first time, absolute diffraction and RID peak intensities as a function of E_i and surface temperature, which should enable an easier comparison with theory. These results showed that diffraction experiments can provide valuable information about the main features of the molecule–surface interaction, and will certainly stimulate further hydrogen diffraction studies on other surfaces. We mention in closing that diffraction of hydrogen dimers from LiF(100) has also been observed (Tepper and Miller 1992). The fraction of dimers which scatter elastically and do not fragment was estimated to 5% from a simple data analysis based on the eikonal approximation. These diffraction results open new possibilities in the study of the interaction of clusters with surfaces, and may also be of interest to generate a beam of hydrogen dimers with well-defined angular momentum.

6. Outlook

The number of investigations of solid surfaces by means of atomic beam diffraction has considerably increased during the last 10 years. The results reviewed in this work show that, besides having been applied to the study of new systems, new phenomena have also become accessible to atomic beam diffraction. In the following we discuss some possible future lines of work and emphasize research areas in which we feel more experimental and/or theoretical work is needed.

Concerning structural determinations of well-ordered adlayers, it can be expected that the increased interest observed in recent years towards investigation of physisorbed systems on insulators by means of HAS will continue. In addition, the possibility of performing three-dimensional wavepacket calculations for different scattering conditions, as done by Carré *et al* (1996) for the (1×1)CO/NaCl(100) system (section 3.2.3), will allow a precise characterization of the surface structure. Similar calculations, if extended to other molecular adlayers on insulators, will certainly encourage new experimental studies of such systems. A somewhat surprising fact is that structural determinations of semiconductor surfaces based on exact close-coupling calculations still remain to be done.

Investigations of structural disorder on surfaces is probably the area which experienced the largest development in the last years. The results summarized in section 3, which include characterization of single adsorbates and step-edge defects as well as substitutionally and structurally disordered adlayers, demonstrate that He diffraction can serve as the basis for a crystallography of disordered surfaces. From the experimental point of view, we emphasize that disorder rainbows (predicted for substitutional disordered monolayers) have not yet been observed. To continue with this development it would be desirable to have theoretical calculations of scattering from collections of defects beyond the overlap approach. Although a few such calculations were done (most of them within the sudden approximation), they should be extended to more complex systems. The results presented in section 3.6 also prove that, due to its high-sensitivity and nondestructive character, HAS is especially well suited to monitor phase transitions on surfaces, although only a few quantitative studies have been reported up until now.

With respect to the Debye–Waller factor, the detailed discussion presented in section 3.3 demonstrates that the general form (3.2) with $W(T)$ given by (3.5) describes quite well most He and H_2 diffraction experiments from clean surfaces. More experimental work is needed in order to check whether this also holds for He diffraction from adsorbed layers. In particular, it would be interesting to investigate experimentally (i) the extent to which a harmonic vibrations model (assumed in most theoretical works) describes well the thermal attenuation from adlayers and (ii) the temperature dependence of resonance line shapes for

He/clean metal surfaces to make comparisons with theoretical predictions.

A very general observation can be made on the basis of the results summarized in tables 1–4: only a few studies have been performed on semiconductor and insulator surfaces as compared with those on metal surfaces. We feel that there are three important areas in which the unique abilities of TEAS should be further explored on nonmetallic surfaces: (i) growth, especially of insulator films, (ii) influence of defects on adsorption and (iii) nucleation and growth of metallic clusters. Among the more recent applications of TEAS on metal surfaces, we would like to stress those which allow the determination of surface diffusion parameters and the dynamics of nucleation and growth as well as the *in situ* monitoring of manipulated growth. Due to the relevance of these subjects in surface science one would expect further development of these applications.

As discussed in section 5.3, diffraction studies with hydrogen molecular beams can help us to understand dissociation of molecules at surfaces by testing the variation in barrier height within the unit cell. A necessary condition to make a comparison with theory possible is to determine experimentally absolute diffraction intensities as a function of incident energy and surface temperature, which up until now has been done for only a few surfaces. It would be of interest to extend such experiments to other systems and in particular to alloy surfaces, which are very important from the point of view of applications (catalysis).

An interesting new approach is the diffraction of neutral, but electronically excited He^* beams to investigate the long-range antiferromagnetic ordering on the surfaces of magnetic insulators, as reported by Swan *et al* (1993) for the NiO(100) surface. The possibility recently reported of focusing in two dimensions a helium beam with an atom mirror (Holst and Allison 1997) suggests that one of the certainly most challenging and attractive future developments could concern the fabrication of a helium microscope with nanometre resolution.

Finally, a concluding remark concerns the general attitude with respect to the scattering of noble gas atoms from surfaces. The picture of a *simple* scattering process is definitely ruled out by recent experimental and theoretical investigations. The interaction mechanism is very subtle and strongly involves electronic degrees of freedom of the surface and of the probe particle. Therefore, wider usage of Ne, He^*, and perhaps also He^3 are promising techniques for mapping the electronic structure of surfaces.

Acknowledgments

This review greatly benefited from the careful and constructive reading of parts of the manuscript by G Comsa, J R Manson and R B Gerber. We are also indebted to M Bertino and P Ruggerone for helpful comments and suggestions. The authors appreciate support from the Deutsche Forschungsgemeinschaft, Sonderforschungsbereich 290.

References

Andersson S, Wilzén L and Persson M 1988 *Phys. Rev.* B **38** 2967–73
Annett J F and Haydock R 1984 *Phys. Rev. Lett.* **53** 838–41
——1986 *Phys. Rev.* B **34** 6860–8
Apel R, Farías D and Rieder K H 1995b *Surf. Rev. Lett* **2** 153–7
Apel R, Farías D, Tröger H, Kirsten E and Rieder K H 1996 *Surf. Sci.* **364** 303–11
Apel R, Farías D, Tröger H and Rieder K H 1995a *Surf. Sci.* **331–333** 57–61
Armand G, Lapujoulade J and Lejay Y 1977 *Surf. Sci.* **63** 143–52
Armand G 1989 *J. Physique* **50** 1493–520
Armand G, Lapujoulade J and Manson J R 1989 *Phys. Rev.* B **39** 10 514–8

Armand G and Manson J R 1978 *Phys. Rev.* B **18** 6510–18
——1979 *Surf. Sci.* **80** 532–42
——1984 *Phys. Rev. Lett.* **53** 1112–15
——1986 *Surf. Sci.* **169** 216–24
——1988 *Phys. Rev.* B **37** 4363–8
Armand G, Manson J R and Jayanthi C S 1986 *Phys. Rev.* B **34** 6627–39
Armand G and Salanon B 1989 *Surf. Sci.* **217** 341–66
Armand G, Schwenger L and Ernst H J 1996 *Phys. Rev.* B **53** R4249–52
Arnott M, McCash E M and Allison W 1992 *Surf. Sci.* **269–270** 724–30
Arumainayagam C R and Madix R J 1991 *Prog. Surf. Sci.* **38** 1–102
Asada H 1979 *Surf. Sci.* **81** 386–408
Aten R M, Blanchard D, Allen L R, Conrad E R, Nelson M and Engel T 1987 *Surf. Sci.* **183** 515–30
Aten R M and Engel T 1985 *J. Chem. Phys.* **84** 434–9
Avrin W F and Merrill R P 1992 *Surf. Sci.* **274** 231–51
——1994 *Surf. Sci.* **311** 269–80
Aziz R A, Buck U, Jónsson H, Ruiz-Suárez J C, Schmidt B, Scoles G, Slaman M J and Xu J 1989 *J. Chem. Phys.* **91** 6477–93
Barbier L and Lapujoulade J 1990 *Vacuum* **40** 615–17
——1991 *Surf. Sci.* **253** 303–12
Barbier L, Salanon B and Sprösser J 1994 *Surf. Rev. Lett* **1** 75–88
Barker J A and Auerbach D J 1985 *Surf. Sci. Rep.* **4** 1–99
Barker J A and Batra I P 1983 *Phys. Rev.* B **27** 3138–43
Batra I P 1984 *Surf. Sci.* **137** L97–102
Becker A F, Rosenfeld G, Poelsema B and Comsa G 1993 *Phys. Rev. Lett.* **70** 477–80
Becker G E, Cardillo M J, Serri J A and Hamann D R 1983 *Phys. Rev.* B **28** 504–14
Becker R S, Golovchenko J A and Swartzentruber B S 1985 *Phys. Rev. Lett.* **54** 2678–80
Bedrossian P, Poelsema B, Rosenfeld G, Jorritsma L C, Lipkin N N and Comsa G 1995 *Surf. Sci.* **334** 1–9
Beeby J L 1971 *J. Phys. C: Solid State Phys.* **4** L359–62
Bellman A F, Cvetko D, Morgante A, Polli M, Tommasini F, Prince K C and Rosei R 1993a *Surf. Sci.* **281** L321–5
Bellman A F, Morgante A, Polli M, Tommasini F, Cvetko D, Dhanak V R, Lausi A, Prince K C and Rosei R 1993b *Surf. Sci.* **298** 1–5
Benedek G, Gerlach R, Glebov A, Lange G, Miret-Artés S, Skofronick J G and Toennies J P 1996 *Phys. Rev.* B **53** 11 211–17
Benedek G, Luo N S, Reichmuth A, Ruggerone P and Toennies J P 1994 *Mater. Sci. Eng.* B **23** 123–9
Benedek G and Miret-Artés S 1995 *Surf. Sci.* **339** L935–9
Bernasek S L, Zappone M and Jiang P 1992 *Surf. Sci.* **272** 53–64
Berndt R, Hinch B J, Toennies J P and Wöll Ch 1990 *J. Chem. Phys.* **92** 1435–41
Bertel E 1996 *Surf. Sci.* **367** L61–5
Bertino M F, Graham A P, Rusin L Y and Toennies J P 1998b *J. Chem. Phys.* in press
Bertino M F, Hofmann F and Toennies J P 1997a *J. Chem. Phys.* **106** 4327–38
Bertino M F, Miret-Artés S and Toennies J P 1998a *Chem. Phys. Lett.* **287** 663–70
Bertino M F, Miret-Artés S, Toennies J P and Benedek G 1997b *Phys. Rev.* B **56** 9964–9
——1997c *Surf. Sci.* **377–379** 714–18
Bilić A and Gumhalter B 1995 *Phys. Rev.* B **52** 12 307–28
Blake R J 1984 *Comput. Phys. Commun.* **33** 425–44
Boato G, Cantini P and Mattera L 1976b *Surf. Sci.* **55** 141–78
Boato G, Cantini P and Tatarek R 1976a *J. Phys. F: Met. Phys.* **6** L237–40
Borondo F, Jaffé Ch and Miret-Artés S 1994 *Surf. Sci.* **317** 211–20
Bortolani V, Celli V, Franchini A, Idiodi J, Santoro G, Kern K, Poelsema B and Comsa G 1989 *Surf. Sci.* **208** 1–12
Bortolani V and Levi A C 1986 *Riv. Nuovo Cimento* **9** 1–77
Bracco G, Cantini P, Cavanna E, Tatarek R and Glachant A 1984 *Surf. Sci.* **136** 169–83
Brault P, Range H, Toennies J P and Wöll Ch 1997 *Z. Phys. Chem.* **198** 1–17
Braun J, Glebov A, Graham A P, Menzel A and Toennies J P 1998 *Phys. Rev. Lett.* **80** 2638–41
Braun J, Kostov K L, Witte G and Wöll Ch 1997 *J. Chem. Phys.* **106** 8262–73
Braun J and Toennies J P 1996 *Surf. Sci.* **368** 226–31
——1997 *Surf. Sci.* **384** L858–64
Bruch L W, Glebov A, Toennies J P and Weiss H 1995 *J. Chem. Phys.* **103** 5109–20

Brune H 1998 *Surf. Sci. Rep.* **31** 121–230
Brusdeylins G and Schmicker D 1995 *Surf. Sci.* **331–333** 237–42
Buongiorno Nardelli M 1996 *Solid State Commun.* **97** 215–19
Buongiorno Nardelli M *et al* 1996a *Phys. Rev.* **53** 1095–8
——1996b *Synth. Met.* **76** 173–6
Butz H P, Feltgen R, Pauly H and Vehmeyer H 1971 *Z. Phys.* **247** 70–82
Cabrera N, Celli V, Goodman F O and Manson R 1970 *Surf. Sci.* **19** 67–92
Cabrera N and Solana J 1974 *Proc. Int. School of Physics Enrico Fermi* vol 58, ed F Goodman (Bologna: Compositori) p 530
Camarero J, Ferrón J, Cros V, Gómez L, Vázques de Parga A L, Gallego J M, Prieto J E, de Miguel J J and Miranda R 1998 *Phys. Rev. Lett.* **81** 850–3
Camarero J, Spendeler L, Schmidt G, Heinz K, de Miguel J J and Miranda R 1994 *Phys. Rev. Lett.* **73** 2448–51
Camillone N, Chidsey C E D, Liu G-Y, Putvinski T M and Scoles G 1991 *J. Chem. Phys.* **94** 8493–502
Camillone N, Chidsey C E D, Liu G-Y and Scoles G 1993a *J. Chem. Phys.* **98** 3503–11
——1993b *J. Chem. Phys.* **98** 4234–45
Canepa M, Cantini P, Cavanna E, Mattera L, Tarditi V and Terreni S 1991 *Surf. Sci.* **251–252** 1142–7
Canepa M, Cantini P, Lo Vetere S, Mattera L, Salvietti M and Terreni S 1993a *Nuovo Cimento* **15** 501–10
Canepa M, Cantini P, Mattera L, Narducci E, Salvietti M and Terreni S 1995a *Surf. Sci.* **322** 271–84
Canepa M, Cantini P, Mattera L, Salvietti M, Terreni S and Valdenazzi F 1993b *Surf. Sci.* **287–288** 273–7
Canepa M, Cantini P, Narducci E, Salvietti M, Terreni S and Mattera L 1995b *Surf. Sci.* **343** 176–84
Canepa M, Mattera L and Narducci E 1997a *Surf. Sci.* **371** 431–7
Canepa M, Terreni S, Cantini P, Campora A and Mattera L 1997b *Phys. Rev.* B **56** 4233–42
Cantini P, Mattera L, de Kieviet M F M, Jalink K, Tassistro C, Terreni S and Linke U 1989 *Surf. Sci.* **211–212** 872–80
Cantini P, Tatarek R and Felcher G P 1979 *Phys. Rev.* B **19** 1161–71
Cardillo M J, Becker G E, Hamann D R, Serri J A, Whitman L and Mattheiss L F 1983 *Phys. Rev.* B **28** 494–503
Cardillo M J, Sibener S J, Becker G E and Miller D R 1981 *Surf. Sci.* **107** 469–93
Carré M-N and Lemoine D 1994 *J. Chem. Phys.* **101** 5305–12
Carré M-N, Lemoine D, Picaud S and Girardet C 1996 *Surf. Sci.* **347** 128–42
Celli V 1992 *Helium Atom Scattering from Surfaces (Springer Series in Surface Sciences 27)* ed E Hulpke (Berlin: Springer) pp 25–40
Celli V, Eichenauer D, Kaufhold A and Toennies J P 1985 *J. Chem. Phys.* **83** 2504–21
Celli V and Maradudin A A 1985 *Phys. Rev.* B **31** 825–42
Chiesa M, Mattera L, Musenich R and Salvo C 1985 *Surf. Sci.* **151** L145–52
Choi B H, Tang K T and Toennies J P 1997 *J. Chem. Phys.* **107** 1631–3
Chow H and Thompson E D 1976 *Surf. Sci.* **59** 225–51
Chung S, Holter N and Cole M W 1985 *Phys. Rev.* B **31** 6660–8
——1986 *Surf. Sci.* **165** 466–76
Cole M W and Tsong T T 1977 *Surf. Sci.* **69** 325–35
Comsa G 1979 *Surf. Sci.* **81** 57–68
Comsa G, Kern K and Poelsema B 1992 *Helium Atom Scattering from Surfaces (Springer Series in Surface Sciences 27)* ed E Hulpke (Berlin: Springer) pp 243–64
Comsa G, Mechtersheimer G and Poelsema B 1982a *Surf. Sci.* **119** 159–71
——1982b *Surf. Sci.* **119** 172–83
Conrad E H, Kaufman D S, Allen L R, Aten R M and Engel T 1985 *J. Chem. Phys.* **83** 5286–92
Cortona P, Dondi M G, Cvetko D, Lausi A, Morgante A, Prince K C and Tommasini F 1993 *Phys. Rev.* B **47** 6705–10
Cortona P, Dondi M G, Lausi A, and Tommasini F 1992b *Surf. Sci.* **276** 333–40
Cortona P, Dondi M G and Tommasini F 1992a *Surf. Sci.* **261** L35–8
Cowin J P, Yu C-F, Sibener S J and Hurst J E 1981 *J. Chem. Phys.* **75** 1033–4
Croci M, Félix C, Vandoni G, Harbich W and Monot R 1993 *Surf. Sci.* **290** L667–72
——1994 *Surf. Sci.* **307–309** 460–4
Crottini A, Cvetko D, Floreano L, Gotter R, Morgante A and Tommasini F 1997 *Phys. Rev. Lett.* **79** 1527–30
Cruz A J and Jackson B 1989 *J. Chem. Phys.* **91** 4985–93
Cui J, White J D, Diehl R D, Annett J F and Cole M W 1992 *Surf. Sci.* **279** 149–58
Curson N J, Bullman H G, Buckland J R and Allison W 1997 *Phys. Rev.* B **55** 10 819–29
Cvetko D, de Renzi V, Floreano L, Lausi A, Morgante A, Peloi M, Tommasini F, Kirsten E and Rieder K H 1995d *Phys. Rev.* B **51** 11 055–60

Cvetko D, de Renzi V, Floreano L and Morgante A 1994c *Solid State Commun.* B **91** 539–43
Cvetko D, de Renzi V, Floreano L, Morgante A, Peloi M, Tommasini F, Cháb V and Prince K C 1995a *Phys. Rev.* B **51** 17 957–64
——1995b *Surf. Sci.* **323** L305–10
——1995c *Phys. Rev.* B **52** 14 941–6
Cvetko D, Floreano L, Morgante A, Peloi M and Tommasini F 1994a *Surf. Sci.* **307–309** 519–25
Cvetko D, Floreano L, Morgante A, Peloi M, Tommasini F, Prince K C, Vendruscolo M and Tosatti E 1994b *Surf. Sci.* **318** L1193–200
Cvetko D, Morgante A, Santianello A and Tommasini F 1996 *J. Chem. Phys.* **104** 7778–83
Darling G R and Holloway S 1990 *J. Chem. Phys.* **93** 9145–56
——1992 *J. Chem. Phys.* **97** 5182–92
——1994 *Surf. Sci.* **304** L461–7
——1995 *Rep. Prog. Phys.* **58** 1595–672
Dastoor P, Arnott M, McCash E M and Allison W 1992 *Surf. Sci.* **272** 154–60
Dastoor P, Ellis J, Reichmuth A, Bullman H, Holst B and Allison W 1994 *Surf. Rev. Lett* **1** 509–12
de Beauvais C, Girard Y, Pérard C, Croset B and Mutaftschiev B 1996 *Surf. Sci.* **367** 129–34
de Beauvais C, Rouxel D, Bigeard B and Mutaftschiev B 1991 *Phys. Rev.* B **44** 4024–7
de Beauvais C, Rouxel D, Michailov M and Mutaftschiev B 1995 *Surf. Sci.* **324** 1–7
de Beauvais C, Rouxel D, Mutaftschiev B and Bigeard B 1992 *Surf. Sci.* **272** 73–80
de Miguel J J, Cebollada A, Gallego J M, Ferrer S, Miranda R, Schneider C M, Bressler P, Garbe J, Bethke K and Kirschner J 1989 *Surf. Sci.* **211–212** 732–9
de Miguel J J, Cebollada A, Gallego J M, Ferrón J and Ferrer S 1988a *J. Cryst. Growth* **88** 442–54
de Miguel J J, Cebollada A, Gallego J M and Miranda R 1990 *Kinetics of Ordering and Growth at Surfaces* ed M G Lagally (New York: Plenum) p 483
de Miguel J J, Ferrón J, Cebollada A, Gallego J M and Ferrer S 1988b *J. Cryst. Growth* **91** 481–9
de Miguel J J, Sánchez A, Cebollada A, Gallego J M, Ferrón J and Ferrer S 1987 *Surf. Sci.* **189–190** 1062–8
D'Evelyn M P and Madix R J 1983 *Surf. Sci. Rep.* **3** 413–95
Diercks V, Goerge J, Zeppenfeld P, David R and Comsa G 1996 *Surf. Sci.* **352–354** 274–9
Doak R B and Nguyen D B 1989 *Phys. Rev.* B **40** 1495–9
Drolshagen G, Kaufhold A and Toennies J P 1985 *J. Chem. Phys.* **83** 827–34
Drolshagen G and Vollmer R 1987 *J. Chem. Phys.* **87** 4948–57
Duan J, Bishop G G, Gillman E S, Chern G, Safron S A and Skofronick J G 1992a *J. Vac. Sci. Technol.* **272** 1999–2005
——1992b *Surf. Sci.* **272** 220–8
Egelhoff W F and Jacob I 1989 *Phys. Rev. Lett.* **62** 921–4
Ellis J, Hermann K, Hofmann F and Toennies J P 1995 *Phys. Rev. Lett.* **75** 886–9
Ellis T H, Scoles G and Valbusa U 1983 *Chem. Phys. Lett.* **94** 247–9
——1985 *Surf. Sci.* **155** 499–534
Engel T and Rieder K H 1982 *Structural Studies of Surfaces with Atomic and Molecular Beam Diffraction (Springer Tracts in Modern Physics 91)* (Berlin: Springer) pp 55–180
Engel T, Rieder K H and Batra I P 1984 *Surf. Sci.* **148** 321–37
Engel T and Weare J H 1985 *Surf. Sci.* **164** 403–16
Ernst H J, Fabre F, Folkerts R and Lapujoulade J 1994 *Phys. Rev. Lett.* **72** 112–15
Ernst H J, Fabre F and Lapujoulade J 1992a *Surf. Sci.* **275** L682–4
——1992b *Phys. Rev.* B **46** R1929–32
——1992c *Phys. Rev. Lett.* **69** 458–61
Ernst H J, Folkerts R and Schwenger L 1995 *Phys. Rev.* B **52** 8461–70
Esbjerg N and Nørskov J K 1980 *Phys. Rev. Lett.* **45** 807–10
Fahsold G, König G, Lehmann A and Rieder K H 1998 *Appl. Surf. Sci.* submitted
Farías D, Eckert I, Burg B and Rieder K H 1993 *Surf. Sci.* **297** 162–6
Farías D, Lange G, Rieder K H and Toennies J P 1997c *Phys. Rev.* B **55** 7023–33
Farías D, Patting M, John F and Rieder K H 1998 to be published
Farías D, Patting M and Rieder K H 1997a *Phys. Status Solidi* A **159** 255–62
——1997b *Surf. Sci.* **385** 115–22
Farías D, Siebentritt S, Apel R, Pues R and Rieder K H 1997d *J. Chem. Phys.* **106** 8254–61
Farías D, Tröger H, Patting M and Rieder K H 1996 *Surf. Sci.* **352–354** 155–60
Farías D, Tröger H and Rieder K H 1995 *Surf. Sci.* **331–333** 150–5
Faubel M, Gianturco F A, Ragnetti F, Rusin L Y, Sondermann F and Tappe U 1994 *J. Chem. Phys.* **101** 8800–11

Félix C, Vandoni G, Harbich W, Buttet J and Monot R 1995 *Surf. Sci.* **331–333** 925–9
——1996 *Phys. Rev.* B **54** 17 039–50
Ferry D, Glebov A, Senz V, Suzanne J, Toennies J P and Weiss H 1996 *J. Chem. Phys.* **105** 1697–701
Fitz D E, Beard L H and Kouri D J 1981 *Chem. Phys.* **59** 257–68
Flach B, Hulpke E and Steinhögl W 1998 *Surf. Sci.* **412–413** 12–23
Foulias S, Curson N J, Cowen M C and Allison W 1995 *Surf. Sci.* **331–333** 522–7
Frenken J W M and Hinch B J 1992 *Helium Atom Scattering from Surfaces (Springer Series in Surface Sciences 27)* ed E Hulpke (Berlin: Springer) pp 287–313
Frisch R and Stern O 1933 *Z. Phys.* **84** 430
García N 1976 *Phys. Rev. Lett.* **37** 912–5
——1977 *J. Chem. Phys.* **67** 897–916
——1978 *Surf. Sci.* **71** 220–30
García N and Cabrera N 1978 *Phys. Rev.* B **18** 576–89
García N, Goodman F O, Celli V and Hill N R 1979 *Phys. Rev.* B **19** 1808–11
García N and Schlup W A 1982 *Surf. Sci.* **122** L657–62
Garibaldi U, Levi A C, Spadacini R and Tommei G E 1975 *Surf. Sci.* **48** 649–75
——1976 *Surf. Sci.* **55** 40–60
Gerber R B 1987 *Chem. Rev.* **87** 29–79
Gerber R B, Beard L H and Kouri D J 1981 *J. Chem. Phys.* **74** 4709–25
Gerber R B and Yinnon A T 1980 *J. Chem. Phys.* **73** 3232–8
——1991 *Chem. Phys. Lett.* **181** 553–7
Gerber R B, Yinnon A T and Kosloff R 1984 *Chem. Phys. Lett.* **105** 523–6
Gerber R B, Yinnon A T, Shimoni Y and Kouri D J 1980 *J. Chem. Phys.* **73** 4397–412
Gerber R B, Yinnon A T, Yanuka M and Chase D 1992 *Surf. Sci.* **272** 81–93
Gerlach R, Glebov A, Lange G, Toennies J P and Weiss H 1995 *Surf. Sci.* **331–333** 1490–5
Gibson K D, Cerjan C, Light J C and Sibener S J 1988 *J. Chem. Phys.* **88** 7911–41
Gibson K D and Sibener S J 1988a *J. Chem. Phys.* **88** 7862–92
——1988b *J. Chem. Phys.* **88** 7893–910
Glebov A, Graham A P, Menzel A and Toennies J P 1997a *J. Chem. Phys.* **106** 9382–5
Glebov A, Manson J R, Skofronick J G and Toennies J P 1997c *Phys. Rev. Lett.* **78** 1508–11
Glebov A, Miller R E and Toennies J P 1997b *J. Chem. Phys.* **106** 6499–506
Glebov A, Toennies J P and Weiss H 1996 *Surf. Sci.* **351** 200–8
Goapper S, Barbier L and Salanon B 1996 *Surf. Sci.* **364** 99–106
Goerge J, Zeppenfeld P, Büchel M, David R and Comsa G 1995 *Surf. Sci.* **331–333** 1038–42
Goerge J, Zeppenfeld P, David R, Büchel M and Comsa G 1993 *Surf. Sci.* **289** 201–13
Gómez L J, Bourgeal S, Ibáñez J and Salmerón M 1985 *Phys. Rev.* B **31** 2551–3
Goodman F O 1977 *J. Chem. Phys.* **66** 976–82
Gorse D, Salanon B, Fabre F, Kara A, Perreau J, Armand G and Lapujoulade J 1984 *Surf. Sci.* **147** 611–46
Graham A P, Allison W and McCash E M 1992 *Surf. Sci.* **269–270** 394–9
Graham A P, Bertino M F, Hofmann F, Silvestri W and Toennies J P 1997 *J. Chem. Phys.* **106** 2502–12
Graham A P, Bertino M F, Hofmann F and Toennies J P 1996a *J. Chem. Soc. Faraday Trans.* **92** 4749–57
Graham A P, Fang D, Cash E M and Allison W 1998 *Phys. Rev.* B **57** 13 158–66
Graham A P, Hinch B J, Kochanski G P, Mc Cash E M and Allison W 1994 *Phys. Rev.* B **50** 15 304–15
Graham A P, Hofmann F and Toennies J P 1996b *J. Chem. Phys.* **105** 2093–8
Graham A P, McCash E M and Allison W 1995 *Phys. Rev.* B **51** 5306–10
Graham A P and Toennies J P 1997 *Phys. Rev.* B **56** 15 378–90
Greene E F and Mason E A 1978 *Surf. Sci.* **75** 549–60
Gross A and Scheffler M 1996 *Chem. Phys. Lett.* **263** 567–73
Gross G, Müller V and Rieder K H 1991 *Phys. Rev.* B **44** 1434–7
Gross G and Rieder K H 1991 *Surf. Sci.* **241** 33–8
Guantes R, Borondo F, Jaffé Ch and Miret-Artés S 1995 *Surf. Sci.* **338** L863–8
——1996 *Phys. Rev.* B **53** 14 117–26
Guantes R, Borondo F, Margalef-Roig J, Miret-Artés S and Manson J R 1997 *Surf. Sci.* **375** L379–84
Gumhalter B 1996 *Surf. Sci.* **347** 237–48
Gumhalter B and Lovric D 1986 *Surf. Sci.* **178** 743–54
Ha J S and Greene E F 1989a *J. Chem. Phys.* **91** 571–6
——1989b *J. Chem. Phys.* **91** 7957–63
Hahn E, Schief H, Marsico V, Fricke A and Kern K 1994 *Phys. Rev. Lett.* **72** 3378–81

Hahn P, Clabes J and Henzler M 1980 *J. Appl. Phys.* **51** 2079–84
Halstead D and Holloway S 1988 *J. Chem. Phys.* **88** 7197–208
Hamburger D A and Gerber R B 1995 *J. Chem. Phys.* **102** 6919–30
Hamburger D A, Yinnon A T, Farbman I, Ben-Shaul A and Gerber R B 1995 *Surf. Sci.* **327** 165–91
Hamburger D A, Yinnon A T and Gerber R B 1996 *Chem. Phys. Lett.* **253** 223–9
Hamburger-Lidar D A 1996 *Phys. Rev.* E **54** 354–70
Hamza A V, Kubiak G D and Stulen R H 1988 *Surf. Sci.* **206** L833–44
Haneman D and Haydock R 1982 *J. Vac. Sci. Technol.* **21** 330
Hansen L, Stoltze P, Jacobsen K W and Nørskov J K 1991 *Phys. Rev.* B **44** 6523–6
Harris J and Zaremba E 1985 *Phys. Rev. Lett.* **55** 1940–3
Hayward D O and Taylor A O 1986 *J. Phys. C: Solid State Phys.* **19** L309–14
Henrion J and Rhead G E 1972 *Surf. Sci.* **29** 20–36
Henry C R and Meunier M 1996 *Mater. Sci. Eng.* A **217–218** 239–43
Henry C R, Meunier M and Morel S 1993 *J. Cryst. Growth* **129** 416–20
Henzler M 1978 *Surf. Sci.* **73** 240–51
——1993 *Surf. Sci.* **298** 369–77
Herman F and Skillman S 1963 *Atomic Structure Calculations* (Englewood Cliffs, NJ: Prentice-Hall)
Hernández J J, Li J A, Baker J, Safron S A and Skofronick J G 1996 *J. Vac. Sci. Technol.* A **14** 1788–93
Hernández M, Miret-Artés S, Villarreal P and Delgado-Barrio G 1991 *Surf. Sci.* **251–252** 369–72
——1992 *Surf. Sci.* **274** 21–34
——1993 *Surf. Sci.* **290** L693–8
Heuer M and Rice T M 1985 *Z. Phys.* B **59** 299–309
Hill N R and Celli V 1978 *Phys. Rev.* B **17** 2478
Hinch B J 1988 *Phys. Rev.* B **38** 5260–6
——1989 *Surf. Sci.* **221** 346–64
Hinch B J, Koziol C, Toennies J P and Zhang G 1989a *Europhys. Lett.* **10** 341–6
——1991 *Vacuum* **42** 309–11
Hinch B J, Lock A, Toennies J P and Zhang G 1989b *J. Vac. Sci. Technol.* B **42** 1260–4
Hinch B J, Lock A, Madden H H, Toennies J P and Witte G 1990 *Phys. Rev.* B **42** 1547–59
Hinch B J, Rohlfing D M, Ellis J, Allison W and Willis R F 1987 *Surf. Sci.* **189–190** 120–6
Hinch B J and Toennies J P 1990 *Phys. Rev.* B **42** 1209–16
Hirschorn E S, Lin D S, Leibsle F M, Samsavar A, Chiang T S 1991 *Phys. Rev.* B **44** R1403–6
Ho T S and Rabitz H 1991 *J. Chem. Phys.* **94** 2305–14
——1992 *J. Chem. Phys.* **96** 7092–8
Höche H, Toennies J P and Vollmer R 1993 *Phys. Rev. Lett.* **71** 1208–11
Hofmann F, Toennies J P and Manson J R 1994 *J. Chem. Phys.* **101** 10 155–72
Hoinkes H 1980 *Rev. Mod. Phys.* **52** 933–70
Hoinkes H, Nahr H and Wilsch H 1972 *Surf. Sci.* **33** 516–24
——1973 *Surf. Sci.* **40** 457
Hoinkes H and Wilsch H 1992 in *Helium Atom Scattering from Surfaces (Springer Series in Surface Sciences 27)* ed E Hulpke (Berlin: Springer) pp 113–72
Holst B and Allison W 1997b *Nature* **390** 244
Holst B, Nohlen M, Wandelt K and Allison W 1997a *Surf. Sci.* **377–379** 891–4
Horne J M, Yerkes S C and Miller D R 1980 *Surf. Sci.* **93** 47–63
Hubbard L M and Miller W H 1983 *J. Chem. Phys.* **78** 1801–7
Hugenschmidt M B and de Beauvais C 1994 *Surf. Sci.* **307–309** 455–9
Hulpke E (ed) 1992 *Helium Atom Scattering from Surfaces (Springer Series in Surface Sciences 27)* (Berlin: Springer)
Hulpke E, Lower J and Reichmuth A 1996 *Phys. Rev.* B **53** 13 901–8
Hutchison J 1980 *Phys. Rev.* B **22** 5671–8
Hutson J M and Schwartz C 1983 *J. Chem. Phys.* **79** 5179–87
Iannotta S, Scoles G and Valbusa U 1985 *J. Phys. C: Solid State Phys.* **89** 1914-21
Idiodi J, Bortolani V, Franchini A, Santoro G and Celli V 1987 *Phys. Rev.* B **35** 6029–33
Jackson B 1988 *J. Chem. Phys.* **89** 2473–81
Jackson B and Metiu H 1986 *J. Chem. Phys.* **84** 3535–44
Jiang P, Zappone M and Bernasek S L 1993a *J. Chem. Phys.* **99** 8120–5
——1993b *J. Chem. Phys.* **99** 8126–35
Jónsson H and Weare J H 1986 *Phys. Rev. Lett.* **57** 412–15

Jónsson H, Weare J H and Levi A C 1984a *Phys. Rev.* B **30** 2241–4
——1984b *Surf. Sci.* **148** 126–38
Jung D R, Cui J and Frankl D R 1991 *Phys. Rev.* B **43** 10 042–50
Kaufman D S, Allen L R, Conrad E H, Aten R M, and Engel T 1986 *Surf. Sci.* **173** 517–37
Kaufman D S, Aten R M, Conrad E H, Allen L R, and Engel T 1987 *J. Chem. Phys.* **86** 3682–92
Kern K and Comsa G 1989 *Molecule Surface Interactions (Advances in Chemical Physics LXXVI)* ed K P Lawley (Chichester: Wiley) pp 211–80
Kern K, David R and Comsa G 1985 *J. Chem. Phys.* **82** 5673–6
Kern K, David R, Palmer R L and Comsa G 1986a *Phys. Rev. Lett.* **56** 620–3
Kern K, Zeppenfeld P, David R and Comsa G 1987 *Phys. Rev. Lett.* **59** 79–82
Kern K, Zeppenfeld P, David R, Palmer R L and Comsa G 1986b *Phys. Rev. Lett.* **57** 3187–90
Kern K, Niehus H, Schatz A, Zeppenfeld P, Goerge J and Comsa G 1991 *Phys. Rev. Lett.* **67** 855–8
Kirsten E, Parschau G and Rieder K H 1990 *Surf. Sci.* **236** L365–8
——1991 *Chem. Phys. Lett.* **181** 544–8
Kirsten E and Rieder K H 1989 *Surf. Sci.* **222** L837–44
Klein J R and Cole M W 1979a *Surf. Sci.* **79** 269–88
——1979b *Surf. Sci.* **81** L319–24
Kolodney E and Amirav A 1985 *Surf. Sci.* **155** 715–31
Kouri D J and Gerber R B 1982 *Israel J. Chem.* **22** 321–8
Kroes G J and Mowrey R C 1995a *Chem. Phys. Lett.* **232** 258–66
——1995b *J. Chem. Phys.* **103** 2186–201
Kroes G J, Snjiders J G and Mowrey R C 1995 *J. Chem. Phys.* **102** 5512–24
Krzyzowski M, Zeppenfeld P, Romainczyk Ch., David R, Comsa G, Kuhnke K E and Kern K 1994 *Phys. Rev.* B **50** 18 505–16
Krzyzowski M, Zeppenfeld P and Comsa G 1995 *J. Chem. Phys.* **103** 8705–12
Kunkel R, Poelsema B, Verheij L K and Comsa G 1990 *Phys. Rev. Lett.* **65** 733–6
Kurz E A and Hudson J B 1988 *Surf. Sci.* **195** 15–30
Lahee A M, Manson J R, Toennies J P and Wöll C 1986a *Phys. Rev. Lett.* **57** 471–4
——1986b *Phys. Rev. Lett.* **57** 2331(E)
——1987 *J. Chem. Phys.* **86** 7194–203
Lambert W R, Trevor P L, Cardillo M J, Sakai A and Hamann D R 1987 *Phys. Rev.* B **35** 8055–64
Lange G, Meli C A, Toennies J P and Greene E F 1997 *Phys. Rev.* B **56** 4642–7
Lange G, Schmicker D, Toennies J P, Vollmer R and Weiss H 1995 *J. Chem. Phys.* **103** 2308–19
Lapujoulade J 1981 *Surf. Sci.* **108** 526–48
——1992 *Helium Atom Scattering from Surfaces (Springer Series in Surface Sciences 27)* ed E Hulpke (Berlin: Springer) pp 95–112
——1994 *Surf. Sci. Rep.* **20** 191–249
Lapujoulade J, Le Cruër Y, Lefort M, Lejay Y and Maurel E 1980b *Phys. Rev.* B **22** 5740–3
——1981b *Surf. Sci.* **103** L85–9
——1982 *Surf. Sci.* **118** 103–20
Lapujoulade J, Le Cruër Y, Lefort M, Lejay Y, Maurel E and Papanicolau N 1981a *J. Physique Lett.* **42** L463–4
Lapujoulade J and Lejay Y 1977 *J. Physique* **38** L303–6
Lapujoulade J, Lejay Y and Armand G 1980a *Surf. Sci.* **95** 107–30
Lapujoulade J and Perreau J 1983 *Phys. Scr.* T **4** 138–40
Lapujoulade J, Perreau J and Kara A 1983 *Surf. Sci.* **129** 59–78
Larese J Z, Leung W Y, Frankl D R, Holter N, Chung S and Cole M W 1985 *Phys. Rev. Lett.* **54** 2533–6
Laughlin R B 1982 *Phys. Rev.* B **25** 2222–47
Lee J, Cowin J P and Wharton L 1983 *Surf. Sci.* **130** 1–28
LeGrand A D and Greene E F 1986 *J. Chem. Phys.* **84** 6483–7
Lehmann A, Fahsold G, König G and Rieder K H 1996 *Surf. Sci.* **369** 289–99
Lehmann A, König G and Rieder K H 1994 *Phys. Rev. Lett.* **73** 3125–8
——1995 *Chem. Phys. Lett.* **235** 65–8
Lennard-Jones J E and Devonshire A F 1936 *Nature* **137** 1069
Lent C S and Cohen P I 1984 *Surf. Sci.* **139** 121–54
Levi A C and Passerone D 1994 *Surf. Rev. Lett* **1** 109–14
Levi A C and Suhl H 1979 *Surf. Sci.* **88** 221–54
Li W, Lin J S, Karimi M, Dowben P A and Vidali G 1992 *Phys. Rev.* B **45** 3708–17
Li W, Lin J S, Karimi M and Vidali G 1991 *J. Vac. Sci. Technol.* A **9** 1707–11

Li W and Vidali G 1992 *Phys. Rev.* B **46** 4356–9
Li W, Vidali G and Biham O 1993 *Phys. Rev.* B **48** 8336–44
Liebsch A and Harris J 1983 *Surf. Sci.* **130** L349–57
Lilienkamp G and Toennies J P 1982 *Phys. Rev.* B **26** 4752–5
——1983 *J. Chem. Phys.* **78** 5210–24
Liu G Y, Robinson G N and Scoles G 1992 *Surf. Sci.* **262** 409–21
Liu G Y, Rowntree P, Scoles G and Xu J 1989 *Surf. Sci.* **224** 43–59
Lu T M and Lagally M G 1982 *Surf. Sci.* **120** 47–66
Luntz A, Mattera L, Rocca M, Terreni S, Tommasini F and Valbusa 1983 *Surf. Sci.* **126** 695–701
Luntz A, Mattera L, Rocca M, Tommasini F and Valbusa 1982 *Surf. Sci.* **120** L447–52
Mahale N K, Kara A and Cole M W 1987 *Solid State Commun.* **62** 225–9
Manolopoulos D E and Wyatt R E 1988 *Chem. Phys. Lett.* **152** 23–32
Manolopoulos D E, Wyatt R E and Clary D C 1990 *J. Chem. Soc. Faraday Trans.* **86** 1641–8
Manson J R 1988 *Phys. Rev.* B **37** 6750–6
——1991 *Phys. Rev.* B **43** 6924–37
——1992 *Helium Atom Scattering from Surfaces (Springer Series in Surface Sciences 27)* ed E Hulpke (Berlin: Springer) pp 173–205
——1994 *Comput. Phys. Commun.* **80** 145–67
Manson J R and Armand G 1987 *Surf. Sci.* **184** 511–29
——1988 *Surf. Sci.* **195** 513–34
Mantovani J G, Manson J R and Armand G 1984 *Surf. Sci.* **143** 536–46
Masel R I, Merrill R P and Miller W H 1975 *Phys. Rev.* B **12** 5545–51
——1976 *J. Chem. Phys.* **65** 2690–9
Mason B F and Williams B R 1991 *Surf. Sci.* **243** L74–80
——1992 *Surf. Sci.* **262** 169–79
Mattera L 1992 *Atomic and Molecular Beam Methods* vol 2, ed G Scoles (Oxford: Oxford University Press) pp 366–83
Mattera L, Musenich R, Salvo C and Terreni S 1985 *Faraday Discuss. Chem. Soc.* **80** 115–26
Mattera L, Salvo C, Terreni S and Tommasini F 1980 *Surf. Sci.* **97** 158–70
McClure J D 1970 *J. Chem. Phys.* **52** 2712–18
——1972a *J. Chem. Phys.* **57** 2810–22
——1972b *J. Chem. Phys.* **57** 2823–9
Meli C A and Greene E F 1994 *J. Chem. Phys.* **101** 7139–43
Meli C A, Greene E F, Lange G and Toennies J P 1995 *Phys. Rev. Lett.* **74** 2054–7
Meunier M and Henry C R 1994 *Surf. Sci.* **307–309** 514–18
Meyer G, Michailov M and Henzler M 1988 *Surf. Sci.* **202** 125–41
Meyer G, Range H and Toennies J P 1997 *Surf. Sci.* **371** 183–99
Meyer H-D 1981 *Surf. Sci.* **104** 117–60
Miret-Artés S 1993 *Surf. Sci.* **294** 141–8
——1995 *Surf. Sci.* **339** 205–20
——1996a *Surf. Sci.* **366** L681–4
——1996b *Surf. Sci.* **366** L735–41
Miret-Artés S, Margalef-Roig J, Guantes R, Borondo F and Jaffé Ch 1996b *Phys. Rev.* B **54** 10 397–400
Miret-Artés S, Toennies J P and Witte G 1996a *Phys. Rev.* B **54** 5881–92
Miyake T, Petek H, Takeda K and Hinode K 1997 *Appl. Phys. Lett.* **70** 1239–41
Mo Y W, Kleiner J, Webb M B and Lagally M G 1991 *Phys. Rev. Lett.* **66** 1998–2001
Modesti S, Dhanak V R, Sancrotti M, Santoni A, Persson B N J and Tossati E 1994 *Phys. Rev. Lett.* **73** 1951–4
Montalenti F, Trioni M I, Brivio G P and Crampin S 1996 *Surf. Sci.* **364** L595–9
Nichtl-Pecher W, Stammler W, Heinz K and Müller K 1991 *Phys. Rev.* **B 43** 6946–51
Nielsen U, Halstead D, Holloway S and Nørskov J K 1995 *J. Chem. Phys.* **93** 2879–84
Niu L, Koleske D D, Gaspar D J, King S F and Sibener S J 1996 *Surf. Sci.* **356** 144–60
O'Keefe D R, Palmer R L and Smith Jr J N 1971 *J. Chem. Phys.* **55** 4572–7
Over H, Schwegmann S, Cvetko D, de Renzi V, Floreano L, Gotter R, Morgante A, Peloi M, Tommasini F and Zennaro S 1997a *Phys. Rev.* B **55** 4717–22
Over H, Schwegmann S, Ertl G, Cvetko D, de Renzi V, Floreano L, Gotter R, Morgante A, Peloi M, Tommasini F and Zennaro S 1997b *Surf. Sci.* **376** 177–84
Park R L, Houston J E and Schreiner D G 1971 *Rev. Sci. Instrum.* **42** 60–5
Parschau G, Burg B and Rieder K H 1993 *Surf. Sci.* **293** L830–4

Parschau G, Kirsten E, Bischof A and Rieder K H 1989 *Phys. Rev.* B **40** 6012–17
Parschau G, Kirsten E and Rieder K H 1990 *Surf. Sci.* **225** 367–72
——1991 *Phys. Rev.* B **43** 12 216–20
Parschau G and Rieder K H 1991 *Surf. Sci.* **257** L628-32
Perreau J and Lapujoulade J 1982a *Surf. Sci.* **119** L292–8
——1982b *Surf. Sci.* **122** 341–54
Peskin U and Moiseyev N 1992a *J. Chem. Phys.* **96** 2347–55
——1992b *J. Chem. Phys.* **97** 2804–8
Peterlinz K A, Curtiss T J and Sibener S J 1991 *J. Chem. Phys.* **95** 6972–88
Peterlinz K A and Sibener S J 1995 *Surf. Sci.* **344** L1239–44
Petersen M, Ruggerone P and Scheffler M 1998 to be published
Petersen M, Wilke S, Ruggerone P, Kohler B and Scheffler M 1996 *Phys. Rev. Lett.* **76** 995–8
Petrella G 1990 *Chem. Phys.* **144** 179–87
——1992 *Chem. Phys.* **161** 237–44
Petrella G and Cassidei L 1993 *Chem. Phys. Lett.* **212** 512–17
——1995 *Chem. Phys.* **191** 203–12
Petrella G, Yinnon A T and Gerber R B 1989 *Chem. Phys. Lett.* **158** 250–6
Picaud S, Girardet C, Glebov A, Toennies J P, Dohrmann J and Weiss H 1997 *J. Chem. Phys.* **106** 5271–83
Pijper E and Kroes G J 1998 *Phys. Rev. Lett.* **80** 488–91
Poelsema B, Becker A F, Rosenfeld G, Kunkel R, Nagel N, Verheij L K and Comsa G 1992 *Surf. Sci.* **272** 269–75
Poelsema B and Comsa G 1989 *Scattering of Thermal Energy Atoms from Disordered Surfaces (Springer Tracts in Modern Physics 115)* (Berlin: Springer)
Poelsema B, de Zwart T S and Comsa G 1982a *Phys. Rev. Lett.* **49** 578–81
——1983a *Phys. Rev. Lett.* **51** 522(E)
Poelsema B, Kunkel R, Nagel N, Becker A F, Rosenfeld G, Verheij L K and Comsa G 1991 *Appl. Phys.* A **53** 369–76
Poelsema B, Palmer R L, de Zwart T S and Comsa G 1983b *Surf. Sci.* **126** 641–6
Poelsema B, Palmer R L, Mechtersheimer G and Comsa G 1982b *Surf. Sci.* **117** 60–6
Poelsema B, Verheij L K and Comsa G 1982c *Phys. Rev. Lett.* **49** 1731–4
——1983c *Phys. Rev. Lett.* **51** 2410–3
——1984 *Phys. Rev. Lett.* **53** 2500–3
——1985 *Surf. Sci.* **152–153** 851–8
Reichmuth A, Graham A P, Bullman H G, Allison W and Rhead G E 1994 *Surf. Sci.* **307–309** 34–40
Rendulic K D, Anger G and Winkler A 1989 *Surf. Sci.* **208** 404–24
Rettner C T 1992 *Phys. Rev. Lett.* **69** 383–6
Rettner C T, Auerbach D J and Michelsen H A 1992a *Phys. Rev. Lett.* **68** 1164–7
——1992b *Phys. Rev. Lett.* **68** 2547–50
Rieder K H 1982a *Surf. Sci.* **117** 13–22
——1982b *Surf. Sci.* **118** 57–65
——1983a *Surf. Sci.* **128** 325–33
——1983b *Phys. Rev.* B **27** 7799–802
——1989 *Phys. Rev.* B **39** 10 708–13
——1992 *Helium Atom Scattering from Surfaces (Springer Series in Surface Sciences 27)* ed E Hulpke (Berlin: Springer) pp 41–71
——1994 *Surf. Rev. Lett.* **1** 51–65
Rieder K H, Baumberger M and Stocker W 1985 *Phys. Rev. Lett.* **55** 390–3
Rieder K H and García 1982 *Phys. Rev. Lett.* **49** 43–6
Rieder K H, Parschau G and Burg B 1993 *Phys. Rev. Lett.* **71** 1059–62
Rieder K H and Stocker W 1983 *J. Phys. C: Solid State Phys.* **16** L783–8
——1984 *Phys. Rev. Lett.* **52** 352–5
——1985a *Surf. Sci.* **150** L66–70
——1985b *Phys. Rev.* B **31** 3392–7
——1985c *Surf. Sci.* **164** 55–84
——1986 *Chem. Phys. Lett.* **126** 297
Rieder K H and Wilsch H 1983 *Surf. Sci.* **131** 245–57
Robinson G N, Camillone N, Rowntree P A, Liu G-Y, Wang J and Scoles G 1992 *J. Chem. Phys.* **96** 9212–20
Robota H J, Vielhaber W, Lin M C, Segner J and Ertl G 1985 *Surf. Sci.* **155** 101–20
Rohlfing D M, Ellis J, Hinch B J, Allison W and Willis R F 1988 *Vacuum* **38** 287–9

Romainczyk Ch, Manson J R, Kern K, Kuhnke K, David R, Zeppenfeld P and Comsa G 1995 *Surf. Sci.* **336** 362–70
Rosenfeld G, Lipkin N N, Wulfhekel W, Kliewer J, Morgenstern K, Poelsema B and Comsa G 1995 *Appl. Phys.* A **61** 455–66
Rosenfeld G, Servaty R, Teichert C, Poelsema B and Comsa G 1993 *Phys. Rev. Lett.* **71** 895–8
Rowntree P A, Scoles G and Ruiz-Suárez J C 1990 *J. Phys. Chem.* **94** 8511–22
Ruiz-Suárez J C, Klein M L, Moller M A, Rowntree P A, Scoles G and Xu J 1988 *Phys. Rev. Lett.* **61** 710–13
Safron S A, Duan J, Bishop G G, Gillman E S and Skofronick J G 1993 *J. Phys. Chem.* **97** 1749–57
Sakai A, Cardillo M J and Hamann D R 1986 *Phys. Rev.* B **33** 5774–81
Salanon B 1984 *J. Physique* **45** 1373–9
Sánchez A and Ferrer S 1987 *Surf. Sci.* **187** L587–91
——1989 *Phys. Rev.* B **39** 5778–86
Sánchez A, Ibáñez J, Miranda R and Ferrer S 1987 *J. Appl. Phys.* **61** 1239–41
Sanders D E and DePristo A E 1992 *Surf. Sci.* **260** 116–28
Santoro G, Franchini A and Bortolani V 1998 *Phys. Rev. Lett.* **80** 2378–81
Schaich Th, Braun J, Toennies J P, Buck M and Wöll Ch 1997 *Surf. Sci.* **385** L958–64
Schinke R 1982a *J. Chem. Phys.* **76** 2352–9
——1982b *Chem. Phys. Lett.* **87** 438–42
Schlup W A and Rieder K H 1986 *Phys. Rev. Lett.* **56** 73–6
Schmicker D, Hibna T, Edwards K A, Howes P B, Mac Donald J E, James M A, Breeman M and Barkema G T 1997 *J. Phys.: Condens. Matter* **9** 969–80
Schmicker D, Schmidt S, Skofronick J G, Toennies J P and Vollmer R 1991b *Phys. Rev.* B **44** 10 995–7
Schmicker D, Toennies J P, Vollmer R and Weiss H 1991a *J. Chem. Phys.* **95** 9412–15
Schulte K F 1976 *Surf. Sci.* **55** 427–44
Schwartz C 1986 *Phys. Rev.* B **34** 2834–9
Schwarz C, Cole H W and Pliva J 1978 *Surf. Sci.* **75** 1–16
Schweizer E K and Rettner C T 1989 *Phys. Rev. Lett.* **62** 3085–8
Schweizer E K, Rettner C T and Holloway S 1991 *Surf. Sci.* **249** 335–49
Schwenger L and Ernst H J 1996 *Surf. Sci.* **347** 25–32
Schwenger L, Folkerts R L and Ernst H J 1997 *Phys. Rev.* B **55** R7406–9
Scoles G (ed) 1988 *Atomic and Molecular Beam Methods* vol 1 (New York: Oxford University Press)
——1992 *Atomic and Molecular Beam Methods* vol 2 (New York: Oxford University Press)
Semerad E and Hörl E M 1983 *Surf. Sci.* **126** 661–5
Šiber A and Gumhalter B 1997 *Surf. Sci.* **385** 270–80
Smith J N Jr, O'Keefe D R and Palmer R L 1970 *J. Chem. Phys.* **52** 315–20
Smith J N Jr, O'Keefe D R, Saltsburg H and Palmer R L 1969 *J. Chem. Phys.* **50** 4667–71
Sprösser J, Salanon B and Lapujoulade J 1991 *Europhys. Lett.* **16** 283–8
Stickney R E 1969 *The Structure and Chemistry of Solid Surfaces* ed G A Somorjai (New York: Wiley) ch 41
Stoll E, Baumberger M and García N 1984 *J. Chem. Phys.* **81** 1496–500
Strutt J W (Lord Rayleigh) 1896 *The Theory of Sound* vol 2 (London: Macmillan) p 272
Swan A, Marynowski M, Franzen W, El-Batanouny M and Martini K M 1993 *Phys. Rev. Lett.* **71** 1250–3
Takeuchi N, Selloni A and Tosatti E 1992 *Phys. Rev. Lett.* **69** 648–51
Tepper G and Miller D 1992 *Phys. Rev. Lett.* **69** 2927–30
Terreni S, Cantini P, Canepa M and Mattera L 1997 *Phys. Rev.* B **56** 6490–3
Tölkes Ch, Struck R, David R, Zeppenfeld P and Comsa G 1998 *Phys. Rev. Lett.* **80** 2877–80
Tölkes Ch, Zeppenfeld P, Krzyzowski M A, David R and Comsa G 1997a *Surf. Sci.* **394** 170–84
——1997b *Phys. Rev.* B **55** 13 932–7
Toennies J P 1982 *Dynamics of Gas–Surface Interaction (Springer Series in Chemical Physics 21)* ed G Benedek and U Valbusa (Heidelberg: Springer) pp 208–26
——1984 *J. Vac. Sci. Technol.* A **2** 1055–65
——1991 *Surface Phonons (Springer Series in Surface Sciences 21)* ed W Kress and F W de Wette (Berlin: Springer) pp 111–66
Toigo F, Marvin A, Celli V and Hill N R 1977 *Phys. Rev.* B **15** 5618–26
Trioni M I, Montalenti F and Brivio G P 1998 *Surf. Sci.* **401** L383–7
Vandoni G, Félix C, Monot R, Buttet J and Harbich W 1994a *Surf. Sci.* **320** L63–7
——1994b *Chem. Phys. Lett.* **229** 51–6
Vandoni G, Félix C, Monot R, Buttet J, Massobrio C and Harbich W 1996 *Surf. Rev. Lett* **1** 949–54
Varga G 1998 *Vacuum* **50** 339–42

Varga G and Füstöss L 1991 *Surf. Sci.* **243** 23–30
Vargas M C and Mochán W L 1996 *Surf. Sci.* **355** 115–26
——1998 *Surf. Sci.* **409** 130–6
Venables J A, Spiller G D T and Hambücken M 1984 *Rep. Prog. Phys.* **47** 399–459
Verheij L K, Freitag M K and Wiegershaus F 1995 *Surf. Sci.* **334** 105–13
Verheij L K, Lux B and Poelsema B 1984 *Surf. Sci.* **144** 385–401
Verheij L K, Poelsema B and Comsa G 1985 *Surf. Sci.* **162** 858–64
Vidali G, Hutchings C W and Karimi M 1988 *Surf. Sci.* **202** L595–602
Vidali G, Ihm G, Kim H-Y and Cole M W 1991 *Surf. Sci. Rep.* **12** 133–81
Wang S C and Ehrlich G 1993 *Phys. Rev. Lett.* **71** 4174–7
Wassermann B, Reif J and Matthias E 1994 *Phys. Rev.* B **50** 2593–7
Whaley K B and Light J C 1984 *J. Chem. Phys.* **81** 3334–43
White J D, Cui J, Strauss M, Diehl R D, Ancilotto F and Toigo F 1994 *Surf. Sci.* **307–309** 1134–40
Williams B R 1971 *J. Chem. Phys.* **55** 1315–22
Wilsch H and Rieder K H 1983 *J. Chem. Phys.* **78** 7491–6
Witte G, Toennies J P and Wöll Ch 1995 *Surf. Sci.* **323** 228–40
Wolken G Jr 1973a *J. Chem. Phys.* **58** 3047–64
——1973b *J. Chem. Phys.* **59** 1159–65
——1973c *Chem. Phys. Lett.* **21** 373–9
——1975 *J. Chem. Phys.* **62** 2730–5
Wulfhekel W, Beckmann I, Lipkin N N, Rosenfeld G, Poelsema B and Comsa G 1996a *Appl. Phys. Lett.* **69** 3492–4
Wulfhekel W, Beckmann I, Rosenfeld G, Poelsema B and Comsa G 1998 *Surf. Sci.* **395** 168–81
Wulfhekel W, Lipkin N N, Kliewer J, Rosenfeld G, Jorritsma L C, Poelsema B and Comsa G 1996b *Surf. Sci.* **348** 227–42
Xu H, Huber D and Heller E J 1988 *J. Chem. Phys.* **89** 2550–7
Xu H, Yang Y and Engel T 1991 *Surf. Sci.* **255** 73–90
Yang Y, Xu H and Engel T 1992 *Surf. Sci.* **276** 341–52
Yanuka M, Yinnon A T, Gerber R B, Zeppenfeld P, Kern K, Becher U and Comsa G 1993 *J. Chem. Phys.* **99** 8280–9
Yinnon A T, Gerber R B, Dacol D K and Rabitz H 1986a *J. Chem. Phys.* **84** 5955–61
Yinnon A T, Kolodney E, Amirav A and Gerber R B 1986b *Chem. Phys. Lett.* **123** 268–72
Yinnon A T, Kosloff R and Gerber R B 1984 *Chem. Phys.* **87** 441–9
——1988b *J. Chem. Phys.* **88** 7209–20
Yinnon A T, Kosloff R, Gerber R B, Poelsema B and Comsa G 1988a *J. Chem. Phys.* **88** 3722–31
Yinnon A T, Lidar (Hamburger) D A, Farbman I, Gerber R B, Zeppenfeld P, Krzyzowski M A and Comsa G 1997 *J. Chem. Phys.* **106** 4228–42
Yinnon A T, Lidar (Hamburger) D A, Gerber R B, Zeppenfeld P, Krzyzowski M A and Comsa G 1998 *Surf. Sci.* **410** L721–5
Yu C-F, Hogg C S, Cowin J P, Whaley K B, Light J C and Sibener S J 1982 *Israel J. Chem.* **22** 305–14
Yu C-F, Whaley K B, Hogg C S and Sibener S J 1983 *Phys. Rev. Lett.* **51** 2210–13
——1985 *J. Chem. Phys.* **83** 4217–34
Zeng H and Vidali G 1995 *Phys. Rev. Lett.* **74** 582–5
Zeng H, Vidali G and Biham O 1994 *J. Vac. Sci. Technol.* A **12** 2058–62
Zeppenfeld P, Becher U, Kern K and Comsa G 1992 *Phys. Rev.* B **45** 5179–86
Zeppenfeld P, Büchel M, Goerge J, David R, Comsa G, Ramseyer C and Girardet C 1996 *Surf. Sci.* **366** 1–18
Zeppenfeld P, Goerge J, Büchel M, David R and Comsa G 1994 *Surf. Sci.* **318** L1187–92
Zeppenfeld P, Goerge J, Diercks V, Halmer R, David R, Comsa G, Marmier A, Ramseyer C and Girardet C 1997 *Phys. Rev. Lett.* **78** 1504–7
Zeppenfeld P, Kern K, David R and Comsa G 1989 *Phys. Rev. Lett.* **62** 63–6
Zuo J-K, Wendelken J F, Dürr H and Liu C-L 1994 *Phys. Rev. Lett.* **72** 3064–7